DYNAMIC ANALYSIS OF RAILWAY WHEELSETS AND COMPLETE VEHICLE SYSTEMS

PROEFSCHRIFT

ter verkrijging van de graad van doctor aan de
Technische Universiteit Delft, op gezag van de
Rector Magnificus, Prof.drs. P.A. Schenck,
in het openbaar te verdedigen ten overstaan van een
commissie aangewezen door het College van Dekanen op
dinsdag 20 april 1993 te 16.00 uur

door

GUANG YANG

geboren te Hebei, China
Master of Science

Dit proefschrift is goedgekeurd door de promotor:

Prof. dr. ir. P. Meijers

CIP-DATA KONINKLIJKE BIBLIOTHEEK, DEN HAAG

Yang, Guang

Dynamic analysis of railway wheelsets
and complete vehicle systems/
Guang Yang. - Delft: Delft University of Technology,
Faculty for Mechanical Engineering and Marine Technology. -111.
Thesis Delft University of Technology. - With ref. - With Dutch summary.
ISBN 90-370-0080-0

To my wife Liye and my parents

Summary

In this thesis, a general mechanical model to predict the dynamic behaviour of railway vehicle systems has been developed based on multibody system methods. The interaction between the rail and the wheel not only ensures the guidance and the running stability of the vehicle but also gives rise to damage because of the high contact forces. These factors should be taken into account in the design of railway vehicles. Attention is especially paid to the geometric, kinematic and dynamic aspects of the track and wheelset system. In the model the geometric and physical nonlinearities due to the contact are incorporated; nonlinearities in the suspensions can also be taken into account. The model has been implemented into a computer package.

By assuming the two contacting bodies to be rigid, the geometric contact between the track and the wheelset becomes a purely geometric problem in three-dimensional space. With the necessary and sufficient conditions for two rigid bodies in contact, the spatial locations of the contact points on the rail and wheel surfaces may be found in terms of two independent generalized coordinates.This requires the solution of a set of nonlinear algebraic equations. The relation between the dependent and independent generalized coordinates is also obtained. A similar analysis has been carried out for the roller-rig system.

In order to reduce the computing time, the set of nonlinear equations is reduced to another set of nonlinear equations for the two-dimensional contact or is simplified by means of the so-called first-order theory. The numerical results indicate that the first-order equations yield a sufficiently accurate solution for the three-dimensional contact. The singularity of the set of nonlinear equations, which is associated with a double-contact position, is studied analytically and numerically. Local parameterization is employed to solve the nonlinear equations. The numerical method to determine double-contact positions is also given. By means of the first-order equations, the numerical analysis is carried out for the well-known combination of UIC60 and S1002 profiles and also for two measured asymmetric profile combinations: *CTO-Measured-Profiles* and *ORE-Benchmark-Profiles*. The influence of the track gauge and the rail inclination is presented too.

In the mechanical model, the motion of the vehicle is described by the nominal motion, which represents the motion of the track reference frame, and the

relative motion, which defines the motion of the body or body-fixed frame relative to the nominal motion. The nominal motion is prescribed as a function of the vehicle nominal speed and the nominal geometry of the track. Due to the contact constraints, a conventional wheelset has only four degrees of freedom. By using the corresponding kinematic constraints, the general equations of motion of the wheelset running along an arbitrary track are derived in terms of the four independent generalized coordinates, two of which are the relative longitudinal translation and the spin rotation of the wheelset. The associated constraint forces which are the normal contact forces between the track and the wheelset are also determined. The theories of rolling contact mechanics are briefly reviewed and Kalker's simplified theory is utilized to calculate the tangential contact forces. Moreover, the equations of motion of a wheelset with independently rotating wheels are derived.

In the dynamic simulation the four general irregularities in tangent tracks may be considered. The variation of the track gauge and the cross-level are incorporated in the determination of the contact position; the lateral and vertical alignments are incorporated in the motion of the track reference frame. The equations of motion of a wheelset are linearized in order to analyze the stability of the stationary motion on a perfect tangent track.

Both single wheelsets and complete vehicle systems have been simulated. First, the solutions of some exercises contained in Pascal's and Kik's railway benchmarks are demonstrated. Comparing the dynamic behaviour of vehicles with different profile combinations indicates that a jump of the contact point destabilizes the vehicle motion. Afterwards, vehicles with independently rotating wheels are investigated numerically. It seems that decoupling the spin motion of the two wheels completely may give rise to destabilization of the systems; at this point further research is necessary.

Acknowledgements

The work presented in the thesis has been carried out at the Laboratory for Engineering Mechanics, Delft University of Technology under financial support provided by the Netherlands Technology Foundation (STW). Throughout the thesis, the influence of Prof. dr. ir. A. D. de Pater and Prof. dr. ir. P. Meijers will be obvious. I would like to express my deepest thanks to them for the invaluable dedication which they gave me and also for their kindness. My grateful thanks go to Prof. dr. ir. J.J Kalker for his seminar on contact mechanics, and go to Prof. ir. N.H.C.E. Zeevenhoven for his helpful comments. I am also sincerely indebted to Ir. P. Wiersma of the Centre of Technical Research (CTO) of the Netherlands Railways in Utrecht for his valuable discussions and suggestions. The support rendered by many colleagues in the laboratory is greatly appreciated. I would also like to gratefully acknowledge the encouragement given by Prof. Zhiyun Shen, Prof. Shitong Chen and Prof. Peixin Fan of Southwest Jiaotong University in Chengdu.

CONTENTS

Chapter 1

Introduction

With the economic growth and the centralisation of the production, trade is booming; tourism and business travel are increasing; homes and places of work are further removed from each other; regional cities are gaining in importance. Consequently, both passenger and freight traffic have risen strongly. The societies we live in are, therefore, under the obligation to develop and enhance transport resources.

The railway transportation system is a system where infrastructure, rolling stock and organisation of operations are very closely integrated. It has not only its own virtues of safety, comfort, speed, reliability and low energy consumption, but it is also environment-friendly. In consequence, the trend is towards an increased demand for railway services.

Both the speed and the load carrying capacity are key factors for the railway system. This is largely because the speed can reduce the travelling time, to which the user is most sensitive, and an increase of the load carrying capacity would heighten the efficiency in the freight traffic. In realising high speed railways two concepts have been implemented successfully. The first is building of completely new lines on which the railway vehicles can travel at very high speed (between 270 and 350 km/h). Besides, upgrading of the existing lines to raise the vehicle speed to 160-250 km/h is very realistic and economic. For freight railway vehicles on special freight traffic lines the speed and the axle loads can be largely increased. With the advent of high speed, the potential of the railway system may be fully exploited so that it can even better compete with other transport systems.

In general, both key factors have negative aspects as well. Increasing the speed induces the tendency to develop unstable lateral oscillations; increasing the axle loads aggravates the damage due to the contact between rail and wheel. Thus, in an optimal design of a railway vehicle system, the dynamic attributes of the system play a very important role. The application of advanced technology will ensure the travel safety, improve the ride comfort and lower the maintenance cost by reducing the wear of the wheels and the rails. In this thesis the main effort is devoted to exposing a general theory for analyzing and simulating the dynamic behaviour of railway vehicles, to predicting the behaviour of newly designed systems and to evaluating the systems in service.

The contact between the profiled steel wheel and the profiled steel rail provides the interface between the moving vehicle and the infrastructure. Through the wheelsets, on which the vehicle is levitated and steered and by which the traction and braking are accomplished, the contact interaction strongly influences the motion of railway vehicles. This interaction solidly depends on the geometric configuration of the track and the wheelset system, the materials and the working circumstances. For instance, track irregularities cause stochastic vibrations of the vehicle system, which are usually investigated for the ride comfort by means of symmetric models related to the vertical and pitch motions of the vehicle.

Above a critical speed the vehicle loses its stability and the hunting motion arises. From the kinematic point of view, Klingel(1883) investigated this kind of motion on the assumptions of conical wheels and pure rolling. He gave the well-known formula to calculate the wavelength of the hunting motion, which is only related to some geometric parameters. Later on, Carter (1926) took into account the relative slip occurring in the contact area between the rail and the wheel; he investigated the two-dimensional case and submitted formulae for the relation between the friction force and the creepage defined by the relative slip. A similar work was done by Rocard (1935) for explaining derailments of steam locomotives.

In reality, the rail and wheel profiles give rise to geometric nonlinearities. These nonlinearities have been investigated by Wickens (1965), Knothe (1975), Cooperrider and Law *et al.*(1976), and De Pater (1988). De Pater derived a set of nonlinear algebraic equations to determine the contact constraints between the track and the wheelset in three dimensions. Carter's theory has been extended to the three-dimensional case by Kalker (1967, 1982b), whose theories of rolling contact mechanics have been broadly employed in the dynamic analysis. Elkins (1991) gave a survey of the investigations on both the geometric and physical contacts.

Due to the geometric and physical nonlinearities associated with the contact, the combination of the track and the wheelset is a very complicated mechanical system. In general, a conventional wheelset on a track subject to two holonomic constraints has four degrees of freedom. De Pater (1979, 1981) studied this system thoroughly; he derived the equations of motion for the single wheelset moving along a perfectly straight track and also the equations for the wheelset moving through a curved track with constant radius and cant. In a complete railway vehicle system comprising several wheelsets, the bodies of the system are assembled by the linkages and a multitude of linear and nonlinear suspensions. In the numerical study of certain vehicle characteristics which were not revealed by analytical studies, deriving the equations of motion "by hand" for such a large nonlinear system with many degrees of freedom and then transforming the equations into computer codes have proven to

be a very tedious, difficult, time consuming and error prone task. With the aid of a library in which many mechanical subsystems such as the wheel and rail subsystem are well modeled, multibody system methods have been developed to enable computers to formulate the equations of motion for many types of mechanical systems (Kortüm and Schiehlen, 1985; Roberson and Schwertassek, 1988). The applications in railway vehicle dynamics were shown by Duffek *et al.*(1977) and Fisette and Samin (1991).

The ideal running gear, which is composed of several elastically connected wheelsets, has to satisfy two conflicting requirements: its motion should be sufficiently stable and it should negotiate a curve as freely as possible. Based on linear models, Wickens (1975) proposed two conditions that have to be held in the optimal design of elastic suspensions. De Pater(1987) gave an additional condition, which enables the running gears to be insensitive to the lateral force due to the cant deficiency in a curved track. The essential properties of the running gear were also studied by Scheffel(1981), Hedrick(1982), Keizer(1985), Smith and Anderson (1988). The forced-steering techniques shown by Fortin (1984), Shen and Yan *et al.* (1987) have been developed and implemented in practice. When a forced-steering vehicle negotiates a curved track, the mechanism linkages between the carbody, bogies and wheelsets tend to force the wheelsets into more radial alignments on the curves. Therefore, the wear of the rail and the wheel is reduced.

The nonlinear dynamic behaviour of railway vehicles has been studied by many investigators. De Pater (1961) used the Krylov-Bogoljubov method to determine the limit cycle of a two-axle bogie system described by a simplified model. Afterwards, the Galerkin method was applied by Knothe and Moelle (1982). The contact non-linearities were treated more appropriately and the suspension nonlinearities were also taken into account. The features of curving behaviour of practical vehicles were investigated by Elkins and Gostling (1977), Endlicher and Lugner (1990), and Bailey and Wormley (1992). Either the Newton-Raphson method or the numerical integration can be employed to study the steady-state motion in circular curves. Analytical and experimental work was also carried out in roller-rig systems in order to validate various theories of a railway vehicle system (Jaschinski, 1990) and to investigate wear of the rail and the wheel (Chollet et al. 1989).

The lateral and yaw motions are coupled in the conventional wheelset because of the rigid connection of the two wheels. Abolishing this coupling is expected to prevent hunting presented in conventional railway vehicles and to reduce wear of the rails and the wheels. But once we completely decouple the spin rotations of the two wheels, vehicles mounted with independently rotating wheels will be sensitive to the track irregularities and also lack the restoring forces to centre the wheelset. These

difficulties may be overcome by utilizing the elasto-damper coupled wheelset or the creep-controlled wheelset (Geuenich *et al.* 1983). Recently, both passive and active-controlled tilting mechanisms have been developed for increasing the operational speed on already existing lines which comprise many curves with relatively small radii (Higaki *et al.*, 1991). When the vehicle passes through a curve at high speed, the tilting system can compensate for the insufficient curve cant, which causes larger lateral acceleration felt by passengers; as a result, the ride comfort is improved remarkably.

The thesis presents a general theory to model railway vehicle systems and especially concentrates on the track and wheelset subsystems. In the next chapter, the basic dynamics of multibody systems are briefly described. The equations of motion of multibody systems are derived based on Jourdain's principle and are written in terms of the independent generalized coordinates.

In Chapter 3, first the general necessary and sufficient conditions of two rigid bodies in contact are stated and formulated. Then a number of coordinate systems are defined to describe the geometry of the track and wheelset system. By means of the contact conditions a set of nonlinear algebraic equations is found for determining the constraints due to the spatial contact between the track and the wheelset; similarly, the equations for the roller-rig system are set up. The former set of nonlinear equations is studied comprehensively. They are simplified by means of the so-called first-order theory (De Pater 1988) and the two-dimensional contact is also discussed as a special case. Numerical results for three different combinations of rail and wheel profiles are presented.

The equations of motion of a single conventional wheelset and the wheelset with independently rotating wheels are derived in Chapter 4 and 5 respectively. At the beginning of Chapter 4, the theory of rolling contact mechanics is briefly reviewed and the creep quantities are defined in a general way. The motion of the wheelset is defined with respect to the motion of the track reference frame, which is prescribed as a function of the vehicle travel distance. The cases of a wheelset moving both along a tangent track and a curved track are discussed. Attention is also paid to track irregularities and to linearization around the stationary motion.

Some exercises contained in Pascal's and Kik's benchmarks are solved in Chapter 6. Comparisons are made for the behaviour of vehicles with three kinds of rail and wheel profiles. A number of vehicles with independently rotating wheels are studied as well. Ultimately, in Chapter 7 the important conclusions of this thesis are given and some problems and topics for further investigations are also mentioned.

Chapter 2

Preliminaries of Multibody System Dynamics

Multibody descriptions have been used to model mechanical systems like vehicles, linkages and robots in an effective way. The development of computer-aided analysis of multibody systems has been presented by Haug (1984, 1989), Besseling, Jonker and Schwab (1985), Roberson and Schwertassek (1988). A survey of a number of computer codes is given by Schiehlen (1990). Special applications in vehicle dynamics have been reviewed by Kortüm, Sharp and De Pater (1991).

In this chapter the kinematics and dynamics of a rigid body and a system of rigid bodies are briefly presented. Jourdain's principle is employed to establish the equations of motion of such systems. By making use of the constraint equations, the equations of motion are derived in terms of the independent generalized coordinates. Finally the constraint forces in the system are calculated.

2.1. Kinematics of a Rigid Body

The motion of a rigid body in space relative to an inertial frame can be described by the translation of a point of the body (the reference point) relative to the inertial frame and the rotation of the body about that point. The rotation can be characterized by the orientations of the axes of a frame, which is located at the reference point and rigidly embedded in the body, relative to the inertial frame. In general, it is most advantageous to choose the mass centre of the body as the reference point. The motion of a rigid body is therefore completely represented by the motion of its body-fixed frame in space.

We suppose that the inertial frame and the body-fixed frame are denoted by $\{o^I, \bar{e}^I\}$ and $\{o^i, \bar{e}^i\}$ respectively (see Fig.2.1). The position vector of the origin of the body-fixed frame relative to the inertial frame is denoted by $\bar{r}$. The rotation matrix of the body-fixed frame relative to the inertial frame is designated by $\boldsymbol{G}$. The absolute angular velocity vector of the body is denoted by $\bar{\omega}$. The general relations between the rotation angles, the rotation matrix, the angular velocity and the angular acceleration are given in the Appendices A and B.

Every point of the body has constant coordinates in the body-fixed frame. The

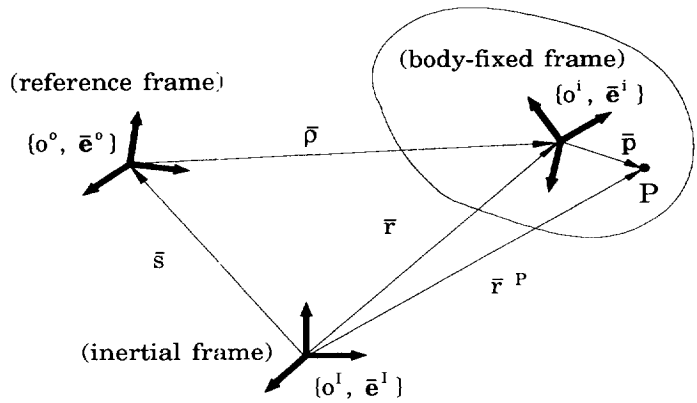

Fig.2.1 A body in space.

position vector $\bar{r}^P$ of a point P in the body relative to the inertial frame is described by the position vector $\bar{r}$ of the body-fixed frame origin relative to the inertial frame and the position vector $\bar{p}$ of the point relative to the body-fixed frame (see Fig. 2.1) so that we can write

$$\bar{r}^P = \bar{r} + \bar{p}\,. \tag{2.1.1}$$

By differentiating both sides of Eq.(2.1.1) once and twice with respect to time, the absolute velocity and the absolute acceleration vectors of point P are determined by

$$\dot{\bar{r}}^P = \dot{\bar{r}} + \bar{\omega} \times \bar{p} \tag{2.1.2}$$

and

$$\ddot{\bar{r}}^P = \ddot{\bar{r}} + \dot{\bar{\omega}} \times \bar{p} + \bar{\omega} \times (\bar{\omega} \times \bar{p})\,. \tag{2.1.3}$$

The body motion can also be described relative to a moving reference frame $\{o^0, \bar{e}^0\}$. In general, the translation and rotation of the reference frame relative to the inertial frame are prescribed as time functions of the position vector $\bar{s}$ of the origin and the rotation angles. The position vector of the body mass centre relative to the inertial frame may now be given by

$$\bar{r} = \bar{s} + \bar{\rho}\,, \tag{2.1.4}$$

where $\bar{\rho}$ is the position vector of the body mass centre relative to the reference frame. The rotation matrix of the body-fixed frame relative to the inertial frame is:

$$\boldsymbol{G} = \boldsymbol{G}^{io}\boldsymbol{G}^{o}, \tag{2.1.5}$$

where $\boldsymbol{G}^{io}$ denotes the rotation matrix of the body-fixed frame relative to the reference frame and $\boldsymbol{G}^{o}$ the rotation matrix of the reference frame relative to the inertial frame. The velocity and the acceleration vectors of the body mass centre are determined by Eqs.(A.14) and (A.15). The absolute angular velocity vector of the body is given by

$$\bar{\omega} = \bar{\omega}^{o} + \bar{\omega}^{io}, \tag{2.1.6}$$

where $\bar{\omega}^{o}$ represents the absolute angular velocity vector of the reference frame and $\bar{\omega}^{io}$ the angular velocity vector of the body relative to the reference frame. By substituting (2.1.4) into Eq.(2.1.1) the position vector of point P can be expressed in terms of the relative quantities.

When the base vectors of the reference frame remain parallel to the base vectors of the inertial frame, the rotation matrix $\boldsymbol{G}^{o}$ reduces to the 3×3 unit matrix and the angular velocity $\bar{\omega}^{o}$ vanishes.

Writing Eqs.(2.1.1)-(2.1.3) in matrix form by using the algebraic representation we find,

$$\boldsymbol{r}^{P} = \boldsymbol{r} + \boldsymbol{G}^{T}\boldsymbol{p}^{*}, \tag{2.1.7}$$

$$\dot{\boldsymbol{r}}^{P} = \dot{\boldsymbol{r}} + \boldsymbol{G}^{T}\tilde{\boldsymbol{\omega}}^{*}\boldsymbol{p}^{*} \tag{2.1.8}$$

and

$$\ddot{\boldsymbol{r}}^{P} = \ddot{\boldsymbol{r}} + \boldsymbol{G}^{T}\dot{\tilde{\boldsymbol{\omega}}}^{*}\boldsymbol{p}^{*} + \boldsymbol{G}^{T}\tilde{\boldsymbol{\omega}}^{*}\tilde{\boldsymbol{\omega}}^{*}\boldsymbol{p}^{*}. \tag{2.1.9}$$

An algebraic vector with a superscript asterisk (*) refers to the body-fixed frame; otherwise its components are taken with respect to the inertial frame.

The algebraic representation of the motion of the body mass centre in a moving reference frame is shown in Appendix A, in which the relative motion between two arbitrary frames is presented.

2.2. Dynamics of a Rigid Body

We first consider a system consisting of a number of particles. Let $\bar{r}^{P}$ be the position vector of particle P relative to the inertial frame, m^{P} the mass of particle P and $\bar{f}^{P}$ the external resultant force applied on the particle. For such a system, Jourdain's

principle of virtual power states

$$\sum_P (\bar{f}^P - m^P \ddot{\bar{r}}^P) \cdot \delta \dot{\bar{r}}^P = 0, \tag{2.2.1}$$

where the virtual velocity $\delta \dot{\bar{r}}^P$ must be compatible with the system constraints.

A rigid body (see Fig.2.1.) can be considered as a system consisting of a large number of particles which are connected by rigid, massless rods. Jourdain's principle reduces to an integration taken over the entire body:

$$\int_m \delta \dot{\bar{r}}^P \cdot \bar{f}^P \, dm(P) - \int_m \delta \dot{\bar{r}}^P \cdot \ddot{\bar{r}}^P \, dm(P) = 0, \tag{2.2.2}$$

where $\bar{f}^P$ is now the external force per unit mass at point P. The virtual velocity at point P must be compatible with Eq.(2.1.2) and this leads to

$$\delta \dot{\bar{r}}^P = \delta \dot{\bar{r}} + \delta \bar{\omega} \times \bar{p}, \tag{2.2.3}$$

where $\delta \dot{\bar{r}}$ denotes the virtual velocity vector of the body mass centre and $\delta \bar{\omega}$ the virtual angular velocity vector of the body.

Substituting (2.1.3) and (2.2.3) into Eq.(2.2.2) and taking into account the definition of the body mass centre, we obtain

$$\delta \dot{\bar{r}} \cdot (\bar{f}_t - m \ddot{\bar{r}}) + \delta \bar{\omega} \cdot \{ \bar{f}_r - \bar{I} \cdot \dot{\bar{\omega}} - \bar{\omega} \times (\bar{I} \cdot \bar{\omega}) \} = 0, \tag{2.2.4}$$

where m is the body mass and $\bar{I}$ the inertia tensor with respect to the mass centre. The symbol $\bar{f}_t$ represents the resultant force and $\bar{f}_r$ the resultant torque about the mass centre; they are defined by

$$\bar{f}_t = \int_m \bar{f}^P \, dm(P), \qquad \bar{f}_r = \int_m \bar{p} \times \bar{f}^P \, dm(P). \tag{2.2.5}$$

As a matter of course the constraint condition that $\bar{p}$ is constant, which ensures the system to be a rigid body, is involved in Eq.(2.2.4). The subsequent consideration of the constraints in systems refers only to constraints between the bodies.

When a rigid body system lacks constraints, the system has six degrees of freedom. The components of both the virtual velocity vector and the virtual angular velocity vector, which can be taken with respect to any frame, are independent. Eq.(2.2.4) gives rise to the Newton-Euler equations

$$m\ddot{\bar{r}} = \bar{f}_t, \tag{2.2.6}$$

and

$$\bar{I}\cdot\dot{\bar{\omega}} + \bar{\omega}\times(\bar{I}\cdot\bar{\omega}) = \bar{f}_r. \tag{2.2.7}$$

For a body subject to a number of n_c (n_c<6) constraints, the number of degrees of freedom n_f is less than six and is defined by $n_f = 6 - n_c$. The equations of motion of the body may again be represented by the Newton-Euler equations (2.2.6) and (2.2.7), which include in that case also the constraint forces and torques. In addition, we have a set of n_c constraint equations.

2.3. Dynamics of Multibody Systems

For a multibody system of n rigid bodies, Jourdain's principle reads

$$\sum_i \left\{ \delta\dot{\bar{r}}_i\cdot(\bar{f}_{ti} - m_i\ddot{\bar{r}}_i) + \delta\bar{\omega}_i\cdot[\bar{f}_{ri} - \bar{I}_i\cdot\dot{\bar{\omega}}_i - \bar{\omega}_i\times(\bar{I}_i\cdot\bar{\omega}_i)] \right\} = 0, \tag{2.3.1}$$

where index i refers to a quantity of body i.

We designate the centroidal body-fixed frame of body i by $\{o^i, \bar{e}^i\}$. If the algebraic vectors of the first term in Eq.(2.3.1), which relate to translations, are taken with respect to the inertial frame and those in the second term, which relate to rotations, are taken with respect to the body-fixed frames, the algebraic representation of Jourdain's principle for a multibody system is

$$\sum_i \left\{ \delta\dot{\boldsymbol{r}}_i^T(\boldsymbol{f}_{ti} - m_i\ddot{\boldsymbol{r}}_i) + \delta\boldsymbol{\omega}_i^{*T}(\boldsymbol{f}_{ri}^* - \boldsymbol{I}_i^*\dot{\boldsymbol{\omega}}_i^* - \tilde{\boldsymbol{\omega}}_i^*\boldsymbol{I}_i^*\boldsymbol{\omega}_i^*) \right\} = 0. \tag{2.3.2}$$

We rewrite these equations in a compact form as:

$$\delta\boldsymbol{v}^T(\boldsymbol{M}\dot{\boldsymbol{v}} - \boldsymbol{g} - \boldsymbol{f}) = 0 \tag{2.3.3}$$

where

$$\boldsymbol{v} = [\dot{\boldsymbol{r}}_1^T, \dot{\boldsymbol{r}}_2^T, \ldots, \dot{\boldsymbol{r}}_n^T, \boldsymbol{\omega}_1^{*T}, \boldsymbol{\omega}_2^{*T}, \ldots, \boldsymbol{\omega}_n^{*T}]^T, \tag{2.3.4}$$

$$\boldsymbol{M} = diag[\, m_1\boldsymbol{E},\ m_2\boldsymbol{E},\ ..\ ,m_n\boldsymbol{E},\ \boldsymbol{I}_1^*,\ \boldsymbol{I}_2^*, ... ,\boldsymbol{I}_n^*\,], \tag{2.3.5}$$

$$\boldsymbol{g} = [\ \boldsymbol{0}^T,\ -(\,\tilde{\boldsymbol{\omega}}_1^*\boldsymbol{I}_1^*\,\boldsymbol{\omega}_1^*\,)^T,\ -(\,\tilde{\boldsymbol{\omega}}_2^*\boldsymbol{I}_2^*\,\boldsymbol{\omega}_2^*\,)^T, ... ,\ -(\,\tilde{\boldsymbol{\omega}}_n^*\boldsymbol{I}_n^*\,\boldsymbol{\omega}_n^*\,)^T\ ]^T, \tag{2.3.6}$$

$$\boldsymbol{f} = [\ \boldsymbol{f}_{t1}^T, \boldsymbol{f}_{t2}^T, ... , \boldsymbol{f}_{tn}^T, \boldsymbol{f}_{r1}^{*T}, \boldsymbol{f}_{r2}^{*T}, ... , \boldsymbol{f}_{rn}^{*T}\ ]^T. \tag{2.3.7}$$

The components of $\boldsymbol{v}$ represent a set of $6n$ velocities which correspond with a set of $6n$ quasi-coordinates (non-integrable coordinates, Haug 1989). $\boldsymbol{E}$ in Eq.(2.3.5) is the 3×3 unit matrix and $\boldsymbol{0}$ in Eq.(2.3.6) is a zero vector with $3n$ components.

For a multibody system without constraints, the system has $6n$ degrees of freedom and the components of the virtual velocity $\delta\boldsymbol{v}$ are independent. The equations of motion of such a system can therefore be written as

$$\boldsymbol{M}\,\dot{\boldsymbol{v}} - \boldsymbol{g} - \boldsymbol{f} = \boldsymbol{0}. \tag{2.3.8}$$

However, in most systems the bodies are connected through various kinds of joints. These joints give rise to constraints on the motion of the bodies. Therefore, the system has less than $6n$ degrees of freedom. In other words, the components of the virtual velocity $\delta\boldsymbol{v}$ in Eq.(2.3.3) are no longer independent and Eq.(2.3.8) is not valid.

We consider only systems subject to holonomic constraints, but it should be noted that the analysis can also be applied to systems with nonholonomic constraints which are linear combinations of the first time derivatives of the generalized coordinates. For a multibody system subject to n_c independent holonomic constraints, the number of the degrees of freedom designated as n_f is equal to $6n$ - n_c.

The differential form of the holonomic constraints, which represents the velocity constraint conditions in the system, can be expressed in terms of the quasi-velocities:

$$\boldsymbol{D}\,\boldsymbol{v} + \boldsymbol{c} = \boldsymbol{0}, \tag{2.3.9}$$

where $\boldsymbol{c} \in \mathbb{R}^{n_c}$ and the rank of the n_c×$6n$ matrix $\boldsymbol{D}$ is equal to the number of the constraints, *i.e.*, n_c. The components of $\boldsymbol{D}$ and $\boldsymbol{c}$ are only functions of time and the generalized coordinates. On the other hand, we know that the quasi-velocity vector $\boldsymbol{v}$ is a linear combination of the generalized velocities. Due to the constraints (2.3.9), only n_f of the $6n$ generalized velocities are independent. Form Eq.(2.3.9), we can find the relationship between the quasi-velocities and the independent generalized

velocities. Denoting q, $q \in \mathbb{R}^{n_f}$, as the vector of the independent generalized coordinates, we have for the quasi-velocities:

$$v = A\,\dot{q} + b\,. \tag{2.3.10}$$

Obviously, the components of the matrix A and the vector b are only functions of time and the generalized coordinates; the rank of the matrix A is equal to the number of the degrees of freedom n_f. It can be proved that the matrix A is orthogonal to the matrix D; *i.e.*

$$DA = 0\,. \tag{2.3.11}$$

Differentiating both sides of Eq.(2.3.10) with respect to time we obtain the accelerations:

$$\dot{v} = A\,\ddot{q} + \dot{A}\dot{q} + \dot{b}. \tag{2.3.12}$$

The virtual vector δv in Eq.(2.3.3) must be compatible with the constraints given by Eq.(2.3.9). Therefore, the relation between δv and $\delta \dot{q}$ is given by the equation

$$\delta v = A\,\delta \dot{q}\,, \tag{2.3.13}$$

where the components of the vector $\delta \dot{q}$ are independent.

Having substituted (2.3.12) and (2.3.13) into Eq.(2.3.3) we obtain the equations of motion:

$$A^T M A\,\ddot{q} - A^T f_g - A^T f = 0\,, \tag{2.3.14}$$

with

$$f_g = g - M(\dot{A}\dot{q} + \dot{b}). \tag{2.3.15}$$

Obviously, Eq.(2.3.14) is a set of n_f second order differential equations in terms of the independent generalized coordinates.

The constraint forces and torques, which are responsible for maintaining the constraints associated with the system, are often of interest and have to be determined in the dynamic analysis, for instance, in a system with a friction joint. When all constraints are disengaged so that every body of the system may have a free motion and the components of δv are completely arbitrary, Eq.(2.3.3) has to be modified to

$$\boldsymbol{M}\dot{\boldsymbol{v}} - \boldsymbol{g} - \boldsymbol{f} - \boldsymbol{D}^T\boldsymbol{\lambda} = \boldsymbol{0}, \tag{2.3.16}$$

where $\boldsymbol{\lambda}$ represents a vector of n_c Lagrangian multipliers, which can be interpreted as the vector of the generalized constraint forces dual to the virtual velocity vector $\boldsymbol{D}\delta\boldsymbol{v}$ (Meijers, 1992). The term $\boldsymbol{D}^T\boldsymbol{\lambda}$ is the effect of the constraint forces and torques on the system.

Premultiplying Eq.(2.3.16) by the product $\boldsymbol{D}\boldsymbol{M}^{-1}$ and using Eqs.(2.3.11) and (2.3.12), we obtain the equations for the generalized constraint forces:

$$\boldsymbol{\lambda} = -(\boldsymbol{D}\boldsymbol{M}^{-1}\boldsymbol{D}^T)^{-1}\boldsymbol{D}\boldsymbol{M}^{-1}(\boldsymbol{f}_g + \boldsymbol{f}). \tag{2.3.17}$$

In the last equation the generalized accelerations have been eliminated; therefore, the generalized constraint forces depend only on the state of the system. The procedure of adding the constraint conditions by Lagrangian multipliers and the method of determining the multipliers indicated above can be found in Lanczos (1952), Schiehlen (1985) and Haug (1989). Other methods were shown by Besseling et al. (1985) and Roberson and Schwertassek (1988).

When we investigate the stationary motion of the system, in which the independent generalized velocities and the independent generalized accelerations vanish, the set of differential equations (2.3.14) changes to the n_f nonlinear equations

$$\boldsymbol{A}^T\boldsymbol{f}_g + \boldsymbol{A}^T\boldsymbol{f} = \boldsymbol{0}, \tag{2.3.18}$$

where the generalized coordinates are considered to be unknown variables. If the system is in a static equilibrium state, the quantity $\boldsymbol{f}_g$ in Eq.(2.3.18) vanishes. Eq.(2.3.17) for the constraint forces is valid in both above-mentioned states.

Chapter 3

Geometric Contact between Track and Wheelset

3.1. Introduction

Railway vehicle dynamics is significantly affected by the interaction between steel rails and steel wheels. The interaction generates the necessary conditions for a railway vehicle running stably on the track but also gives rise to damage of the rails and the wheels because of the high contact stresses. The motion stability of a railway vehicle concerns the critical operating speed, the lateral dynamic behaviour, adequate guidance and the ability of negotiating a curved track. The damage of the rails and the wheels involves wear of rails and wheels, corrugation, fatigue etc. An optimized railway system is one satisfying high stability requirements and a low damage rate of the rails and the wheels; these two aspects should strongly be integrated in the design of a bogie device or a complete railway vehicle.

Contact mechanics do therefore play an important role in the investigations of railway dynamics. An early important contribution to this subject was due to Carter (1926), who was the first to propose the concept of "creepage". Later on, De Pater (1962) predicted the friction forces based on the so-called linear theory. Meanwhile, Vermeulen and Johnson (1964) contributed in the direct generalization of Carter's theory to three dimensions and established an approximate creep-force law. Since the middle of the 1960's, Kalker's theories on rolling contact mechanics have been the most widely used theories both in the simulation of railway vehicle dynamics and in the damage analysis of the profiles of rails and wheels. For the use in practical applications, Shen, Hedrick and Elkins (1983) proposed an alternative creep-force law based on Kalker's creep coefficients and Johnson-Vermeulen's method. Another creep-force law also based on Kalker's creep coefficients was established by Jaschinski (1990). Moreover, a dynamic creep-force law has been developed by Knothe and Gross-Thebing (1986).

In Kalker's theories of rolling contact mechanics, it is supposed that the contact area is very small as compared with the dimensions of the contacting bodies (rail and wheel), so that we can consider each contact body as a half space. Also, it is assumed that in the contact area no plastic deformation occurs and Hooke's law remains valid. Therefore, the rolling contact problem can be reduced to the

minimization of a function subject to the geometric condition that the contacting bodies can not penetrate each other. Meanwhile the traction force, i.e., the friction force, is determined based on Coulomb's law (Kalker, 1990).

As is well known, in practical simulation of railway vehicle dynamics it is sufficiently accurate to consider the normal problem as a Hertz problem(Love, 1926) and to solve the tangent problem by means of Kalker's simplified theory(Kalker, 1982). In Hertz's problem, each surface of the contacting bodies around the contact point is approximated by a surface of second order. As a result, the boundary of the contact area between the rails and the wheels is an ellipse and the pressure distribution over the contact area is semi-ellipsoidal. It is to be noted that in the simplified theory, other appropriate form of pressure distribution was used (Kalker, 1982).

Both for the application of the simplified theory of rolling contact mechanics and for the dynamic analyses, the location of the contact patch has to be determined. Because the patch is very small with respect to the dimensions of the track-wheelset system such as the diameter of the wheel and the track gauge, the location of the contact patch is commonly represented by the location of a contact point which is calculated by postulating the bodies to be rigid. In this contact problem, the ratio of the two semi-axes of the contact ellipse depends only on the principal radii of curvature at the contact point. In the dynamic analyses, the resultant friction force, the resultant normal contact force and the spin moment are applied at the contact point; the tangent forces are situated in the contact plane and the normal force and the spin moment are perpendicular to that plane. The determination of the positions of the contact points and the associated geometric parameters gives rise to a purely geometric problem when the wheelset and track are assumed to be rigid.

The fact that a wheelset with two profiled wheels is placed upon a track with two profiled rails makes the geometric constraints between track and wheelset very complicated. An early analysis about a conical wheelset which is purely rolling on knife edge rails, was studied by Klingel (1883). In reality, wheels and rails in service soon wear to profiles that have radii of curvature varying across the width of the wheel and rail. Moreover, in modern designs of railway vehicles, the new wheel profiles also have non-conical forms. Wickens (1965) improved the accuracy of Klingel's analysis for the case where the rail and wheel profiles are assumed to be circular arcs. But the variations in radii of curvature may be quite considerable; as a result, the solution for circular arc profiles is normally only valid for small lateral wheelset displacements. Therefore it is necessary to use numerical analysis techniques to determine the geometric contact for a track-wheelset system with arbitrary rail and wheel profiles. These profiles may be derived from either design drawings or profile measurements.

In the early numerical methods, the geometric contact between track and wheelset is considered to be two-dimensional (Cooperrider and Law, 1976), so that the effect of the wheelset yaw angle is ignored. More accurate theories for determining the geometric contact in three dimensions have been developed by De Pater (1979, 1988), Duffek (1982) and Fisette and Samin (1991). De Pater (1988) has also simplified the exact theory by means of his first-order theory; this reduces the three-dimensional contact problem to the solution of a set of four nonlinear equations. Comparing the results obtained from both the exact equations, which are a set of eight nonlinear algebraic equations, and the first-order equations, we find that the difference is so small that the first-order theory can be considered to yield sufficiently accurate results (Yang and De Pater, 1991). Thus, the first-order theory has been employed to determine the geometric contact during the dynamic simulations.

When a body contacts with another body in space, the following three conditions must be satisfied:

(1) There is a point in one body that has the same location in space as a point in the other body.

(2) The normal on the surface of one body at the contact point is parallel to that of the other body.

(3) Not any part of one of the bodies penetrates the other body.

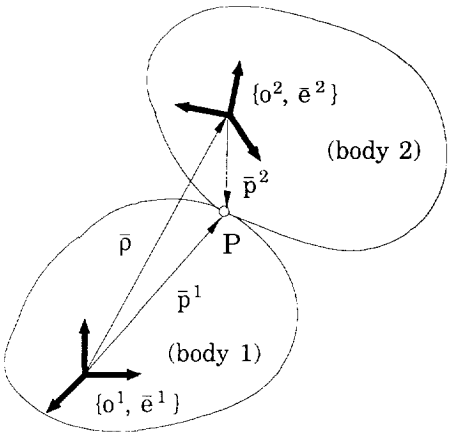

Fig.3.1.1. Two bodies in contact.

In case the contacting bodies are assumed to be rigid, the geometry of a body remains the same with respect to the body-fixed frame. We assume that body 1 is in contact with body 2 at point P (see Fig.3.1.1), so that the first condition can be expressed by

$$\bar{p}^{\,1} = \bar{\rho} + \bar{p}^{\,2}, \tag{3.1.1}$$

where $\bar{p}^1$ and $\bar{p}^2$ are the position vectors of the contact point relative to the frames $\{o^1, \bar{e}^{\,1}\}$ and $\{o^2, \bar{e}^{\,2}\}$ respectively, and $\bar{\rho}$ is the position vector of the origin o^2 relative to the other origin o^1.

The second condition leads to

$$\bar{n}^{\,1}(P) = \bar{n}^{\,2}(P). \tag{3.1.2}$$

The vectors $\overline{n}^1$ and $\overline{n}^2$ represent the unit normal vectors of the two surfaces. Moreover, one vector, for instance $\overline{n}^1$, is the outer normal of body 1 and the other, $\overline{n}^2$ is the inner normal of body 2. The second condition only confirms that there is no penetration in the neighbourhood of the contact point P and does not globally ensure the third contact condition. Therefore the first two conditions are necessary conditions for two bodies in contact but they are not sufficient.

Eqs.(3.1.1) and (3.1.2) together with the two surface functions of the contacting bodies represent a set of nonlinear algebraic equations, but only two of the three equations generated by the second contact condition are independent because the vectors $\overline{n}^1$ and $\overline{n}^2$ are normalized.

In railway vehicle systems, there may be at one side more than one contact point between a track and a wheelset even if the track and wheelset are assumed to be rigid bodies. We first establish the exact theory for the common case in which there is only one contact point at each side of the track-wheelset system. Subsequently, a similar treatment for the geometric contact problem in roller rig systems is presented in Section 3.3. Afterwards, in Section 3.4 three approximate methods for modifying and solving the exact equations obtained in Section 3.2 are discussed in detail. Moreover, a method to determine a double contact point is proposed. In the last section of this chapter, numerical results are shown for several track-wheelset systems. In order to verify the accuracy of the approximate methods, we solve both the exact and the approximate equations. The effects of parameters such as the track gauge and the rail inclination are investigated by means of the first-order equations. The numerical results show that for certain combinations of profiles at a certain position the rail and the wheel have two contact points at one side and only one contact point at the other side.

3.2. Geometric Contact between Track and Wheelset

3.2.1. Coordinate Systems

A track with two rails is considered to be fixed upon a rigid base. When a wheelset, which is composed of two wheels connected through a shaft, is placed upon the track, the forces between a rigid wheel and a rigid rail at the contact point do not alter the pure geometric properties of the system such as the contours of the rail and the wheel. Hence, the geometric contact between the track and the wheelset depends only on their geometric configurations. In reality, corresponding to a position where the wheelset contacts the track, only the region of the track around the location of

the wheelset centre needs to be taken into account. Therefore, at each instant, we can restrict ourselves to a small segment of the track around the contact points in the investigation of the geometric contact constraints. We may certainly assume the track in the small segment to be cylindrical, so that the profiles of the cross-sections of the rails remain the same along the track.

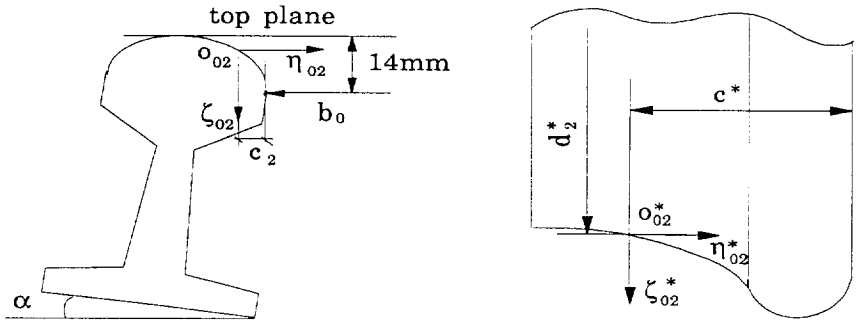

(a) Rail contour. (b) Wheel contour.

Fig.3.2.1. Rail and wheel local coordinate systems.

First of all the profile functions of the rails and wheels have to be ascertained with respect to some coordinate systems. These coordinate systems are taken from measurements for "worn" profiles and from the design drawings in the case of "new" profiles. It is shown in Fig.3.2.1 that the coordinates of a profile are originally given with respect to the coordinate system (o_{0j}, η_{0j}, ζ_{0j}) for the rails and with respect to (o_{0j}*, η_{0j}*, ζ_{0j}*) for the wheels. These coordinate systems are designated as the local coordinate systems.

Here the index j (j=1,2) signifies the side of the track-wheelset system in such a way that j=1 for the right-hand side and j=2 for the left-hand side. In addition, a symbol with a superscript asterisk (*) indicates that the quantity refers to the wheelset; one without the asterisk refers to the track.

For a wheel, for instance the left-hand wheel shown in Fig.3.2.1, the local coordinate system is defined as follows: the origin is a point on the profile and the distance from the origin to the inside surface of the wheel is equal to the constant c*, which is in general equal to 70mm in the European railway system; the axis o_{0j}*η_{0j}* is perpendicular to the inside surface. The wheel diameter at the origin o_{0j}* is denoted by d_j*. When the wheelset is supposed to be symmetric, the diameters d_j* of both wheels are the same; in general they will not be equal. The mean value of the rolling radii at both origins of the wheels is considered as the nominal rolling

radius r_0.

We assume that the top line of both cross-sections of the rails is parallel to the support base (e.g. the sleeper plane) in the nominal track system where the imperfections of the rail profiles are zero. The track gauge denoted by $2b_0$ is measured 14mm below the top of the rails. The location of the origin of the rail local coordinate system is taken at the rail tread centre for a new profile; otherwise, it is somewhat arbitrary and often related to measurements. The axis $o_{0j}\eta_{0j}$ is parallel to the top line and in our applications we stipulate that the axes $o_{01}\eta_{01}$ and $o_{02}\eta_{02}$ are collinear.

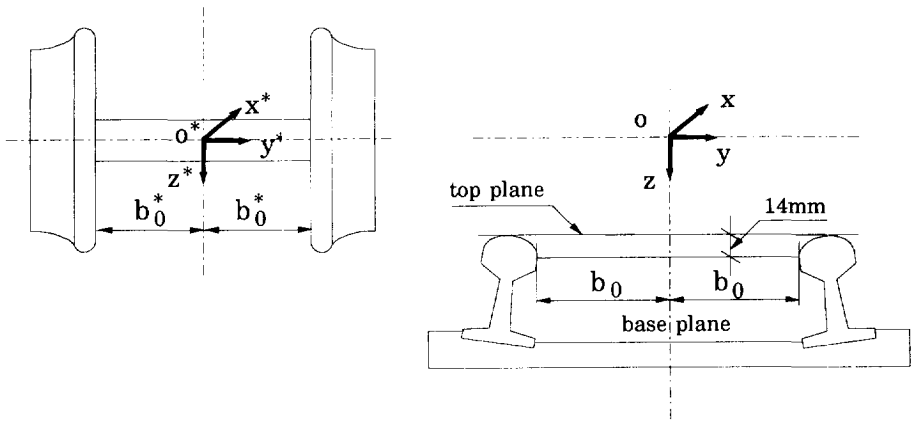

Fig. 3.2.2. Track and wheelset.

Both the track reference frame (o, x, y, z) and the wheelset body frame (o^*, x^*, y^*, z^*) are shown in Fig.3.2.2; they are designated by $\{o^1, \bar{e}^1\}$ and $\{o^2, \bar{e}^2\}$ respectively. The origin of the wheelset body frame is located at the mass centre of the body and the spin (pitch) axis o^*y^* of the frame coincides with the axis of revolution of the body. The rolling axis o^*x^* is perpendicular to the spin axis o^*y^* and is the forward axis of the wheelset. The remaining axis of the wheelset body frame is the yaw axis, which points downwards. The wheelset body frame moves with the wheelset with the exception of the rotation of the wheelset about its axis of revolution. In other words, the wheelset body frame is not really rigidly embedded in the wheelset body. However, due to the axisymmetry of the wheelset, the three axes of the frame remain constantly principal inertia axes of the wheelset body.

The origin of the track reference frame is located at a distance r_0 above the local coordinate systems of the rails; the x-axis of the track reference frame is parallel to the track direction; the z-axis is perpendicular to the top plane of the rails

and passes the track gauge centre; the y-axis is determined by virtue of the right-hand rule. These definitions imply that the x-y plane of the track reference frame is certainly parallel to the top plane of the rails.

The absolute motion of the wheelset can be determined by its motion relative to the track reference frame and the motion of the track reference frame relative to the inertial frame. The latter motion is described as the nominal motion of the railway vehicle. It will be convenient to study the geometric contact constraints in the track reference frame.

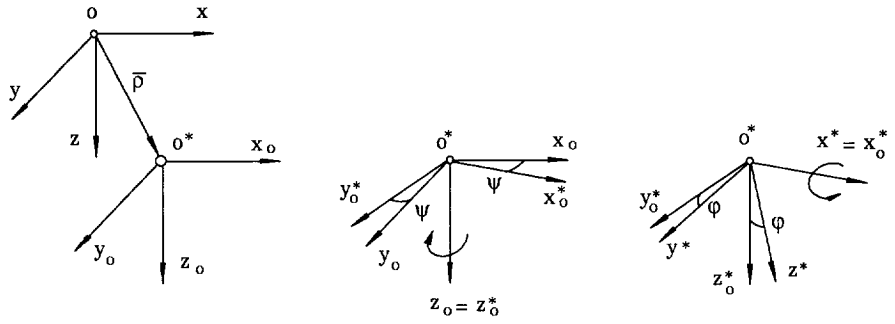

Fig.3.2.3. Relation between track reference frame and wheelset body frame.

We designate the position where the track reference frame and the wheelset body frame coincide as the geometric central position of the track-wheelset system. In this position all the generalized coordinates describing the motion of wheelset relative to the track reference frame vanish. This position needs not to be a physical contact position for the track-wheelset system because it may be quite well possible that a wheel penetrates a rail or that the wheelset does not touch the track anywhere. In general, the relation between the track reference frame and the wheelset frame is shown in Fig.3.2.3. The translation of the wheelset body frame relative to the track reference frame is designated by the vector

$$\bar{\rho} = \boldsymbol{\rho}^T \bar{e}^1 \tag{3.2.1}$$

where the components are

$$\boldsymbol{\rho} = [\, u,\ v,\ w \,]^T . \tag{3.2.2}$$

The quantities u, v and w represent the generalized coordinates and are the longitudinal, lateral and vertical translations of the wheelset mass centre relative to the track reference frame $\{o, \bar{e}^1\}$ respectively.

The rotation of the wheelset body frame relative to the track frame is usually described by the yaw rotation ψ about the axis o^*z_o, followed by the rolling rotation ϕ about the axis o^*x^* (see Fig.3.2.3) and then followed by the spin rotation θ about the axis o^*y^*. But by means of the above definition of the wheelset body frame, the spin rotation does not change the positions of the axes o^*z^* and o^*x^* relative to the track frame. Therefore, according to the theory given in Appendix B, the rotation matrix $\boldsymbol{G}^{21}$ from the track reference frame to the wheelset body frame, which is only related to the first and the second rotations, is determined by

$$\boldsymbol{G}^{21} = \boldsymbol{A}^1(\phi)\boldsymbol{A}^3(\psi), \tag{3.2.3}$$

where the matrices $\boldsymbol{A}^1$ and $\boldsymbol{A}^3$ are given by Eq.(B.2); its full expression is

$$\boldsymbol{G}^{21} = \begin{bmatrix} \cos\psi & \sin\psi & 0 \\ -\cos\phi\sin\psi & \cos\phi\cos\psi & \sin\phi \\ \sin\phi\sin\psi & -\sin\phi\cos\psi & \cos\phi \end{bmatrix} \tag{3.2.4}$$

The matrix $\boldsymbol{G}^{21}$ is an orthogonal transformation matrix, hence,

$$\boldsymbol{G}^{12} = [\boldsymbol{G}^{21}]^T = [\boldsymbol{G}^{21}]^{-1}, \tag{3.2.5a}$$

where $\boldsymbol{G}^{12}$ is the rotation matrix from the wheelset body frame to the track reference frame, which is equal to

$$\boldsymbol{G}^{12} = \begin{bmatrix} \cos\psi & -\cos\phi\sin\psi & \sin\phi\sin\psi \\ \sin\psi & \cos\phi\cos\psi & -\sin\phi\cos\psi \\ 0 & \sin\phi & \cos\phi \end{bmatrix} \tag{3.2.5b}$$

3.2.2. Theoretical Analysis

As has already been stated in the previous section, the wheels always contact their corresponding rails during the motion of the wheelset through the track and the bodies are assumed to be rigid. This implies that there is at least one contact point at each side of the track-wheelset system. At every contact point, the first and second contact conditions given in the previous section must be satisfied. The third condition guarantees a unique set of contact positions in which the track and wheelset are in contact but do not penetrate each other. In general, at each side of the track-wheelset system the wheel is in contact with the rail at a single point.

The motion of the single wheelset relative to the track reference frame is described by six generalized coordinates, which are the longitudinal, lateral and vertical displacements u, v and w of the wheelset body mass centre and the rolling, spin (pitch) and yaw angles ϕ, θ and ψ of the body. Due to the geometric contact constraints, only four of them are independent. The wheelset is an axisymmetric body and later on it will be shown that the spin rotation about the revolution axis of the wheelset and the longitudinal translation of the wheelset centre relative to the track reference frame do not affect the location of the contact point on the wheel surface with respect to the wheelset body frame. On the other hand, the spin rotation of the wheelset does not influence the location of the contact point in the rail surface; the longitudinal displacement only changes the longitudinal coordinate of the contact point with respect to the track reference frame, because the related small track segment is supposed to be cylindrical. As a result, the longitudinal displacement u and the spin rotation of the wheelset θ do not influence the geometric contact constraints. These two generalized coordinates should certainly be chosen as independent ones and of the remaining four generalized coordinates, which are the lateral and the vertical displacements and the rolling and the yaw angles, only two are independent because of the geometric contact constraints.

Most researchers in railway dynamics have chosen the translation v and the yaw rotation ψ as the independent generalized coordinates because the amplitudes of ϕ and w are very small as compared with the amplitudes of ψ and v respectively. However, it is shown by De Pater (1988) and Yang (1991) that choosing the rolling and yaw rotations ϕ and ψ as the independent generalized coordinates is preferable in the theoretical analysis.

In determining the contact position between track and wheelset, we have assumed that the track is tangent in a small segment around the wheelset. As a result, the x-coordinate disappears in the equation of the rail surface with respect to the track reference system (o, x, y, z) and the equation can be written as:

$$z - f_j(y) = 0, \tag{3.2.6}$$

where $f_j(y)$ is the profile function of the rail cross-section (it should be noted that De Pater (1988) defined the profile functions in a different way but his results agree with ours). For the wheelset, which is an axisymmetric body, its wheel surface is generated by rotating the curve $z^*=f_j^*(y^*)$ in the y*z* plane about the axis o^*y^*. Consequently, the equation of a wheel surface can be designated by

$$\sqrt{x^{*2} + z^{*2}} - f_j^*(y^*) = 0, \tag{3.2.7}$$

where $f_j^*(y^*)$ is the profile function of the wheel cross-section.

Meanwhile we can determine the unit normal vectors of the surfaces by calculating the partial derivatives of the surface equations. We stipulate that the unit normal vectors of the rail and the wheel surfaces are positive when the vectors point in the direction of the inner normal of the rail. Therefore, the expression for the unit normal vector of the rail at a point (x, y, z) reads

$$\bar{n}_j = \boldsymbol{n}_j^T \bar{\boldsymbol{e}}^1 , \tag{3.2.8}$$

with

$$\boldsymbol{n}_j = \frac{1}{\sqrt{1 + f_j'^2(y)}} [\, 0, \; -f_j'(y), \; 1 \,]^T . \tag{3.2.9}$$

The unit normal vector of the wheel surface at a point (x^*, y^*, z^*) is

$$\bar{n}_j^* = \boldsymbol{n}_j^{*T} \bar{\boldsymbol{e}}^2 , \tag{3.2.10}$$

with

$$\boldsymbol{n}_j^* = \frac{1}{\sqrt{1+f_j^{*\prime 2}(y^*)}} \left[\frac{x^*}{\sqrt{x^{*2} + z^{*2}}}, \; -f_j^{*\prime}(y^*), \; \frac{z^*}{\sqrt{x^{*2} + z^{*2}}} \right]^T . \tag{3.2.11}$$

The prime ($'$) indicates the derivative of the function with respect to its own argument.

We introduce the following notations:

$$r^* = \sqrt{x^{*2} + z^{*2}} , \tag{3.2.12}$$

$$\mathrm{tg}\gamma_j = \mp f_j'(y) , \tag{3.2.13}$$

$$\mathrm{tg}\gamma_j^* = \mp f_j^{*\prime}(y^*) , \tag{3.2.14}$$

where the upper sign in $\pm$ and $\mp$ refers to the right-hand side j=1 and the lower sign to the left-hand side j=2. Correspondingly, we have

$$\cos\gamma_j = \frac{1}{\sqrt{1 + f_j'^2(y)}} , \qquad \sin\gamma_j = \frac{\mp f_j'(y)}{\sqrt{1 + f_j'^2(y)}} ; \tag{3.2.15}$$

$$\cos\gamma_j^* = \frac{1}{\sqrt{1 + f_j^{*\prime 2}(y^*)}}, \qquad \sin\gamma_j^* = \frac{\mp f_j^{*\prime}(y^*)}{\sqrt{1 + f_j^{*\prime 2}(y^*)}}. \tag{3.2.16}$$

Using these notations we can rewrite Eqs.(3.2.9) and (3.2.11) as:

$$\boldsymbol{n}_j = \left[0, \ \pm\sin\gamma_j, \ \cos\gamma_j\right]^T \tag{3.2.17}$$

and

$$\boldsymbol{n}_j^* = \left[\frac{x^*}{r^*}\cos\gamma_j^*, \ \pm\sin\gamma_j^*, \ \frac{z^*}{r^*}\cos\gamma_j^*\right]^T. \tag{3.2.18}$$

Here the quantity r^* is the rolling radius of the wheel at point (x^*, y^*, z^*); the angle γ_j is the conicity of the rail and $\mp\gamma_j$ is the angle that the tangent of the rail cross-section $f_j(y)$ at the point y makes with the axis oy. In a similar way, the angle $\mp\gamma_j^*$ is the angle that the tangent of the wheel cross-section $f_j^*(y^*)$ at the position y^* makes with the axis o^*y^*. All these angles are called contact angles.

When the wheel is in contact with the rail at a point P_j (see Fig.3.2.4), the coordinates of the contact point on the rail surface are assumed to be (x_j, y_j, z_j) with respect to the track reference frame (o, x, y, z); correspondingly, the coordinates of the contact point on the wheel surface are (x_j^*, y_j^*, z_j^*) with respect to the wheelset body frame (o^*, x^*, y^*, z^*). Because every point on a surface must satisfy the equation of that surface, according to Eq.(3.2.6) and (3.2.7), the following relations hold:

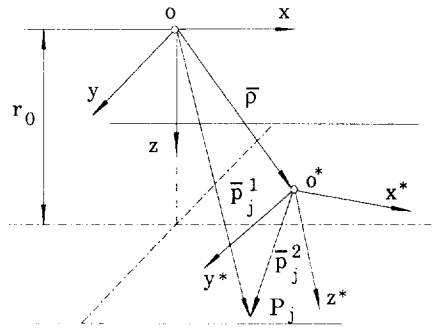

Fig. 3.2.4. Relation between track and wheelset

for the rails: $z_j - f_j(y_j) = 0$ (3.2.19)

and

for the wheels: $\sqrt{x_j^{*2} + z_j^{*2}} - f_j^*(y_j^*) = 0.$ (3.2.20)

We designate the position vector of the contact point relative to the track reference frame $\{o^1, \bar{e}^1\}$ as

$$\bar{p}_j^{\,1} = \boldsymbol{p}_j^T \bar{e}^1 \tag{3.2.21}$$

with

$$\boldsymbol{p}_j = [x_j, y_j, z_j]^T \tag{3.2.22}$$

and that relative to the wheelset body frame $\{o^2, \bar{e}^2\}$ as

$$\bar{p}_j^{\,2} = \boldsymbol{p}_j^{*T} \bar{e}^2 \tag{3.2.23}$$

with

$$\boldsymbol{p}_j^* = [x_j^*, y_j^*, z_j^*]^T . \tag{3.2.24}$$

Here it is to be noted that the algebraic vectors $\boldsymbol{p}$ and $\boldsymbol{p}^*$ do not correspond to the same geometric vector; they indicate only the same contact point P_j.

The first contact condition requires that the positions of the contact points of the bodies should be identical in space, this gives rise to the equation (see Fig.3.2.4)

$$\bar{p}_j^{\,1} = \bar{\rho} + \bar{p}_j^{\,2}, \tag{3.2.25}$$

where the position vector of the wheelset mass centre $\bar{\rho}$ is given by Eq.(3.2.1).

With respect to the track reference frame $\{o^1, \bar{e}^1\}$, we may reduce the last equation from the geometric vector form to the algebraic vector form. Using the rotation matrix $\boldsymbol{G}^{12}$ given by Eq.(3.2.5), we obtain

$$\boldsymbol{p}_j = \boldsymbol{\rho} + \boldsymbol{G}^{12} \boldsymbol{p}_j^* . \tag{3.2.26}$$

By considering the case of the track and the wheelset in contact at both sides, (3.2.26) generates the set of six equations

$$x_j = u + x_j^* \cos\psi - y_j^* \cos\phi \sin\psi + z_j^* \sin\phi \sin\psi , \tag{3.2.27}$$

$$y_j = v + x_j^* \sin\psi + y_j^* \cos\phi \cos\psi - z_j^* \sin\phi \cos\psi , \tag{3.2.28}$$

$$z_j = w + y_j^* \sin\phi + z_j^* \cos\phi . \tag{3.2.29}$$

The second contact condition demands that at the contact point the unit normal vector of the rail surface coincides with the one of the corresponding wheel surface, viz.

$$\bar{n}_j = \bar{n}_j^* \,. \tag{3.2.30}$$

Thus, the algebraic representation of Eq.(3.2.30) with respect to the wheelset body frame $\{o^2, \bar{e}^2\}$ is:

$$\boldsymbol{n}_j^* = \boldsymbol{G}^{21}\,\boldsymbol{n}_j \,. \tag{3.2.31}$$

In detail, the last equation may be written as

$$\begin{bmatrix} \dfrac{x_j^*}{r_j^*}\cos\gamma_j^* \\ \pm\sin\gamma_j^* \\ \dfrac{z_j^*}{r_j^*}\cos\gamma_j^* \end{bmatrix} = \begin{bmatrix} \cos\psi & \sin\psi & 0 \\ -\cos\phi\sin\psi & \cos\phi\cos\psi & \sin\phi \\ \sin\phi\sin\psi & -\sin\phi\cos\psi & \cos\phi \end{bmatrix} \begin{bmatrix} 0 \\ \pm\sin\gamma_j \\ \cos\gamma_j \end{bmatrix}. \tag{3.2.32}$$

For each of the sides of the track-wheelset system, only two of the three equations in (3.2.32) are independent because the normal vectors are unit vectors. The first two equations are chosen to be the independent ones.

When we consider the contact angles and the rolling radii of the wheels to be explicit functions of the coordinates of the contact points, the geometric problem that has to be solved, contains the following 17 variables:

- six coordinates of the contact points with respect to the track reference frame, i.e. x_j , y_j and z_j;
- six coordinates of the contact points with respect to the wheelset body frame, i.e. x_j^*, y_j^* and z_j^*;
- five generalized coordinates of the wheelset with respect to the track reference frame, i.e. u, v, w, ϕ, ψ.

On the other hand, we have a set of 14 nonlinear algebraic equations for these 17 variables:

- four surface equations (3.2.19) and (3.2.20);
- six equations (3.2.27)-(3.2.29) from the first contact condition;

- four equations in (3.2.32) from the second contact condition.

The number of variables exceeds the number of independent equations; therefore, three of the 17 variables have to be considered as free parameters and the remaining ones will be determined in terms of these three parameters. In principle, the independent parameters can be chosen arbitrarily from all the variables, but normally they are taken from the five generalized coordinates. The selected three generalized coordinates together with the spin rotation of the wheelset will be chosen as the independent generalized coordinates in the dynamic analysis.

We may reduce the equations for the geometric problem even further. First we eliminate the lateral displacement v and the vertical displacement w from Eq.(3.2.28) and Eq.(3.2.29) respectively. Subsequently, the coordinate z_j is considered as an explicit function of the coordinate y_j. Including only the first two equations in (3.2.32) together with the equations of the wheel surfaces, we obtain the following set of 12 nonlinear equations

$$(y_1-y_2)-[(x_1^*-x_2^*)\sin\psi+(y_1^*-y_2^*)\cos\psi\cos\phi-(z_1^*-z_2^*)\cos\psi\sin\phi] = 0, \quad (3.2.33)$$

$$[f_1(y_1)-f_2(y_2)]-[(y_1^*-y_2^*)\sin\phi+(z_1^*-z_2^*)\cos\phi] = 0, \quad (3.2.34)$$

$$\sqrt{x_j^{*2}+z_j^{*2}}-f_j^*(y_j^*) = 0, \quad (3.2.35)$$

$$\frac{x_j^*}{r_j^*}\cos\gamma_j^* \mp \sin\gamma_j\sin\psi = 0, \quad (3.2.36)$$

$$\sin\gamma_j^* \mp \cos\gamma_j\sin\phi - \sin\gamma_j\cos\psi\cos\phi = 0, \quad (3.2.37)$$

$$v-\frac{1}{2}\left\{(y_1+y_2)-[(x_1^*+x_2^*)\sin\psi+(y_1^*+y_2^*)\cos\phi\cos\psi-(z_1^*+z_2^*)\sin\phi\cos\psi]\right\}=0, \quad (3.2.38)$$

$$w-\frac{1}{2}\left\{[f_1(y_1)+f_2(y_2)]-[(y_1^*+y_2^*)\sin\phi+(z_1^*+z_2^*)\cos\phi]\right\} = 0, \quad (3.2.39)$$

$$x_j-\left\{u+x_j^*\cos\psi-y_j^*\sin\psi\cos\phi+z_j^*\sin\phi\sin\psi\right\} = 0. \quad (3.2.40)$$

The longitudinal displacement u is certainly chosen as one of the three independent generalized coordinates. Comparing Eq.(3.2.40) with the set of

Eqs.(3.2.33)-(3.2.39) we realise that the longitudinal displacement affects only the coordinates x_j. In other words, if the rails in the small track segment have cylindrical surfaces, the quantities x_j do not influence the geometric constraints and as we will see later it will neither influence the dynamic analysis; the longitudinal displacement needs only to be considered in the dynamic analysis. Consequently, the geometric constraints are independent of the longitudinal displacement and of the rotation of the wheelset about its axis of revolution.

When the rolling and yaw angles are treated as the other two independent generalized coordinates, the eight variables y_j , x_j^*, y_j^* and z_j^* can be solved in terms of these two generalized coordinates from the set of eight nonlinear algebraic equations (3.2.33)-(3.2.37). From the solutions for certain values of ϕ and ψ we can determine the two variables v and w by means of (3.2.38) and (3.2.39). On the other hand, if the lateral displacement and the yaw angle are chosen as two independent generalized coordinates, the eight unknowns together with the rolling angle have to be solved by the set of equations (3.2.33)-(3.2.37) combined with Eq.(3.2.38). The vertical displacement w is usually selected as a dependent generalized coordinate and it can be calculated by the relation (3.2.39) after the coordinates of the contact point have been identified.

In principle, we could have retained all the three equations in (3.2.32) and have replaced the wheel surface equation (3.2.35) by the third equation of (3.2.32). But this has the disadvantage that the condition of the Jacobian matrix of the new set of nonlinear algebraic equations required in the Newton-Raphson procedure is worse than that of the actual set for small values of the yaw angle. Especially, when the yaw angle is equal to zero, the coordinate x_j^* vanishes and the rolling radius r_j^* is identical with the coordinate z_j^*. In that case, the third equation of (3.2.32) reduces to

$$\cos\gamma_j^* = \mp \sin\gamma_j \sin\phi + \cos\gamma_j \cos\phi \, . \tag{3.2.41}$$

Comparing the last equation with Eq.(3.2.37) for the case of zero yaw angle, we discover that the two equations are dependent and the new set of equations fails to solve the geometric problem, because the Jacobian matrix will become singular.

In general, the original profiles of the cross-sections of the rails and the wheels are measured in the local coordinate systems (see Fig.3.2.1). The profile functions of these sections are denoted by

$$\zeta_{oj} = f_{oj}(\eta_{oj}) \tag{3.2.42}$$

and

$$\zeta_{oj}^{*} = f_{oj}^{*}(\eta_{oj}^{*}). \tag{3.2.43}$$

Certainly, we can not apply these functions to solve Eqs.(3.2.33)-(3.2.40) directly and we have to transform the coordinates which are taken with respect to the local coordinate systems to those taken with respect to the track reference frame for the rails or to the wheelset body frame for the wheels. As shown in Fig.3.2.1(b) and Fig.3.2.2, with respect to the wheelset body system the location of the origin of a local coordinate system of a wheel is determined by the diameter of the wheel at the origin and the distance from the origin to the inside surface of the wheel. Thereby, this yields:

$$y_j^{*} = \pm [(b_{0j}^{*} + c^{*}) - \eta_{0j}^{*}] \tag{3.2.44}$$

and

$$z_j^{*} = \frac{1}{2} d_j^{*} + \zeta_{0j}^{*}. \tag{3.2.45}$$

The relations between the profile functions given in Eq.(3.2.20) and those in Eq.(3.2.43) can easily be indicated by

$$f_j^{*}(y_j^{*}) = \frac{1}{2} d_j^{*} + f_{oj}^{*}(\eta_{oj}^{*}), \tag{3.2.46}$$

There is no unique way to locate the origin of the local coordinate systems for the rails and we may consider the points to measure the track gauge as the reference points for the location of the origin. Suppose the lateral coordinate of this point to be c_j with respect to the local coordinate system (o_{0j}, η_{0j}, ζ_{0j}) (see Fig.3.2.1), we obtain the following relations

$$y_j = \pm [(b_0 + c_j) - \eta_{0j}], \tag{3.2.47}$$

$$z_j = r_0 + \zeta_{0j} \tag{3.2.48}$$

and

$$f_j(y_j) = r_0 + f_{0j}(\eta_{0j}). \tag{3.2.49}$$

When we have the profile functions with respect to the local coordinate systems, Eqs.(3.2.33)-(3.2.40) may be solved by using (3.2.46) and (3.2.49).

3.3. Geometric Contact in Roller Rig Systems

Roller rig systems are often used in experiments either to predict the behaviour of railway vehicle systems (Elkins, 1985; Heliot, 1985; Jaschinski, 1990) or to investigate the wheel/rail interaction phenomena, such as the identification of the creep coefficients and the wear ratio of the rail and wheel surface (Ul-Haque and Law, 1982; Kumar, 1982). In such a roller rig the vehicle is placed with the wheels on pairs of rollers. In general, the rollers can only rotate about their axes of revolution and the other five generalized coordinates are locked. In some test facilities such as the one reported by Hahn (1986), full-scale bogies or vehicles can be analyzed but it requires a lot of effort when vehicle types or parameters of the vehicle have to be changed. In contrast, the scaled vehicles can be investigated in an economic way and the experimental results may be transformed to the full scale system based on the similarity laws, as shown by Heliot (1985) and Jaschinski (1990). However, as pointed out by De Pater (1990), the results obtained in the roller rig system should be interpreted carefully because the mechanics of the roller rig differ in some aspects essentially from the mechanics of the usual track-vehicle system.

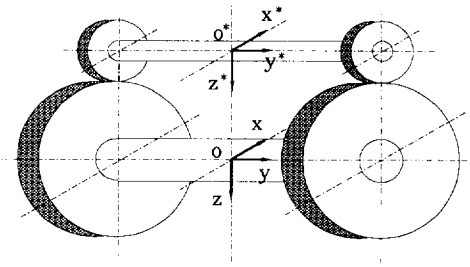

Fig.3.3.1. A roller rig system.

When we consider a single wheelset resting upon a pair of rollers (see Fig.3.3.1), there are also two constraint relations between the translations u, v, w and the rotations ϕ, θ and ψ of the wheelset. In general, the pair of rollers can be considered as a single rigid, axisymmetric body which is supported upon a rigid base. In order to solve the geometric constraints associated with the roller rig system, we have to specify a coordinate system to describe the geometry of the roller body. We may naturally define the roller-body frame in the same way as we did the wheelset-body frame in the previous section (see Fig.3.2.2) because both bodies have the same geometric properties. The origin of the roller body frame is chosen at the body mass centre. With respect to this frame, which is also denoted by $\{o^1, \bar{e}^1\}$, the roller-body surface equation can be written as

$$\sqrt{x^2 + z^2} - f_j(y) = 0, \tag{3.3.1}$$

where $f_j(y)$ is the profile function of the roller cross-section.

In a way similar to that indicated at the end of Section 3.2, we can find the transformation from the roller body frame to the local coordinate systems with respect to which the original rail contours are described. In comparison with the procedure for the track-wheelset system, the vertical displacement of the wheelset and the z-coordinates of the contact points should be treated carefully in the roller-rig system because the roller body frame is defined in a different manner.

In addition to the notations introduced in Eqs.(3.2.12)-(3.2.16), we define the rolling radius r of the roller as

$$r = \sqrt{x^2 + z^2}\,. \tag{3.3.2}$$

The unit normal vector of the roller surface at a point (x, y, z) can be expressed by

$$\bar{n}_j = \boldsymbol{n}_j^T \bar{\boldsymbol{e}}^1 \tag{3.3.3}$$

with

$$\boldsymbol{n}_j = \left[\frac{x}{r}\sin\gamma_j \;\; \pm\sin\gamma_j \;\; \frac{z}{r}\cos\gamma_j \right]^T. \tag{3.3.4}$$

When the diameter of the rollers tends to infinity, the roller-rig reduces to the track-wheelset system.

The motion of the wheelset will be described with respect to the roller body frame. We may still utilize Fig.(3.2.3) to indicate the relation between the roller body frame (o, x, y, z) and the wheelset body frame (o^*, x^*, y^*, z^*), but in this case the roller body frame is no longer related to the radius r_0 in Fig.(3.2.4). Supposed that the coordinates (x_j, y_j, z_j) indicate a contact point with respect to the roller-body frame, all equations corresponding to the first contact condition derived for the track-wheelset system in the previous section remain valid. Only Eq.(3.2.32) generated from the second contact condition have to be modified to

$$\begin{bmatrix} \frac{x_j^*}{r_j^*}\cos\gamma_j^* \\ \pm\sin\gamma_j^* \\ \frac{z_j^*}{r_j^*}\cos\gamma_j^* \end{bmatrix} = \begin{bmatrix} \cos\psi & \sin\psi & 0 \\ -\cos\phi\sin\psi & \cos\phi\cos\psi & \sin\phi \\ \sin\phi\sin\psi & -\sin\phi\cos\psi & \cos\phi \end{bmatrix} \begin{bmatrix} \frac{x_j}{r_j}\cos\gamma_j \\ \pm\sin\gamma_j \\ \frac{z_j}{r_j}\cos\gamma_j \end{bmatrix}. \tag{3.3.5}$$

The first two equations of (3.3.5) are chosen as the independent ones.

Finally we obtain the following set of 14 equations for the 17 variables:

$$(x_1 - x_2) - [\,(x_1^* - x_2^*)\cos\psi - (y_1^* - y_2^*)\cos\phi\sin\psi + (z_j^* - z_2^*)\sin\phi\,\sin\psi\,] = 0, \quad (3.3.6)$$

$$(y_1 - y_2) - [\,(x_1^* - x_2^*)\sin\psi + (y_1^* - y_2^*)\cos\phi\cos\psi - (z_1^* - z_2^*)\sin\phi\cos\psi\,] = 0, \quad (3.3.7)$$

$$[\,z_1 - z_2\,] - [\,(y_1^* - y_2^*)\sin\phi + (z_1^* - z_2^*)\cos\phi\,] = 0, \quad (3.3.8)$$

$$\sqrt{x_j^2 + z_j^2} - f_j(y) = 0, \quad (3.3.9)$$

$$\sqrt{x_j^{*2} + z_j^{*2}} - f_j^*(y_j^*) = 0, \quad (3.3.10)$$

$$\frac{x_j^*}{r_j^*}\cos\gamma_j^* = \frac{x_j}{r_j}\cos\gamma_j\cos\psi \pm \sin\gamma_j\sin\psi, \quad (3.3.11)$$

$$\pm\sin\gamma_j^* = -\frac{x_j}{r_j}\cos\gamma_j\cos\phi\,\sin\psi \pm \sin\gamma_j\cos\phi\,\cos\psi + \frac{z_j}{r_j}\cos\gamma_j\sin\phi, \quad (3.3.12)$$

$$u = \frac{1}{2}\left\{(x_1+x_2) - [(x_1^*+x_2^*)\cos\psi - (y_1^*+y_2^*)\cos\phi\sin\psi + (z_j^*+z_2^*)\sin\phi\sin\psi]\right\} \quad (3.3.13)$$

$$v = \frac{1}{2}\left\{(y_1+y_2) - [(x_1^*+x_2^*)\sin\psi + (y_1^*+y_2^*)\cos\phi\cos\psi - (z_1^*+z_2^*)\sin\phi\cos\psi]\right\}, \quad (3.3.14)$$

$$w = \frac{1}{2}\left\{[f_1(y_1)+f_2(y_2)] - [(y_1^*+y_2^*)\sin\phi + (z_1^*+z_2^*)\cos\phi\,]\right\}. \quad (3.3.15)$$

This set of nonlinear algebraic equations can be handled in a similar way as the one for the track-wheelset system. Having given values of three variables, for instance the longitudinal displacement u, the rolling angle ϕ and the yaw angle ψ, we may completely solve the twelve equations (3.3.6)-(3.3.13) to obtain the coordinates of the contact points. Afterward, the lateral and vertical displacements are determined from the last two equations. In contrast with the track-wheelset system, the longitudinal displacement of the wheelset mass centre strongly influences the geometric contact of the roller rig system.

3.4. Approximate Methods for Solving the Geometric Constraint Equations.

Even though we may choose the rolling angle and the yaw angle as the independent generalized coordinates in the geometric contact problem, we have to solve a set of eight nonlinear algebraic equations to determine the eight coordinates of the contact points in terms of these two angles. The computer time for solving these equations is considerable but it can be reduced to a very large extent by simplifying the equations either to the two-dimensional equations or to the so-called first-order equations. In contrast with the two-dimensional approach, the first-order theory still gives rise to three-dimensional solutions. In Section 3.5, we shall see that the simplification has the important additional advantage that certain nonlinear properties of the solution can be found in a much easier way.

3.4.1. Two-dimensional Approach

A direct simplification of the geometric contact problem is achieved by reducing the three-dimensional problem to a two-dimensional one in which the influence of the yaw rotation is neglected. This simplification may be reasonable with the exception of the case that there is contact on the flange in the presence of a large yaw angle.

When the yaw angle is equal to zero, the longitudinal coordinate of the contact point with respect to the wheelset body frame vanishes, so that the rolling radius r_j^* is equal to the vertical coordinate z_j^* of the point. We can therefore find the geometric contact constraints more easily, because the set of eight Eqs.(3.2.33)-(3.2.37) can be reduced to the following four equations:

$$(y_1 - y_2) - (y_1^* - y_2^*)\cos\phi + [f_1^*(y_1^*) - f_2^*(y_2^*)]\sin\phi = 0, \tag{3.4.1}$$

$$[f_1(y_1) - f_2(y_2)] - (y_1^* - y_2^*)\sin\phi - [f_1^*(y_1^*) - f_2^*(y_2^*)]\cos\phi = 0, \tag{3.4.2}$$

$$\gamma_j = \gamma_j^* \mp \phi . \tag{3.4.3}$$

Using the relationship between the local coordinate systems and the frames of the track and the wheelset given in Eqs.(3.2.42)-(3.2.49), we find

$$\mathrm{tg}\gamma_j = \mp f_j'(y_j) = f_{0j}'(\eta_{0j}), \tag{3.4.4}$$

and

$$\mathrm{tg}\gamma_j^* = \mp f_j^{*\prime}(y_j^*) = f_{0j}^{*\prime}(\eta_{0j}^*). \tag{3.4.5}$$

Substituting these relations into Eqs.(3.4.1)-(3.4.3) and using the expressions (3.2.42)-(3.2.49) again, we may rewrite Eqs.(3.4.1)-(3.4.3) with variables that refer to the local coordinate systems:

$$\begin{aligned}&(\eta_{01}+\eta_{02}) - (\eta_{01}^*+\eta_{02}^*)\cos\phi - [f_{01}^*(\eta_{01}^*) - f_{02}^*(\eta_{02}^*)]\sin\phi \\ &- (2b_0+c_1+c_2) + 2(b_0^*+c^*)\cos\phi - \frac{1}{2}(d_1^*-d_2^*)\sin\phi = 0,\end{aligned} \tag{3.4.6}$$

$$\begin{aligned}&[f_{01}(\eta_{01}) - f_{02}(\eta_{02})] + (\eta_{01}^*+\eta_{02}^*)\sin\phi \\ &- [f_{01}^*(\eta_{01}^*) - f_{02}^*(\eta_{02}^*)]\cos\phi - 2(b_0^*+c^*)\sin\phi - \frac{1}{2}(d_1^*-d_2^*)\cos\phi = 0,\end{aligned} \tag{3.4.7}$$

$$f_{01}^{*\prime}(\eta_{01}^*) - \mathrm{tg}\phi - f_{01}'(\eta_{01})[1 + f_{01}^{*\prime}(\eta_{01}^*)\,\mathrm{tg}\phi] = 0, \tag{3.4.8}$$

$$f_{02}^{*\prime}(\eta_{02}^*) + \mathrm{tg}\phi - f_{02}'(\eta_{02})[1 - f_{02}^{*\prime}(\eta_{02}^*)\,\mathrm{tg}\phi] = 0. \tag{3.4.9}$$

Obviously, the last equations involve only five variables, viz. the four lateral coordinates of the contact points and the rolling angle ϕ. This implies that also the lateral and the vertical displacements v and w given by Eqs.(3.2.38) and (3.2.39) may be expressed in the contact coordinates and the rolling angle ϕ:

$$\begin{aligned}&v - \frac{1}{2}\{-(\eta_{01}-\eta_{02}) + (\eta_{01}^*-\eta_{02}^*)\cos\phi + [f_{01}^*(\eta_{01}^*) + f_{02}^*(\eta_{02}^*)]\sin\phi \\ &+ (c_1-c_2) + 2r_0\sin\phi\} = 0,\end{aligned} \tag{3.4.10}$$

$$\begin{aligned}&w - \frac{1}{2}\{[f_{01}(\eta_{01}) + f_{02}(\eta_{02})] + (\eta_{01}^*-\eta_{02}^*)\sin\phi \\ &- [f_{01}^*(\eta_{01}^*) + f_{02}^*(\eta_{02}^*)]\cos\phi + 2r_0(1-\cos\phi)\} = 0,\end{aligned} \tag{3.4.11}$$

Having solved Eqs.(3.4.6)-(3.4.9) for a given small value ϕ_0 of ϕ, for instance ϕ_0=0, we obtain the coordinates of the contact points ($\eta_{0\,j}$, $\zeta_{0\,j}$) and ($\eta_{0\,j}$*, ζ_{0j}*) for the rails and wheels respectively. This contact position is designated as the initial contact position, in which the contact coordinates are considered as initial values for

the Newton-Raphson procedure to solve Eqs.(3.4.6)-(3.4.9) with varying values of the rolling angle ϕ. More importantly, these coordinates are also employed as initial values for solving either the exact equations (3.2.33)-(3.2.37) or the first-order equations to be derived in the next section. Corresponding to the initial contact position, we introduce the following notations for the track:

$$b_{0j} = (b_0 + c_j - \eta_{0j}), \tag{3.4.12}$$

$$r_{0j} = r_0 + f_{0j}(\eta_{0j}) \tag{3.4.13}$$

and for the wheelset:

$$b^*_{0j} = (b^*_0 + c^* - \eta^*_{0j}), \tag{3.4.14}$$

$$r^*_{0j} = \frac{1}{2} d^*_j + f^*_{0j}(\eta^*_{0j}). \tag{3.4.15}$$

These quantities represent the absolute coordinates of the contact points with respect to the track reference frame and the wheelset body frame for $\phi=\phi_0$ and $\psi=0$.

When the geometry of the track-wheelset system is asymmetric, we can easily find that for $\phi=0$ both the lateral and vertical displacements v and w are unequal to zero. For a symmetric geometry, v becomes zero for $\phi=0$ but in general w not.

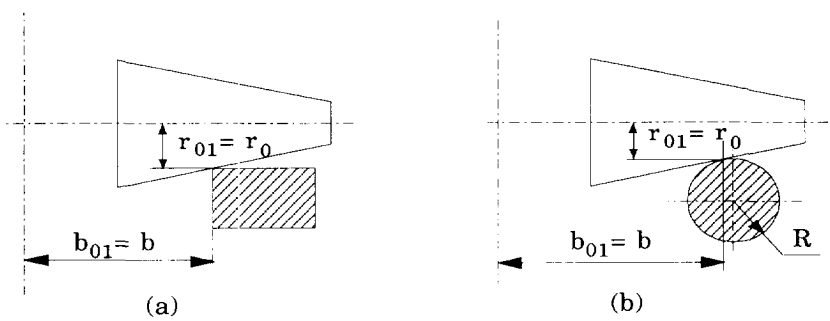

Fig.3.4.1. (a). dicone upon knife edge rails and (b) dicone upon circular cylindrical rails.

Only for a few special combinations of rail and wheel profiles, we can find analytical solutions of Eqs.(3.4.6)-(3.4.9). One of such cases is indicated in Fig.3.4.1a, where a dicone rolls upon knife edge rails. In this case, Eqs.(3.4.8) and (3.4.9) are eliminated and the coordinates of the contact points of the rails are

permanently equal to zero in their local coordinate systems. On the other hand, because a profile function of the dicone is a linear function of the lateral coordinate, Eqs.(3.4.6) and (3.4.7) reduce to linear algebraic equations for the lateral contact coordinates η_{01}^* and η_{02}^*. Therefore, the reduced equations can be solved in an analytical way.

In another case, the dicone is placed upon two circular cylindrical rails as shown in Fig.3.4.1b. The contact coordinates of the rails can be determined analytically from Eqs.(3.4.8) and (3.4.9) due to the constant contact angles of the wheels. Substituting the solutions for the rail coordinates into Eqs.(3.4.6) and (3.4.7) yields a set of two linear algebraic equations from which the lateral contact coordinates of the wheels can be solved analytically in terms of the rolling angle ϕ. Obviously, the system of a dicone upon knife edge rails is a limit case of the system of a dicone upon circular cylindrical rails for which the rail radii approach to zero.

As examples, we consider more special cases in which we assume that the two above-mentioned track-wheelset systems are symmetric and that the initial contact position coincides with the central position of the wheelset. By means of the relations (3.4.12)-(3.4.15) we may have:

$$b = b_{01} = b_{02} = b_{01}^* = b_{02}^* , \tag{3.4.16}$$

$$r_0 = r_{01} = r_{02} = r_{01}^* = r_{02}^* . \tag{3.4.17}$$

When the dicone rests upon the knife edge rails, the lateral and the vertical displacements can be expressed by:

$$v = (-\frac{b}{k}\cos\phi + r_0)\sin\phi + kb(1-\cos\phi)\sin\phi , \tag{3.4.18}$$

$$w = -\frac{b}{k}\sin^2\phi + r_0(1-\cos\phi) - kb(1-\cos\phi)\cos\phi . \tag{3.4.19}$$

where k represents the tangent of the cone angle γ_0. For the system of the dicone upon the circular cylindrical rails, we can find the following results:

$$\begin{aligned} v = {} & (-\frac{b}{k}\cos\phi + r_0)\sin\phi + kb(1-\cos\phi)\sin\phi \\ & + \frac{R}{\cos\gamma_0}(1-\cos\phi)\sin\phi , \end{aligned} \tag{3.4.20}$$

$$w = -\frac{b}{k}\sin^2\phi + r_0(1-\cos\phi) - kb(1-\cos\phi)\cos\phi - \frac{R}{\cos\gamma_0}(1-\cos\phi)\cos\phi, \tag{3.4.21}$$

where R is the radius of the rail cross-section. The approximate results obtained from the first-order theory (De Pater, 1988) are in excellent agreement with our results.

Under the conditions that the rolling angle and the cone angle are small ($\phi \ll 1$ and $\gamma_0 \ll 1$), we may approximate Eqs.(3.4.18) and (3.4.20) by:

$$\phi \approx -\frac{k}{b - kr_0} y \tag{3.4.22}$$

and Eqs.(3.4.19) and (3.4.21) lead to

$$w \approx -\frac{k}{b-2kr_0} y^2. \tag{3.4.23}$$

The analytical results indicate that in these two track-wheelset systems the geometric contact constraints are strongly dependent on the cone angle and, in contrast, they are hardly affected by the radii of curvature of the rails.

3.4.2. First-order Theory

Both experimental and theoretical investigations of the dynamic behaviour of practical railway vehicle systems evidence the fact that vehicles perform, in general, small yaw and rolling rotations as well as small lateral and vertical translations. For instance, as compared with a typical dimension of the wheelset such as the wheelset gauge, which is about 1360mm in the standardized European railway systems, the amplitude of the lateral wheelset displacement is only of the order of magnitude of 5mm. Thus, we may draw up a first-order theory (De Pater, 1988) to simplify the geometric contact problem; in contradistinction to the two-dimensional approach of the previous section, the first-order theory is completely three-dimensional.

First of all, we introduce a group of new coordinate systems called initial coordinate systems to describe the rail and wheel profiles. As stated in the preceding section, under the conditions $\phi=\phi_0$ and $\psi=0$ we have obtained the contact position associated with the contact coordinates $(0, \pm b_{0j}, r_{0j})$ with respect to the track

reference frame for the rails and the coordinates $(0, \pm b_{0j}^*, r_{0j}^*)$ in the wheelset body frame for the wheels. We define that the origins of the initial systems, which are denoted by $(o_j, \xi_j, \eta_j, \zeta_j)$ and $(o_j^*, \xi_j^*, \eta_j^*, \zeta_j^*)$ for the rails and wheels respectively, are located at these initial contact points and that their axes remain parallel to the axes of the respective local coordinate systems. The relations between the coordinates of the initial systems and those of the track body frame and the wheelset body frame are therefore determined by

$$x_j = \xi_j \,, \quad y_j = \pm(b_{0j} - \eta_j) \,, \quad z_j = r_{0j} + \zeta_j \,, \tag{3.4.24}$$

and

$$x_j^* = \xi_j^* \,, \quad y_j^* = \pm(b_{0j}^* - \eta_j^*) \,, \quad z_j^* = r_{0j}^* + \zeta_j^* \,. \tag{3.4.25}$$

Correspondingly, the profile functions of the rails and the wheels can be written in the initial systems. For the rails, we obtain

$$f_j(y_j) = r_{0j} + \zeta_j, \tag{3.4.26}$$

with

$$\zeta_j = \tilde{f}_j(\eta_j) = f_{0j}(\eta_j + \eta_{0j}) - \zeta_{0j} \tag{3.4.27}$$

and for the wheels,

$$f_j^*(y_j^*) = r_{0j}^* + \rho_j^*, \tag{3.4.28}$$

with

$$\rho_j^* = \tilde{f}_j^*(\eta_j^*) = f_{0j}^*(\eta_j^* + \eta_{0j}^*) - \zeta_{0j}^*. \tag{3.4.29}$$

The angles γ_j and γ_j^* are still determined by Eqs.(3.2.13) and (3.2.14), which yield

$$\mathrm{tg}\gamma_j = f_j'(\eta_j) \tag{3.4.30}$$

and

$$\mathrm{tg}\gamma_j^* = f_j^{*\prime}(\eta_j^*). \tag{3.4.31}$$

In Eqs.(3.4.30), (3.4.31) and henceforth the tilde (" ~ ") has been dropped and the notations $\tilde{f}_j$ and $\tilde{f}_j^*$ have been replaced by f_j and f_j^* respectively.

In addition, we define the following quantities for the subsequent analysis:

$$b = \frac{1}{2}(b_{01} + b_{02}), \qquad \Delta b = (b_{01} - b_{02}), \tag{3.4.32}$$

$$r = \frac{1}{2}(r_{01} + r_{02}), \qquad \Delta r = (r_{01} - r_{02}), \tag{3.4.33}$$

$$b^* = \frac{1}{2}(b_{01}^* + b_{02}^*), \qquad \Delta b^* = (b_{01}^* - b_{02}^*), \tag{3.4.34}$$

$$r^* = \frac{1}{2}(r_{01}^* + r_{02}^*), \qquad \Delta r^* = (r_{01}^* - r_{02}^*). \tag{3.4.35}$$

In railway practice the following inequalities hold:

$$|v| \ll b, \quad |w| \ll b, \quad |\phi| \ll 1, \quad |\psi| \ll 1. \tag{3.4.36}$$

These inequalities give rise to inequalities for the small contact coordinates $\xi_j,...,\zeta_j^*$ and ρ_j^* of (3.4.24-25) and (3.4.29), viz.

$$|\xi_j| \ll b, \ ..., \ |\zeta_j^*| \ll b^*, \ |\rho_j^*| \ll b^* \tag{3.4.37}$$

and they also ensure that:

$$\Delta b \ll b, \quad \Delta r \ll r, \quad \Delta b^* \ll b^*, \quad \Delta r^* \ll r^*. \tag{3.4.38}$$

By taking into account the condition (3.4.36), Eq.(3.2.37) may be approximated by

$$\gamma_j^* = \gamma_j \pm \phi - \frac{1}{2}\psi^2 \mathrm{tg}\gamma_j + O_3(\phi,\psi), \tag{3.4.39}$$

where $O_3(\phi,\psi)$ represents terms of the third and higher order in ϕ and ψ. In the first-order theory, these higher order terms are neglected. The third equation of (3.2.32) yields

$$\frac{z_j^*}{r_{0j}^* + \rho_j^*}\cos\gamma_j^* \pm \sin\gamma_j \sin\phi\cos\psi - \cos\gamma_j\cos\phi = 0 \tag{3.4.40}$$

and using Eq.(3.4.39), we may obtain

$$\zeta_j^* = \rho_j^* - \frac{1}{2} r_{0j}^* \psi^2 \mathrm{tg}^2\gamma_j. \tag{3.4.41}$$

In a similar way, Eq.(3.2.36) reduces to

$$\xi_j^* = \pm r_{0j}^* \psi \, \mathrm{tg}\gamma_j \pm \rho_j^* \psi \, \mathrm{tg}\gamma_j + r_{0j}^* \psi \phi \, \mathrm{tg}^2 \gamma_j . \tag{3.4.42}$$

By the last two relations, both the vertical and the longitudinal coordinates of the contact points on the wheels are expressed as functions of the lateral contact coordinates η_j^*, η_j and the rotation angles ϕ, ψ. This is due to the fact that both the wheel profiles ρ_j^* and the rail contact angles γ_j are only functions of their own lateral coordinates.

Thus, transforming Eqs.(3.2.33) and (3.2.34) to the local coordinates and using the relations (3.4.41) and (3.4.42), we obtain the following approximate equations:

$$\begin{aligned}&(\eta_1 + \eta_2) - (\eta_1^* + \eta_2^*) - \phi \, [f_1^*(\eta_1^*) - f_2^*(\eta_2^*)] \\ &+ r^* \psi^2 [f_1'(\eta_1) + f_2'(\eta_2)] - 2(b - b^*) - \Delta r^* \phi - b^* (\phi^2 + \psi^2) = 0 ,\end{aligned} \tag{3.4.43}$$

$$\begin{aligned}&[f_1(\eta_1) - f_2(\eta_2)] - [f_1^*(\eta_1^*) - f_2^*(\eta_2^*)] + \phi \, (\eta_1^* + \eta_2^*) \\ &+ \frac{1}{2} r^* \psi^2 [f_1'^{\,2}(\eta_1) - f_2'^{\,2}(\eta_2)] + \Delta r - \Delta r^* - 2 b^* \phi = 0 .\end{aligned} \tag{3.4.44}$$

Moreover, calculating the tangent of both sides of Eqs.(3.4.39) yields:

$$f_1^{*\prime}(\eta_1^*) - f_1'(\eta_1) - [\phi + (\phi^2 - \frac{1}{2}\psi^2) f_1'(\eta_1)] [1 + f_1'^{\,2}(\eta_1)] = 0, \tag{3.4.45}$$

and

$$f_2^{*\prime}(\eta_2^*) - f_2'(\eta_2) - [-\phi + (\phi^2 - \frac{1}{2}\psi^2) f_2'(\eta_2)] [1 + f_2'^{\,2}(\eta_2)] = 0 . \tag{3.4.46}$$

Evidently, Eqs.(3.4.43)-(3.4.46) contain only six variables: the four lateral contact coordinates η_j, η_j^* and the rolling and yaw angels ϕ, ψ. With varying values of the rolling and yaw angles, the four lateral contact coordinates may be determined from these four equations. Because the rail and wheel profiles are described in their corresponding initial coordinate systems, the zero values of the lateral contact coordinates are the solution of these four equations with $\phi=\phi_0$ and $\psi=0$. Thus, this contact position provides the four equations with the most convenient initial values of the lateral contact coordinates when the rolling and yaw angle take values around ϕ_0 and zero respectively. Afterwards, the contact angles γ_j and γ_j^* are calculated by means of Eqs.(3.4.30) and (3.4.31); the vertical contact coordinates ζ_j of the rails can directly be obtained from the rail surface equations (3.4.27); the longitudinal and

vertical contact coordinates ξ_j^*, ζ_j^* of the wheels are determined by Eqs.(3.4.41) and (3.4.42).

Using (3.4.41) and (3.4.42), we can reduce Eqs.(3.2.38) and (3.2.39) to the following equations, in which the lateral and vertical displacements v, w are expressed in the lateral contact coordinates and the generalized coordinates:

$$v - \frac{1}{2}\{(-\eta_1+\eta_2+\eta_1^*-\eta_2^*)+\phi\,[f_1^*(\eta_1^*)+f_2^*(\eta_2^*)] - r^*\psi^2\,[f_1'(\eta_1)-f_2'(\eta_2)]+r^*\phi+\Delta b-\Delta b^*+\frac{1}{2}\Delta b^*(\phi^2+\psi^2)\} = 0, \tag{3.4.47}$$

$$w - \frac{1}{2}\{[f_1(\eta_1)+f_2(\eta_2)-f_1^*(\eta_1^*)-f_2^*(\eta_2^*)]+\phi(\eta_1^*-\eta_2^*) + \frac{1}{2}r_0\psi^2\,[f_1'^2(\eta_1)+f_2'^2(\eta_2)]+2(r+r^*)-\Delta b^*\phi+\frac{1}{2}r^*\phi^2\} = 0. \tag{3.4.48}$$

When the lateral displacement v is considered as one of the independent coordinates and the rolling angle ϕ as a dependent generalized coordinate, we have to solve a set of five equations (3.4.43)-(3.4.47) for the five unknowns which are the four lateral contact coordinates and the rolling angle.

In contrast to the exact theory, in the first-order theory the longitudinal and vertical coordinates of the contact points on the wheels are not treated as variables; they are approximately given by the relations (3.4.41) and (3.4.42) in terms of the lateral contact coordinates, the rolling angle ϕ and the yaw angle ψ, which comprise terms up to the second order in the small quantities. Therefore, the three-dimensional geometric contact between the track and the wheelset is determined approximately by the first-order equations (3.4.43)-(3.4.48). As compared with the exact equations (3.2.33)-(3.2.40), the reduction of computer time is considerable when the first-order theory is adopted in solving the geometric contact problem.

3.4.3. Perturbation Method

The perturbation method is widely employed in the analysis of nonlinear systems (Nayfeh, 1976). Recently, De Pater has made use of this method to determine the effect of the yaw angle on the geometric contact. In the first-order equations, the rolling and the yaw angles are chosen to be the independent parameters and the solutions of the lateral coordinates may be written as power series in terms of these

two parameter. When we investigate the influence of the yaw angle on the lateral contact coordinates at a fixed value of the rolling angle ϕ, we need only express these coordinates as a power series development of the yaw angle. Moreover, the contribution of the first order terms in the yaw angle vanishes due to the fact that only second order terms of this yaw angle appear in the equations. As a result, we may write:

$$\eta_j = \eta_{Ij} + \frac{1}{2}\eta_{IIj}\psi^2, \tag{3.4.49}$$

and

$$\eta_j^* = \eta_{Ij}^* + \frac{1}{2}\eta_{IIj}^*\psi^2. \tag{3.4.50}$$

Correspondingly, we may express the profile functions ζ_j and ρ_j^* and their first derivatives around η_{Ij} and η_{Ij}^* in Taylor series, so that

$$f_j(\eta_j) = f_j(\eta_{Ij}) + \frac{1}{2}\eta_{IIj}\psi^2 f_j'(\eta_{Ij}), \tag{3.4.51}$$

$$f_j'(\eta_j) = f_j'(\eta_{Ij}) + \frac{1}{2}\eta_{IIj}\psi^2 f_j''(\eta_{Ij}), \tag{3.4.52}$$

and

$$f_j^*(\eta_j^*) = f_j^*(\eta_{Ij}^*) + \frac{1}{2}\eta_{IIj}^*\psi^2 f_j^{*\prime}(\eta_{Ij}^*), \tag{3.4.53}$$

$$f_j^{*\prime}(\eta_j^*) = f_j^{*\prime}(\eta_{Ij}^*) + \frac{1}{2}\eta_{IIj}^*\psi^2 f_j^{*\prime\prime}(\eta_{Ij}^*). \tag{3.4.54}$$

Substituting (3.4.49)-(3.4.54) into Eqs.(3.4.43)-(3.4.46) yields two sets of equations, one of which refers to the equations for two-dimensional contact, whereas the other is related to the second order terms in the yaw angle. In fact, the first set involving only the rolling angle ϕ and the quantities η_{Ij}, η_{Ij}^* is the set of first-order equations in the case ψ=0, from which η_{Ij} and η_{Ij}^* can be solved in terms of the rolling angle.

The other set of equations is:

$$(\eta_{II1}+\eta_{II2})-(\eta_{II1}^*+\eta_{II2}^*) = 2b^* - 2r^*[f_1'(\eta_{I1})+f_2'(\eta_{I2})], \tag{3.4.55}$$

$$[\eta_{II1}f_1'(\eta_{I1}) - \eta_{II2}f_2'(\eta_{I2})] - [\eta_{II1}^*f_1^{*\prime}(\eta_{I1}^*) - \eta_{II2}^*f_2^{*\prime}(\eta_{I2}^*)] = -r^*[f_1'^2(\eta_{I1}) - f_2'^2(\eta_{I2})], \tag{3.4.56}$$

$$\eta_{II1}^*f_1^{*\prime\prime}(\eta_{I1}^*) - \eta_{II1}f_1''(\eta_{I1}) = f_1'(\eta_{I1})[1 + f_1'^2(\eta_{I1})], \tag{3.4.57}$$

$$\eta_{II2}^*f_2^{*\prime\prime}(\eta_{I2}^*) - \eta_{II2}f_2''(\eta_{I2}) = f_2'(\eta_{I2})[1 + f_2'^2(\eta_{I2})]. \tag{3.4.58}$$

These four equations are linear algebraic equations for the quantities η_{IIj} and η_{IIj}^*. Once η_{Ij} and η_{Ij}^* have been obtained from the first-order equations with ψ=0 by the Newton-Raphson procedure, these linear equations can be solved. Now, the lateral coordinates of the contact points are determined by taking into account the first correction for the yaw angles.

3.5. Numerical Methods and Results

To determine the geometric contact between track and wheelset either by the exact theory or by the approximate approaches one has to solve a set of nonlinear algebraic equations with a number of parameters. Techniques for solving such equations, which originate from many practical problems such as stability of structures and nonlinear behaviour of dynamic systems, are summarized by Keller (1987) and Seydel (1988).

3.5.1. Numerical Methods

The general form of nonlinear algebraic equations is expressed as

$$\boldsymbol{g}(\boldsymbol{x}, \lambda) = \boldsymbol{0}, \tag{3.5.1}$$

with $\boldsymbol{g} \in \mathbb{R}^n$, $\boldsymbol{x} \in \mathbb{R}^n$ and $\lambda \in \mathbb{R}$. $\boldsymbol{g}$ consists of n smooth functions and λ is a control parameter. In many applications, the system may have more than one parameter; if so, only one of them is supposed to vary over a certain specified range and the others are assigned to some constant values during a computation procedure.

At a given value of the parameter λ, it is expected that the solution $\boldsymbol{x}$ of Eq.(3.5.1) can be found iteratively by means of the Newton-Raphson method. Let

$x^{(0)}$ be an approximation of x; in the neighbourhood of $x^{(0)}$ we have

$$g(x) = g(x^{(0)}) + g_x(x^{(0)})(x - x^{(0)}) + \text{higher-order terms}. \tag{3.5.2}$$

Here, g_x is the Jacobian matrix of $g(x)$. This relation establishes a way to calculate a better approximation $x^{(1)}$ of x by solving the set of linear algebraic equations:

$$g(x^{(0)}) + g_x(x^{(0)})(x^{(1)} - x^{(0)}) = 0. \tag{3.5.3}$$

Applying Eq.(3.5.3) repeatedly leads to the iterative procedure:

$$x^{(k+1)} = x^{(k)} - g_x^{-1}(x^{(k)})\, g(x^{(k)}), \tag{3.5.4}$$

through which a sequence $x^{(0)}$, $x^{(1)}$, $x^{(2)}$, ... is generated. If this sequence is convergent, the solution of Eq.(3.5.1) is the limit of the sequence.

The method is generally performed in two steps. First, we introduce the vector $d^{(k)}$ for the difference between two successive iterations, so that $d^{(k)}$ is found by:

$$g_x(x^{(k)})\, d^{(k)} = -g(x^{(k)}). \tag{3.5.5}$$

Afterwards, the new approximation $x^{(k+1)}$ is obtained by:

$$x^{(k+1)} = x^{(k)} + d^{(k)}. \tag{3.5.6}$$

When the approximation $x^{(k)}$ is in the neighbourhood of the solution, both $g(x^{(k)})$ and $d^{(k)}$ quickly approach zero and we may simply establish the convergence criterion by:

$$\| d^{(k)} \| \le \varepsilon, \tag{3.5.7}$$

or by

$$\| g(x^{(k)}) \| \le \varepsilon, \tag{3.5.8}$$

where ε is a prescribed tolerance.

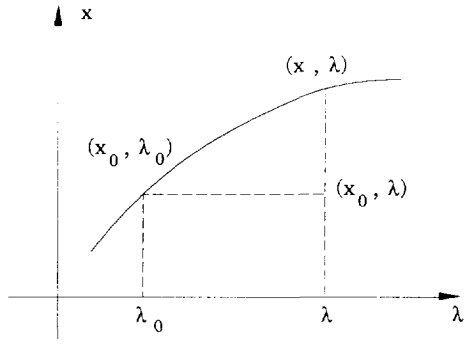

Fig.3.5.1. Trivial predictor.

Evidently, the Newton-Raphson method fails in case the Jacobian matrix $g_x(x)$ is singular. Another difficulty may arise when the first approximation $x^{(0)}$ is far away from the solution; as a result, the iteration procedure may lead to a divergent sequence. In finding the solution of nonlinear equations, the main effort is often to estimate a good initial approximation of the solution.

Varying the parameter λ over a certain range, we expect the solution of Eq.(3.5.1) to be a function of the parameter: $\boldsymbol{x} = \boldsymbol{x}(\lambda)$. Suppose we have a solution $(\boldsymbol{x}_0, \lambda_0)$. Let the Jacobian matrix $\boldsymbol{g}_x(\boldsymbol{x}_0)$ be nonsingular, then the implicit function theorem (Keller (1987)) states the existence of a unique branch of solutions $\boldsymbol{x} = \boldsymbol{x}(\lambda)$ in the neighbourhood of λ_0. Various kinds of so-called predictor-solver methods are used to find a solution $\boldsymbol{x}(\lambda)$ at $\lambda=(\lambda_0+\Delta\lambda)$ where $\Delta\lambda$ is a small perturbation. In a predictor, the solution $(\boldsymbol{x}_0, \lambda_0)$ is utilized to construct an approximation $\boldsymbol{x}^{(0)}(\lambda)$ of the actual solution $\boldsymbol{x}(\lambda)$. For example, a direct procedure takes the solution at λ_0 as the initial guess at λ, *viz.* $\boldsymbol{x}^{(0)}(\lambda) = \boldsymbol{x}_0 = \boldsymbol{x}(\lambda_0)$; this approximation, called the trivial predictor, is interpreted geometrically in Fig.3.5.1. After obtaining an initial approximation, we apply a solver such as the Newton-Raphson method to obtain the solution in an iteration scheme.

When the Jacobian matrix $\boldsymbol{g}_x(\boldsymbol{x}, \lambda)$ at the point $(\boldsymbol{x}_0, \lambda_0)$ is singular, this point is a turning point or a bifurcation point (Seydel (1988)) so that near this point there is more than one solution. Based on the implicit function theorem and the Newton-Raphson method, we cannot get a solution of Eq.(3.5.1) because of the singularity of the Jacobian matrix. There are a wealth of continuation methods to overcome the numerical difficulties and to determine the global solution of Eq.(3.5.1). But for our application, we restrict ourselves to a system of equations with turning points.

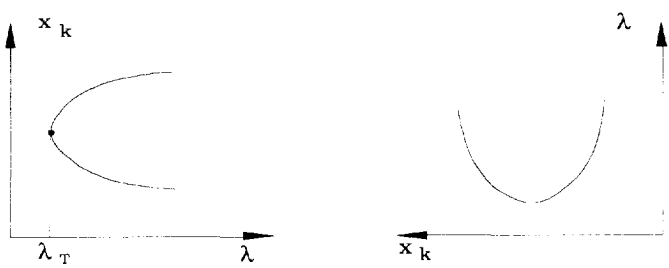

Fig.3.5.2. Removal of a turning point.

We define $\boldsymbol{y} = [\ \boldsymbol{x}^T, \lambda\ ]^T$ and consider Eq.(3.5.1) to be a set of n equations in n+1 variables:

$$\boldsymbol{g}(\boldsymbol{y}) = \boldsymbol{0}. \tag{3.5.9}$$

We assume that the rank of the $n\times(n+1)$ matrix $\boldsymbol{g}_y = [\ \boldsymbol{g}_x, \boldsymbol{g}_\lambda\ ]$ is equal to n in the concerning range of $\boldsymbol{y}$; then only turning points may exist in this region. In other words, there always exists a nonsingular n x n square submatrix in the matrix $\boldsymbol{g}_y$ even at the turning point $\boldsymbol{y}_T$ where the Jacobian matrix $\boldsymbol{g}_x(\boldsymbol{x}, \lambda)$ is singular. Without

losing generality, every component of $\boldsymbol{y}$ is admitted to be a parameter so that the remaining variables can be determined in terms of this parameter. At the turning point $\boldsymbol{y}_T$, where $y_{n+1}=\lambda$ is a parameter, a nonsingular submatrix

$$\left[\frac{\partial \boldsymbol{g}}{\partial x_1}, \ldots, \frac{\partial \boldsymbol{g}}{\partial x_{k-1}}, \frac{\partial \boldsymbol{g}}{\partial \lambda}, \frac{\partial \boldsymbol{g}}{\partial x_{k+1}}, \ldots, \frac{\partial \boldsymbol{g}}{\partial x_n} \right] \tag{3.5.10}$$

is constructed by replacing the k-th column vector of $\boldsymbol{g}_x$ (which is singular) by the vector $\boldsymbol{g}_\lambda$. If we consider the variable x_k as a new parameter and the parameter λ as a variable, the n variables $x_1,\ldots,x_{k-1}$, λ, $x_{k+1},\ldots,x_n$ can be solved as functions of the new parameter x_k in the neighbourhood of the turning point $(\boldsymbol{x}_T, \lambda_T)$ (Rheinboldt, 1986). The Jacobian matrix (3.5.10) for this combination of the variables and the parameter is no longer singular and the implicit function theorem is valid again. Some other methods are mentioned by Seydel (1988) and Meijaard (1991). The geometric interpretation of the above-mentioned procedure is illustrated in Fig.3.5.2; the turning point disappears after rotating the diagram x_k-versus-λ over an angle of 90^o.

3.5.2. Implementation in the Geometric Contact Problem

3.5.2.1. Singularity and Double-contact Position

As stated in Sections 3.2 and 3.4, the geometric contact problem reduces to a system of nonlinear equations, from which the contact coordinates are determined in terms of two physical parameters: the rolling and yaw angles ϕ and ψ. Because we consider arbitrary combinations of rail and wheel profiles, some nonlinear phenomena such as jumps of the contact points may occur when varying the two angles. The numerical difficulties which may arise with the nonlinear phenomena, are analyzed through the two-dimensional geometric contact equations.

Making use of Eqs.(3.4.4) and (3.4.5), we rewrite Eq.(3.4.3) as follows:

$$\arctan f_1'(y_1) - \arctan f_1^{*\prime}(y_1^*) - \phi = 0 \tag{3.5.11}$$

$$\arctan f_2'(y_2) - \arctan f_2^{*\prime}(y_2^*) - \phi = 0. \tag{3.5.12}$$

These two equations together with Eqs.(3.4.1) and (3.4.2) make up a set of four equations in five unknowns: the four lateral contact coordinates and the rolling angle ϕ. As usual, the rolling angle ϕ is considered as a parameter and the four contact

coordinates are chosen as variables; hence we have

$$\boldsymbol{g}(\boldsymbol{x}, \lambda) = \mathbf{0} \tag{3.5.13}$$

with $\boldsymbol{x} = [\, y_1, y_2, y_1^*, y_2^* \,]^T$ and $\lambda = \phi$. The Jacobian matrix of Eq.(3.5.13) is found to be:

$$\boldsymbol{g}_x = \begin{bmatrix} 1 & -1 & -\cos\phi + f_1^{*\prime}\sin\phi & \cos\phi - f_2^{*\prime}\sin\phi \\ f_1' & -f_2' & -\sin\phi - f_1^{*\prime}\cos\phi & \sin\phi + f_2^{*\prime}\cos\phi \\ \dfrac{f_1''}{1+f_1'^2} & 0 & -\dfrac{f_1^{*\prime\prime}}{1+f_1^{*\prime 2}} & 0 \\ 0 & \dfrac{f_2''}{1+f_2'^2} & 0 & -\dfrac{f_2^{*\prime\prime}}{1+f_2^{*\prime 2}} \end{bmatrix}. \tag{3.5.14}$$

In order to simplify this matrix, we introduce R_j and R_j^* to designate the radii of curvature of the profile functions:

$$\frac{1}{R_j} = \frac{f_j''}{\sqrt{(1+f_j'^2)^3}}, \qquad \frac{1}{R_j^*} = \frac{f_j^{*\prime\prime}}{\sqrt{(1+f_j^{*\prime 2})^3}}. \tag{3.5.15}$$

Replacing the first derivatives of the profile functions f_j and f_j^* by the corresponding tangents of the contact angles, Eq.(3.5.14) reduces to

$$\boldsymbol{g}_x = \begin{bmatrix} 1 & -1 & -\dfrac{\cos(\gamma_1^* - \phi)}{\cos\gamma_1^*} & \dfrac{\cos(\gamma_2^* + \phi)}{\cos\gamma_2^*} \\ -\mathrm{tg}\gamma_1 & -\mathrm{tg}\gamma_2 & \dfrac{\sin(\gamma_1^* - \phi)}{\cos\gamma_1^*} & \dfrac{\sin(\gamma_2^* + \phi)}{\cos\gamma_2^*} \\ \dfrac{1}{R_1\cos\gamma_1} & 0 & -\dfrac{1}{R_1^*\cos\gamma_1^*} & 0 \\ 0 & \dfrac{1}{R_2\cos\gamma_2} & 0 & -\dfrac{1}{R_2^*\cos\gamma_2^*} \end{bmatrix}. \tag{3.5.16}$$

The determinant of the Jacobian matrix $\boldsymbol{g}_x$ is calculated by

$$|\boldsymbol{g}_x| = -\frac{\mathrm{tg}\gamma_1 + \mathrm{tg}\gamma_2}{\cos\gamma_1^* \cos\gamma_2^*} \left(\frac{1}{R_1} - \frac{1}{R_1^*}\right)\left(\frac{1}{R_2} - \frac{1}{R_2^*}\right). \tag{3.5.17}$$

Corresponding to the zero value of this determinant, there are three possibilities to give rise to a singular matrix $\boldsymbol{g}_x$: (1) at one side, the radii of curvature of the rail and wheel profiles are equal at the contact point; (2) the radii are the same at both sides and (3) the contact angles in both rails have opposite values. All these singularities lead to failure of the Newton-Raphson method.

In the second case there is a bifurcation. Because the second and the third cases rarely happen in railway vehicle systems, they remain out of consideration.

To investigate whether there is a turning point in the first case, we have to calculate the partial derivative of $\boldsymbol{g}(\boldsymbol{x},\lambda)$ with respect to the parameter $\lambda=\phi$,

$$\boldsymbol{g}_\lambda = \begin{bmatrix} (y_1^* - y_2^*)\sin\phi + (f_1^* - f_2^*)\cos\phi \\ -(y_1^* - y_2^*)\cos\phi + (f_1^* - f_2^*)\sin\phi \\ -1 \\ -1 \end{bmatrix}. \tag{3.5.18}$$

Apparently, it is impossible that the vector $\boldsymbol{g}_\lambda$ is a linear combination of the columns of matrix $\boldsymbol{g}_x$; this implies that in the first singular case the rank of the matrix $\boldsymbol{g}_y$ remains equal to the number of equations. Consequently, the singularity of $\boldsymbol{g}_x$ corresponds to a turning point and there exists a unique relationship between the contact coordinates and the rolling angle.

These results remain valid for the three-dimensional case with a small yaw angle. The subsequent analysis refers to the first-order theory because in our computations only this theory is used to determine the geometric contact constraints. The first-order equations are rewritten in the general form:

$$\boldsymbol{g}(\boldsymbol{x}, \lambda, \psi) = \boldsymbol{0}, \tag{3.5.19}$$

with $\boldsymbol{x} = [\,\eta_1, \eta_2, \eta_1^*, \eta_2^*\,]^T$. The control parameter λ represents the rolling angle ϕ and ψ is a fixed yaw angle.

The singularity of the Jacobian matrix $\boldsymbol{g}_x$ leads to a jump of a contact point on the rail and wheel surfaces. In railway vehicle dynamics such a nonlinear phenomenon is called a double-contact position because at this instant there exist two contact points at one side corresponding to the same values of the rolling angle ϕ and the yaw angle ψ. It is known that double-contacts may occur on the flange as well as in the tread part of the wheel surfaces.

A typical solution path is shown in Fig.3.5.3 where two turning points **C** and **E** appear. The results have been obtained from the combination of the UIC 60 rails and S1002 wheels with 1435mm track gauge, 1/40 inclination and 1360mm wheelset gauge in the case of ψ=0. Fig.3.5.3(a) indicates the relation between the lateral displacement v and the rolling angle ϕ; Fig.3.5.3(b) shows the lateral contact coordinate of the right-hand rail as a function of the rolling angle ϕ and Fig.3.5.3(c) explains qualitatively what happens.

When the rolling angle ϕ decreases, the contact coordinate shifts along the curve **AB** (see Fig.3.5.3.b) until it arrives at the critical point **B**; at the corresponding rolling angle ϕ_B and the lateral displacement v_B there is another contact point at **F**. Between **B** and **C**, there is penetration in the neighbourhood of the point **F** but not nearby the contact points in the **ABC** region. At **C** and **E** the radii of curvature of the rail and the wheel are identical so that these two points correspond to turning points with respect to the rolling angle. Because from **C** to **E** the rail radius of curvature is greater than that of the wheel, there is penetration around the solutions in the region **CDE**. When the contact coordinate varies along the curve **EF**, the rail penetrates the wheel in the region around **ABC** but not nearby the contact points on **EF**. **F** is the other critical point where the penetration in **ABC** alters to the contact point **B**. From **F** to **G** (excluding the critical point **F**), a wheel is in contact with its corresponding rail at one point.

From a numerical point of view, by choosing the lateral contact coordinate instead of the rolling angle ϕ as the control parameter, the numerical difficulties around the two turning points **C** and **E** can be completely avoided; the numerical procedures will be discussed in detail in the subsequent sections.

In reality, penetration is not admitted, therefore, the solutions in the open region **BCDEF** do not exist and only the parts **AB** and **FG** of the curve have physical meaning. The two critical points **B** and **F** correspond with a double-contact position; these two points can be determined on the basis of the fact that the lateral displacement v calculated by means of (3.4.47) at **B** is identical with that at **F**.

We may establish the following nonlinear equations to find these two points:

$$\boldsymbol{h}(\boldsymbol{y},\psi) = \begin{bmatrix} \boldsymbol{g}(y_1, y_2, y_3, y_4, y_9, \psi) \\ \boldsymbol{g}(y_5, y_6, y_7, y_8, y_9, \psi) \\ y_{10} - v(y_1, y_2, y_3, y_4, y_9, \psi) \\ y_{11} - v(y_5, y_6, y_7, y_8, y_9, \psi) \\ y_{10} - y_{11} \end{bmatrix} = \mathbf{0} \qquad (3.5.20)$$

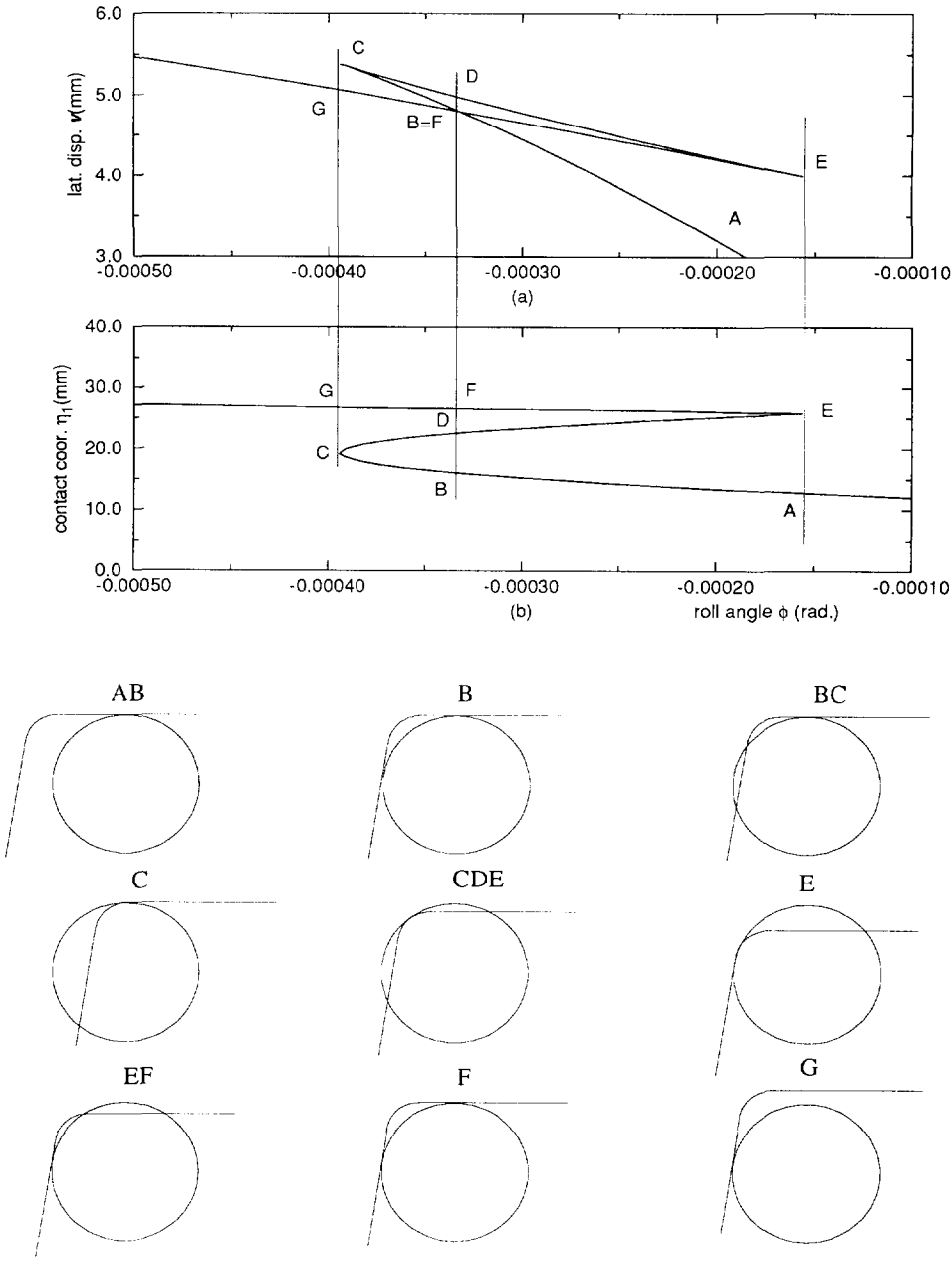

(c) qualitative explanation of rail/wheel contact

Fig. 3.5.3. A typical solution path of Eqs.(3.4.43)-(3.4.46).

with $\boldsymbol{h} \in \mathbf{R}^{11}$, $\boldsymbol{y} \in \mathbf{R}^{11}$. In this equation, $\boldsymbol{g}$ is given by means of the first-order equations; y_9 represents the rolling angle ϕ; y_{10} and y_{11} are two auxiliary variables; the four variables (y_1, y_2, y_3, y_4) and the other four variables (y_5, y_6, y_7, y_8) are two sets of the lateral contact coordinates. Eq.(3.5.20) is a set of eleven nonlinear equations in eleven variables with the yaw angle as a parameter. When the initial approximation of the set of variables (y_1, y_2, y_3, y_4) is a solution of Eq.(3.5.19) around point **B**, the initial approximation of (y_5, y_6, y_7, y_8) is a solution in the neighbourhood of point **F** and y_9 is an approximation of the rolling angle ϕ near the points **B** and **F**, Eq.(3.5.20) may be solved by means of the Newton-Raphson method. The solution (y_1, y_2, y_3, y_4) coincides with point **B** and (y_5, y_6, y_7, y_8) with point **F**, so that the double-contact problem is completely solved. In real computations, the two auxiliary variables y_{10} and y_{11} are eliminated from Eq.(3.5.20) and only a set of nine nonlinear equations in nine variables is solved.

To show that a solution satisfies the third contact condition, which prohibits penetration between the rails and the wheels, is very complex, especially for three-dimensional solutions. There are no ways to ensure that a solution is a real solution in two-dimensional contact with the exception of comparing the vertical coordinates of the whole surfaces of the rails and the wheels in the track reference frame. Suppose that **A** in Fig.3.5.3 corresponds with a real contact position, we may then expect that solutions in its neighbourhood also hold even in three-dimensional contact with a small yaw angle because the implicit function theorem guarantees the unique solution path passing **A**. This can be proved numerically for a two-dimensional contact and the above-mentioned analysis concerning the solution path **ABCDEFG** is also based on the numerical calculations.

3.5.2.2. Summary of the Numerical Procedure

The geometry of the track-wheelset system is completely specified by the profiles of the rails and the wheels in the local coordinate systems together with the track gauge, the inclination, the wheelset gauge and the diameters of the wheels. Each of the profiles and every parameter should be considered individually as a factor to affect the geometric contact.

A computer program named "GeoCont" has been drawn up for solving the geometric contact between track and wheelset. The program accomplishes the problem in three steps:

- choosing the profiles and the parameters, then transforming the profiles to the initial coordinate systems;

- determining the global solution paths;
- finding the double-contact position if there is one and generating the output files.

We follow this sequence to illustrate the numerical procedure in the program.

In the first step, the theoretical or measured profiles have to be represented by numerical tables which contain the lateral and the vertical coordinates and their first and second derivatives. For measured profiles, the original experimental data have to be smoothed because of the accuracy of the instruments, the errors of the observers and the flaking of the surfaces. The smoothed results obtained by means of a least square method or a linear programming method as shown by Sauvage (1975) are expected to be continuous up to the second derivatives. If the inclination needs to be taken into account, the right-hand rail has to rotate anticlockwise over the inclination angle and the other rail rotates clockwise. Notice that for measured rail profiles, the inclination is already incorporated in the experimental data.

So far, the points used to measure the track gauge are unknown, but they are incorporated in the rail profiles and change with the inclination. To find the points we have to determine the tops of the rails where the first derivatives are equal to zero; then, we can find the points the positions of which are 14mm below the top plane (Fig.3.2.1). Their lateral coordinates in the local coordinate systems have already been denoted by c_j in Section 3.2.

According to Eqs.(3.4.6)-(3.4.9) for the two-dimensional approach, we may work out a solution for a given track-wheelset system at zero rolling angle ϕ with certain initial values of the lateral contact coordinates η_{01}, η_{02}, η_{01}^* and η_{02}^*. Whether the rails penetrate the wheels at this solution is checked by comparing the vertical coordinates of the rail and wheel surfaces in the track reference frame. If the solution is associated with penetration, the initial approximations of the lateral coordinates have to be modified to obtain a real solution. After this has been accomplished, the profile functions are transformed from the local coordinate systems to the initial coordinate systems by means of Eqs.(3.4.24) and (3.4.25).

Solving the first-order equations is the aim in the applications of the program. As stated in the preceding section numerical difficulties arise when the radii of curvature of the rail and the wheel are equal or approach each other at a contact position. Taking the lateral contact coordinate of the right-hand rail η_1 as the parameter λ in the set of first-order equations (3.5.19), we can overcome such difficulties only when they occur at the right-hand side of the system but not at the left-hand side. In some cases this requires the coordinate of the left-hand rail η_2 to be the parameter rather than one of the four variables. Therefore, at each computation step the parameter λ has to be chosen out of the two coordinates η_1 and

η_2 to ensure a nonsingular Jacobian matrix. It is advisable not to choose the rolling angle as the parameter in case of passing a turning point.

The zero coordinates η_1, η_2, η_3 and η_4, *viz.* the origins of the initial coordinate systems, are always a solution of Eq.(3.5.19) with ϕ=0 and ψ=0; meanwhile, they are also good approximations of the coordinates for the case of small rolling and yaw angles. From these origins we may start the whole solution path. In general the yaw angle ψ remains constant in the analysis.

The last two solutions denoted by $(\boldsymbol{x}_{(i-1)}, \phi_{(i-1)})$ and $(\boldsymbol{x}_{(i)}, \phi_{(i)})$ must be kept available during the computation. In case the coordinate η_1 (say x_1) is the parameter, the next solution $(\boldsymbol{x}_{(i+1)}, \phi_{(i+1)})$ for an increment $\Delta\lambda_{(i+1)}$ of η_1 may be determined from the approximations given by the trivial predictor. Because the slope of the tangent approaches infinity in the neighbourhood of the turning point (Fig.3.5.3), we establish an inequality to assure that the solution is still sufficiently far away from the turning point. Hence,

$$K < K_{\text{lim}}, \tag{3.5.21}$$

where

$$K = \left| \frac{\eta_{2(i+1)} - \eta_{2(i)}}{\eta_{1(i+1)} - \eta_{1(i)}} \right|. \tag{3.5.22}$$

The quantity K_{lim} is the critical slope; the optimal value is about 6.0 in the program "GeoCont". When the inequality (3.5.21) is deficient, the coordinate η_2 becomes the parameter λ instead of η_1 and the step size for the new parameter η_2 is given by

$$\Delta\lambda_{(i+1)} = 0.1 \frac{(\eta_{2(i)} - \eta_{2(i-1)})}{|(\eta_{2(i)} - \eta_{2(i-1)})|} (mm). \tag{3.5.23}$$

Correspondingly, the quantity K is then equal to the inverse number of the right-hand member of Eq.(3.5.22). Applying this process repeatedly may generate the global solution path we need.

Both the value of K and the number of the iterations (N) in obtaining a solution of Eq.(3.5.19) are used to adjust the step size of the parameter, which is one of the coordinates η_1 and η_2. In case the number of iterations N is less than an optimal value N_{opt} ($\approx$ 10) and the slope K is less than 1.0, the step size increases to $\Delta\lambda_{(i+1)}$=1.618$\Delta\lambda_{(i)}$, but it is limited by the maximum value 0.4. On the other hand, when $N \geq N_{opt}$, $K \geq 1.0$ and $\Delta\lambda_{(i)} \geq 0.2$, we take $\Delta\lambda_{(i+1)}$=0.618$\Delta\lambda_{(i)}$

The useless data that correspond to penetration have to be deleted from the results. As indicated in Fig.3.5.3, the increment of the lateral displacement v as a

function of the rolling angle ϕ changes its sign around the turning points **C** and **E**. On the basis of this fact, the two points in which the sign changes, can be found in the results saved in the sequence of **A** to **G**; therefore, it is easy to get some solutions in **AC** nearby the turning point **C** and in **EG** closed to **E**. By making use of these solutions to determine the initial approximations of Eq.(3.5.20), which are expected nearby the double-contact position **B** and **F**, this equation may be solved iteratively to obtain the contact coordinates of the double-contact position **B** and **F** as well as the corresponding lateral displacement and the rolling angle. Afterwards, the data on **BDEF** are deleted and the information of **B** and **F** is inserted into the data file.

The most essential data files contain the lateral displacement, the rolling angle, the difference of the rolling radii and the four lateral contact coordinates in addition to the information of the system, the positions of double-contact and the constant value of the yaw angle. Some other quantities such as the contact angles, the vertical displacement, the longitudinal and vertical contact coordinates can easily be calculated by means of the essential output data.

3.5.3. Numerical Solutions and Discussions

A typical combination of theoretical profiles of rails and wheels, *viz.* the UIC60 rails and the S1002 wheels is handled as an example of a symmetrical track-wheelset system. Two other asymmetric combinations, called *CTO-Measured-Profiles* and *ORE-Benchmark-Profiles* (see Appendix D), have been measured from tracks and wheelsets in service, so that the inclinations of their rails are already incorporated in the experimental results. In all three combinations which are considered in the computations, the distance between the inside surface of the wheels (or the wheelset gauge) is equal to 1360mm and the nominal rolling radius is 460mm. In order to compare the numerical results, the contact coordinates are taken with respect to the local coordinate systems of the profiles with the exception of the contact coordinates mentioned in Table.3.5.1.

First of all, in order to validate of the approximate methods numerically, we compare the numerical results determined by the exact theory with those determined by the approximate methods described in Section 3.4. The track-wheelset system used in these computations is the combination of the UIC60 rails and the S1002 wheels with the rail inclination 1 in 40 and 1435mm track gauge. In this thesis it is designated as *UIC60-S1002-Standard*. As we expected, Fig.3.5.4 indicates that the differences between the results obtained by solving the exact equations and the first-

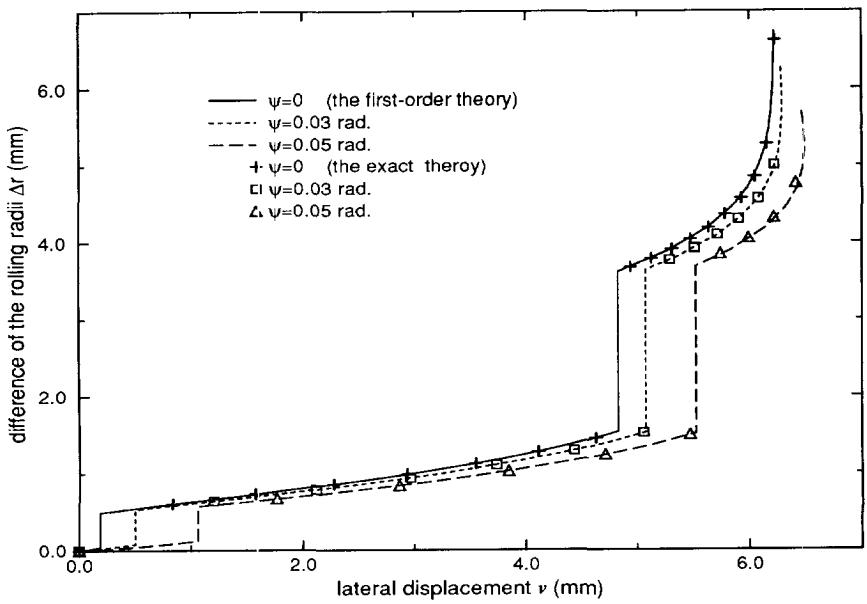

Fig.3.5.4. Comparison of the exact theory and the first-order theory for the *UIC60-S1002-Standard.*

	ν (mm)	Δr (mm)	η_1^* (mm)	η_2^* (mm)	ξ_1^* (mm)	ξ_2^* (mm)
exact theory	5.190	1.389	19.700	-11.106	2.648	-0.190
two-dimensional approach	4.462	1.387	19.824	-9.308	0.0	0.0
first-order theory	5.210	1.389	19.702	-11.114	2.709	-0.194
perturbation method	5.201	1.388	19.680	-11.284	2.704	-0.180

Table.3.5.1. Comparison of the results obtained by various methods for ψ=0.05 rad. and ϕ=0.0003 rad. (the contact coordinates are taken with respect to the initial coordinate systems).

order theory equations are so small that the first-order theory can be considered to yield sufficiently accurate results. Moreover, the computer time to solve the set of four nonlinear algebraic equations of the first-order theory is certainly much less than that to solve the set of eight nonlinear algebraic equations of the exact theory. Fig.3.5.4 and Table.3.5.1 show that the two-dimensional approach is applicable only

when the yaw angle and the lateral displacement are very small. The first-order theory and the perturbation method are recommended for the dynamic simulations. They can be applied both to the tabulation of the contact constraints in advance and to the online calculations. In our computations the first-order theory is adopted.

In the first-order equations (3.4.43)-(3.4.46), the geometric contact of a track-wheelset system primarily depends on the following factors: the profiles of the rails and the wheels, the track gauge, the wheelset gauge, the diameters of the two wheels and the rail inclination, which is only a design variable in the design of new tracks. For the combination of the UIC60 rails and the S1002 wheels, Fig.3.5.5 shows the change of the initial contact position, where the rolling angle and the yaw angle are both equal to zero, in a large range of the track gauge (1420mm-1460mm) for the different rail inclinations. With the largest rail inclination (1 in 20), the initial lateral contact coordinates of the rails and the wheels are smooth functions of the track gauge. By contrast, for the other inclined rails, the coordinates and the contact angles of the initial contact position change discontinuously to the flange of the profiles when the track gauge is varied (see Fig.3.5.6). These contact angles strongly affect the stability of railway vehicles; for a normal rail inclination 1 in 40, the tangent of the initial rail contact angle jumps from the value 0.027 to 0.065 at 1434.62mm track gauge and from 0.128 to 0.302 at 1425mm. In the range of 1434.62mm-1460mm the initial contact angle remains low with values from 0.0088 to 0.027.

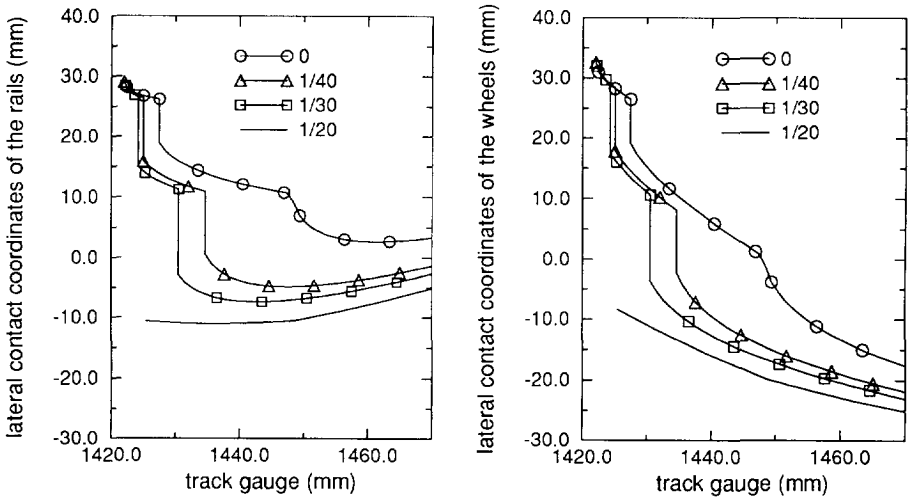

Fig.3.5.5. The lateral coordinate of the initial contact position as a function of the track gauge and the rail inclination for the *UIC60-S1002* combination.

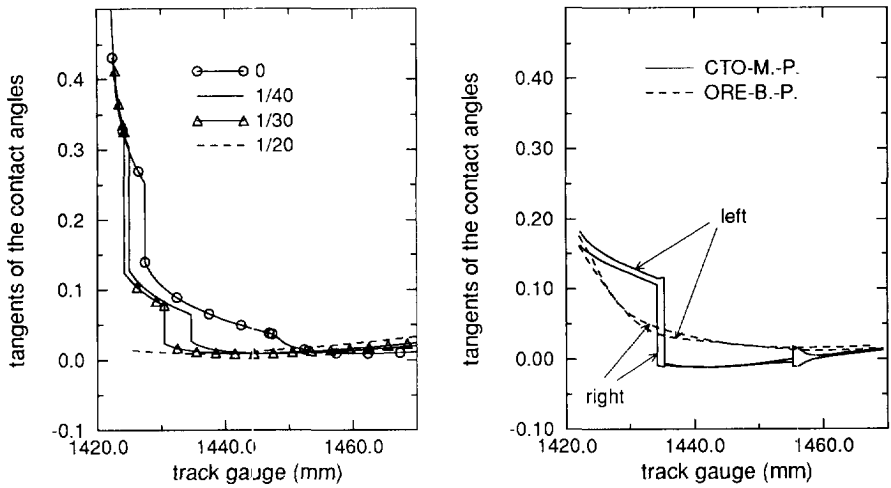

Fig.3.5.6. (a) The contact angles at the initial contact position as functions of the track gauge and the rail inclination for the *UIC60-S1002* combination. (b) The initial contact angles as functions of the track gauge for the *ORE-Benchmark-Profiles* and the *CTO-Measured-Profiles*.

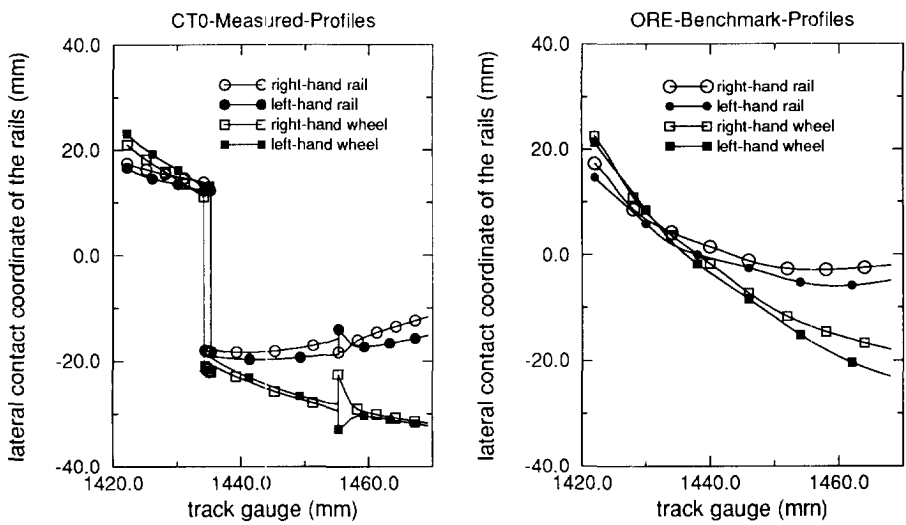

Fig.3.5.7. The lateral coordinate of the initial contact position as a function of the track gauge for *ORE-Benchmark-Profiles* and *CTO-Measured-Profiles*.

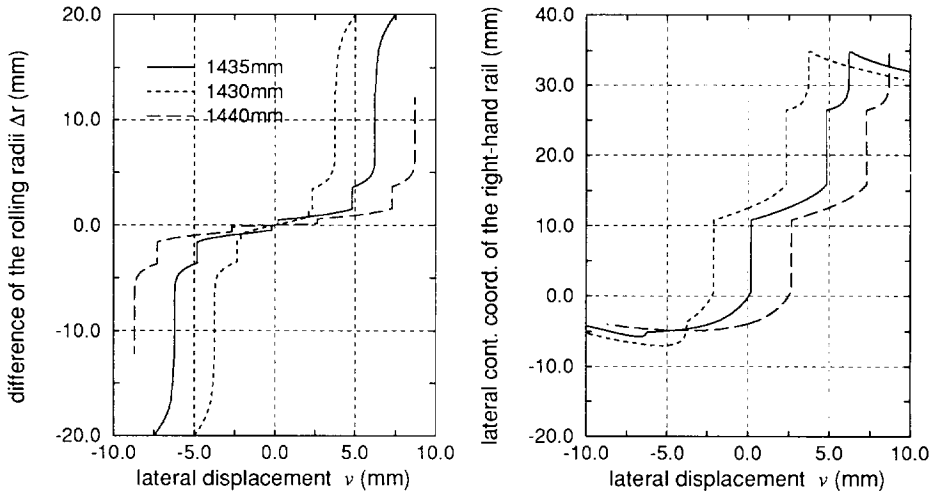

Fig.3.5.8. The influence of the track gauge on the geometric contact for the *UIC60-S1002* combination with the rail inclination 1 in 40.

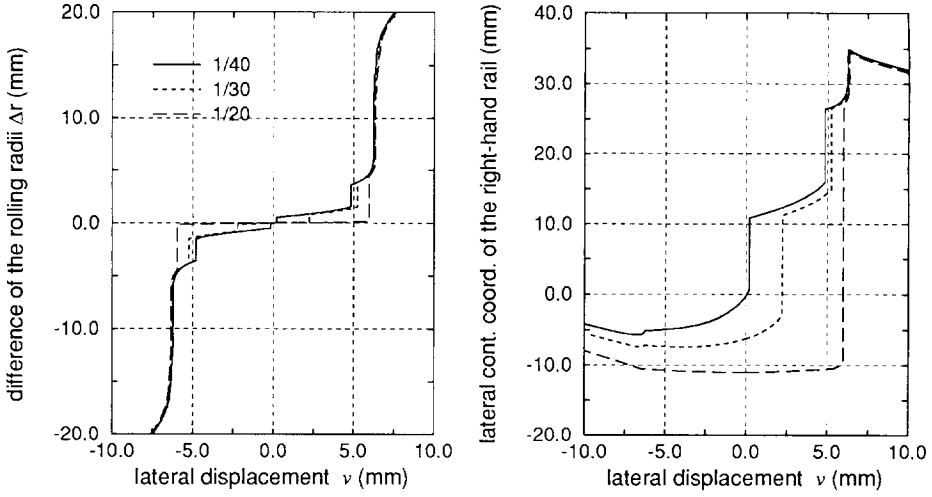

Fig.3.5.9. The influence of the rail inclination on the geometric contact for the *UIC60-S1002* combination with the track gauge 1435mm.

For the other two asymmetric combinations the initial contact angles and the initial contact coordinates are indicated in Figs.3.5.6 and 3.5.7. Around 1434mm track gauge, the contact angles jump from -0.01 to 0.1 for the *CTO-Measured-Profiles*. This combination is the only one having (small) negative contact angles for certain values of the track gauge. Another remarkable result refers to the *ORE-Benchmark-Profiles*; the variation of the track gauge does not induce a jump of the contact position in the whole range from 1425 to 1460mm.

The further investigations of the influences of the track gauge and the inclination on the geometric contact are demonstrated in Fig.3.5.8 and Fig.3.5.9 respectively for the combination of the UIC60 rails and the S1002 wheels, the yaw angle being zero. Because the considered inclinations of the rails are so small as compared to unity that they only slightly change the lateral coordinate of the rail profiles, we can still compare the lateral contact coordinates for the different inclinations in one diagram.

When rail inclination approaches zero, or when the track gauge is reduced, for the same lateral displacement the lateral contact coordinates move towards the flange area, thereby increasing the contact angles. According to the two figures, the lateral displacements corresponding to the double-contact position vary with the track gauge and the rail inclination. In the case of 1 in 40 rail inclination, the contact point on a surface of a rail or a wheel can only be located in three ranges of the profile and between two ranges there is a contact jump, which corresponds to a double-contact position. A jump induces a discontinuity of both the rolling radii difference and the contact angle.

track gauge = 1430mm						
double-contact	v(mm)	Δr(mm)	η_{01}(mm)	η_{02}(mm)	η_{01}^*(mm)	η_{02}^*(mm)
1st	2.113	0.810	15.349	10.863	17.066	8.111
		1.268	15.349	0.542	17.066	-2.210
2nd	2.36	1.397	15.892	-0.444	17.854	-3.441
		3.475	26.397	-0.444	28.359	-3.441
track gauge = 1440mm						
1st	2.658	0.173	0.682	-4.842	-2.156	13.040
		0.623	10.853	-4.842	8.015	13.040
2nd	7.308	1.578	15.900	-4.401	17.858	-17.394
		3.653	26.395	-4.401	28.354	-17.394

Table.3.5.2. The influence of the track gauge on the double-contact positions of *UIC60-S1002-Standard* (see also Fig.3.5.8).

Table.3.5.2 lists the double-contact positions and some associated parameters. From this table and Fig.3.5.8 we find that in spite of the track gauge varying the lateral displacement v where a double-contact occurs, the lateral contact coordinates of the jump positions are almost independent of the track gauge. The numerical results listed in Table.3.5.2 also indicate that at a double-contact position, there exist three contact points in the contacting bodies and hence, the jump of the contact point occurs only at one side. Moreover, for 1430mm track gauge, the first double-contact at v=2.113mm is caused by a jump of the contact point at the left-hand side but the double-contact at v=2.360mm is caused by a jump at the right-hand side.

For the rail inclination 1 in 20, there are only two contact ranges in a profile. When the lateral displacement is in the range from -5.97mm to +5.97mm, the contact point lays on the tread segments of the profiles at both sides and the contact angle is very low (approximately 0.013); once the amplitude of the lateral displacement exceeds 5.97mm, at one side the contact point directly jumps to the flange.

The accuracy of the dynamic analyses can be improved by treating the geometric contact between track and wheelset three-dimensionally, in other words, by taking into account the influence of the yaw angle, especially in case of a conventional vehicle negotiating a narrow curved track.

For the *UIC60-S1002-Standard* combination we have applied the three-dimensional theory and the results are shown in Figs.3.5.10 to 3.5.12. The relations between the generalized coordinates are indicated in Fig.3.5.10; the amplitude of the vertical displacement w is much smaller than that of the lateral displacement in the absence of flange contact. Due to the jump of the contact position, the first derivative of the rolling angle is no longer a continuous function of the lateral displacement. According to Fig.3.5.11, the longitudinal contact coordinate of the left-hand wheel hardly changes with the yaw angle for a positive lateral displacement v; however, the coordinate of the right-hand wheel varies strongly at large positive lateral displacements for non-zero yaw angles. As indicated in Fig 3.5.12 and Table.3.5.3, the yaw angle, like the track gauge, hardly alters the three possible contact ranges on the surfaces of the rails and the wheels. By contrast, the lateral displacement v corresponding to the double-contact position is significantly affected by the yaw angle.

In the *ORE-Benchmark-Profiles*, there is no jump in the tread contact, thus therefore the relations of the generalized coordinates are smooth functions. Because the combination is asymmetric, the zero difference of the rolling radii does no longer correspond to the zero rolling angle and the zero lateral displacement: Δr=0 at $\phi=1.84\text{x}10^{-5}$rad. and v = -0.81mm.

yaw angle ψ = 0						
double-contact	v(mm)	Δr(mm)	η_{01}(mm)	η_{02}(mm)	η_{01}^*(mm)	η_{02}^*(mm)
1st	0.187	0.044	0.663	-0.738	-2.164	-3.948
		0.496	10.854	-0.738	-8.027	-3.948
2nd	4.823	1.537	15.897	-4.913	17.856	-12.908
		3.613	26.396	-4.913	28.356	-12.908
yaw angle ψ = 0.05 rad.						
1st	1.062	0.123	0.621	-3.517	-2.234	-8.535
		0.579	10.876	-3.517	8.065	-8.535
2nd	5.521	1.513	15.700	-4.963	17.557	-14.585
		3.681	26.470	-4.963	28.534	-14.585

Table.3.5.3. The influence of the yaw angle on the double-contact positions of *UIC60-S1002-Standard* (see Fig.3.5.1).

The results shown in Fig.3.5.14 are for the asymmetric combination of the *CTO-Measured-Profiles*. There is a special interval of the lateral displacement v (-1.93mm to -1.14mm for ψ=0rad.) where the difference of the rolling radii is almost zero (Δr=0.012 to 0.028mm). In this interval the contact angles of both rails are small and negative; when the lateral displacement is beyond this interval, one of the rail contact angles still remains negative. By contrast, in the UIC60-S1002 combination and for the *ORE-Benchmark-Profiles*, both rail contact angles are always positive.

When the *CTO-Measured-Rails* are combined with the new wheel profiles S1002, the difference of the rolling radii is found to be almost zero (Δr = -0.058 to 0.063mm) in a larger range of the lateral displacement (v = -5.216 to 1.962mm, see Fig.3.5.15). In this range, the contact angles of both rails are very small. Another example refers to the combination of the *CTO-Measured-Rails* and the BR P8 wheel profiles, which are utilized on major lines in Britain; this combination generates no special range with zero difference of rolling radii so that it may provide suitable conicities in the tread contact area.

As has been shown above, the geometric contact between track and wheelset is very sensitive to the profiles and other geometric parameters. Because the contact strongly influences the dynamic behaviour of railway vehicles, the optimization of these factors is extremely important in the design of the vehicles.

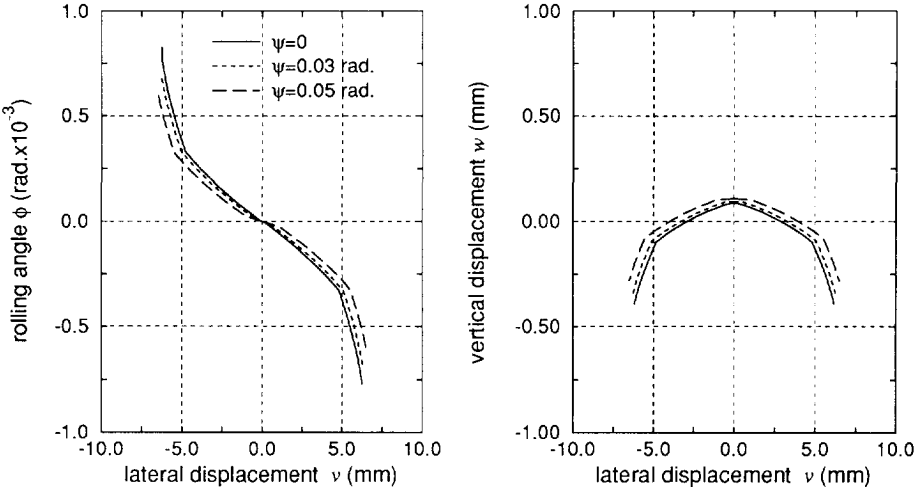

Fig.3.5.10. The relations between the generalized coordinates for the *UIC60-S1002-Standard.*

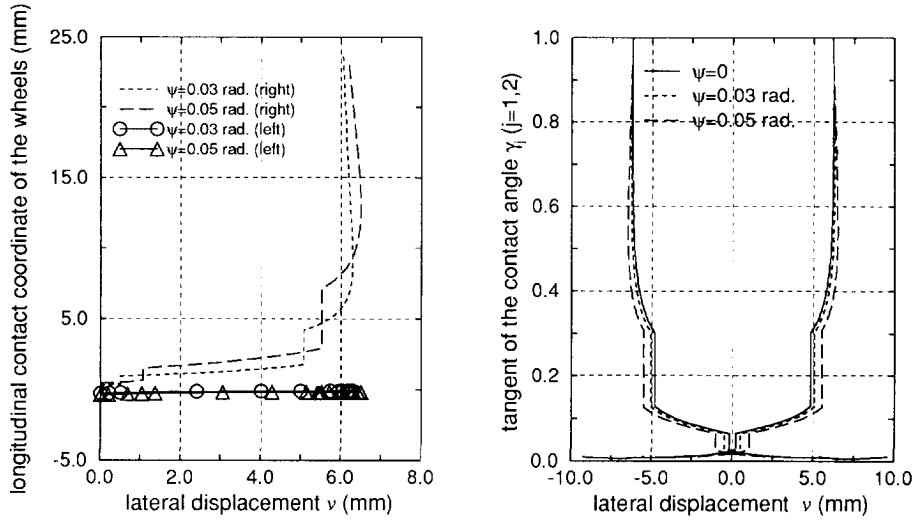

Fig.3.5.11. The longitudinal contact coordinates of the wheels and the contact angles of the rails as functions of the lateral displacement and the yaw angle for the *UIC60-S1002-Standard.*

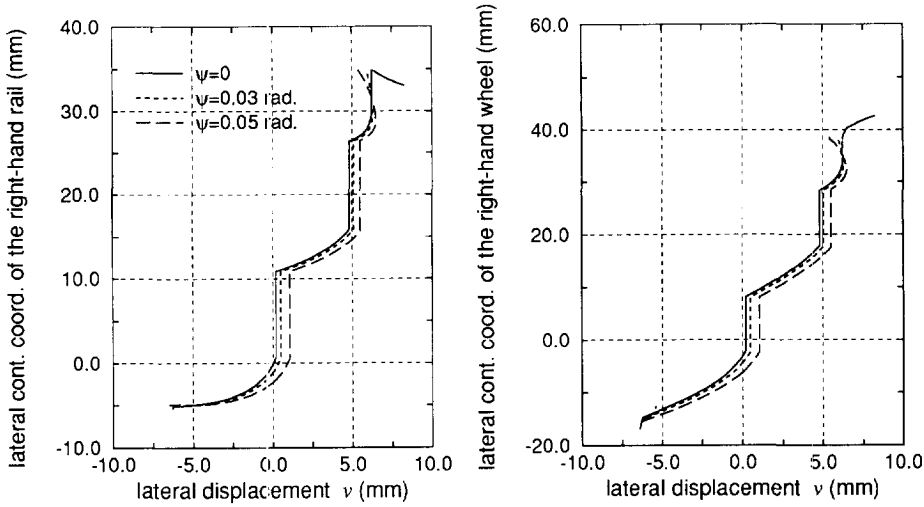

Fig.3.5.12. The lateral contact coordinates of the right-hand rail and wheel as functions of the lateral displacement and the yaw angle for the *UIC60-S1002-Standard.*

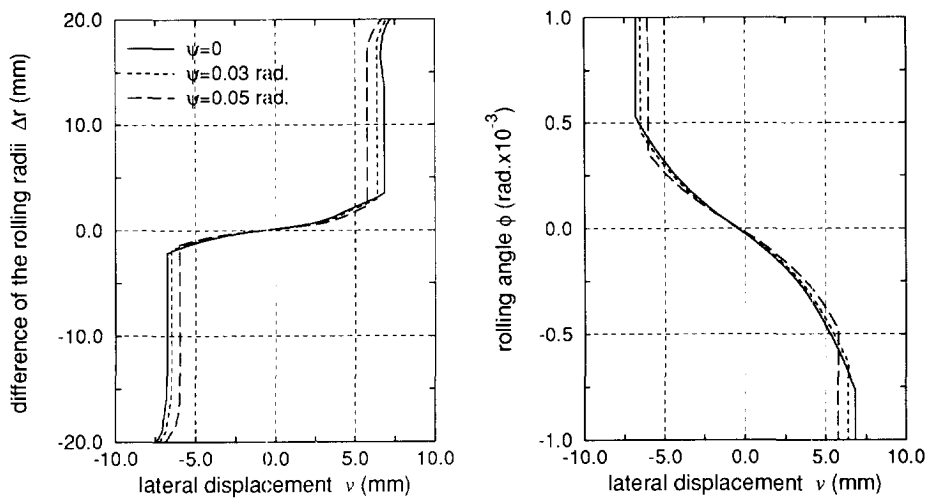

Fig.3.5.13. The rolling radii difference and the rolling angle as functions of the lateral displacement and the yaw angle for the *ORE-Benchmark-Profiles.*

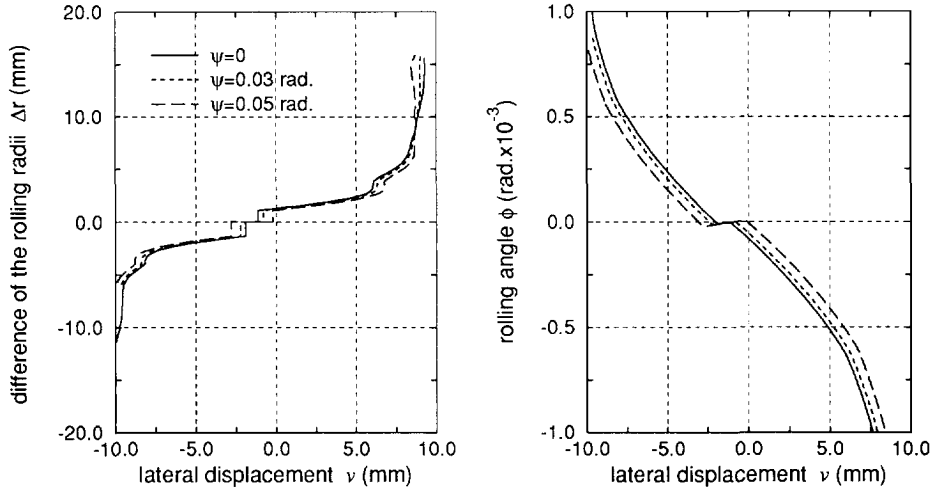

Fig.3.5.14. The rolling radii difference and the rolling angle as functions of the lateral displacement and the yaw angle for the *CTO-Measured-Profiles*.

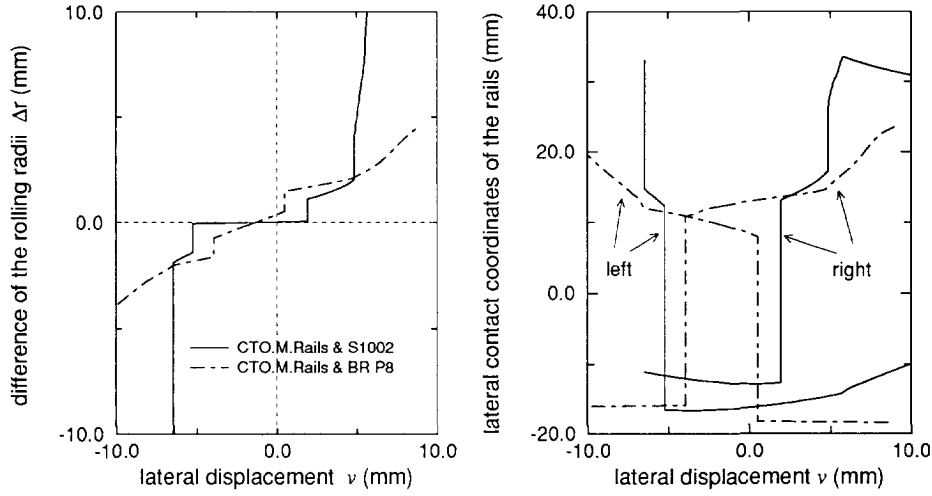

Fig.3.5.15. The rolling radii difference and the lateral contact coordinates as functions of the lateral displacement for the *S1002* or the *BR P8* wheels upon the *CTO-Measured-Rails*.

Chapter 4

Dynamic Models of a Single Wheelset on Various Tracks

4.1. Introduction

The dynamics of a railway vehicle wheelset have long been of interest to specialists in the dynamic field and to railway companies. The hunting of the wheelset observed above a critical vehicle speed is the primary source of the instability of railway vehicles. It is also a significant factor of wear of the rails and the wheels, ride discomfort and derailment. A peak of the acceleration due to the hunting motion also produces high dynamic loads on the suspension through which the wheelset is connected with the bogie, so that the suspension may easily be damaged. This chapter presents the achievements in establishing dynamic models of a single wheelset.

It is well known that the dynamics of a wheelset are inherently nonlinear. Among the sources of nonlinearity especially are important:

- the geometric contact between the rails and the wheels (geometric nonlinearity);
- the creep forces which are the interaction forces between the rails and the wheels (physical nonlinearity);
- the nonlinear characteristics of the suspension.

Only the first and the second types of nonlinearity are taken into account because in this chapter only the motion of a single wheelset is investigated.

De Pater (1961) attempted to investigate analytically the effect of nonlinear elements in railway vehicles by means of the method of Krylov and Bogoliubov. In his nonlinear model contact between wheel flange and rail was described as a collision phenomenon and the linear creep law was assumed to be valid. The limit-cycle and its stability for a two-axle vehicle were determined by means of the so-called equivalent linear equations. Later on, the method of Krylov and Bogoliubov was also applied by Van Bommel (1964), and Law and Brand (1973). Cooperrider and Hedrick *et al.* (1975) developed the quasi-linearization technique to predict the nonlinear response of railway vehicles. Hauschild (1981), Knothe and Moelle (1982) used the Galerkin method to transform the nonlinear equations of motion to a set of

nonlinear algebraic equations; the frequencies, amplitudes and phases of possible limit-cycles were determined from these nonlinear algebraic equations. True (1983) investigated the nonlinear phenomena of Cooperrider's vehicle model by means of the Hopf bifurcation analysis.

It has been shown by De Pater(1979, 1981) that it is possible to derive exact equations of motion for a wheelset moving along a tangent track or a track with constant radius of curvature and with constant cant. From the dynamic point of view, the six equations of motion of the wheelset together with the two constraint equations due to the contact between track and wheelset can be solved for the six generalized coordinates and the two normal contact forces. The tangential forces are determined in terms of the normal contact forces and the geometric and kinematic parameters at the contact points. The theoretical and numerical analysis of a vehicle passing through a curved track were also done by Elkins and Gostling (1977), Duffek *et al.* (1977), and Kortüm and Wormley (1981). Recently, Fisette and Samin (1991) have developed symbolic software to generate the equations of motion and employed the software in the investigation of a railway vehicle system with independent wheels. Nonlinear models of the wheelset have been developed by many investigators such as Burton and Whitman (1980), Mufti and Dukkipati (1982), Kik (1991), Pascal and Sauvage (1991). The problems arising in the development of the mechanical models of the wheelset are well discussed by Elkins (1991).

In the preceding chapter, the geometric constraints between the rigid track and the rigid wheelset have been investigated in detail. The dependent generalized coordinates and the contact position can be determined numerically from the postulation that both wheels remain in contact with their corresponding rails. This finally gives rise to two holonomic constraint equations. The dependent generalized accelerations and the constraint forces can be eliminated from the unreduced differential equation by utilising the corresponding kinematic constraint equations (Yang and De Pater 1991).

In the present chapter, first the creep-force laws used in the dynamic simulations are discussed; see Section 4.2. In Section 4.3, the kinematics of a conventional wheelset are discussed and the kinematic constraints between the track and the wheelset are given in the following section. The general equations of motion of the wheelset given in Section 4.5 are established on the basis of Jourdain's principle. In Sections 4.6 and 4.7, the dynamic models of the wheelset moving along a tangent track and a curved track are derived from the general equations of motion. The effect of track irregularities on the dynamic models is studied in Section 4.8. Finally, in the last section a linear dynamic model for the linear stability analysis is given.

4.2 Rolling Contact Theory

The determination of the contact forces between the rails and the wheels plays an important and critical role in the analysis of the performance of railway vehicles. A detailed and systematic classification of all rolling contact problems was given by Kalker (1990); a brief review has been given in Chapter 3. The linear theory is extensively used in linear lateral stability analyses of railway vehicles for the determination of the critical speed. The Shen-Hedrick-Elkins theory and Kalker's simplified theory (FASTSIM) are both recommended to be utilised in dynamic simulations. The former loses its validity for large values of the spin, so that it is only applicable to cases without flange contact. All these three theories have been numerically verified by the exact contact theory of Kalker (1990) related with the program CONTACT.

4.2.1 Creepages and Spin Creep

Due to the fact that the rolling radii of the two wheels vary along their axis of revolution, the wheelset will, in general, not perform a pure rolling along the track; there exists relative motion in the contact area between a rail and a wheel. The longitudinal creepage υ_x and the lateral creepage υ_y are used to describe the deviations from a pure rolling motion of the two contacting bodies.

In order to define the directions of the creepages and the contact forces, we introduce the contact frame $\{P_j, \bar{e}^{Pj}\}$ (see Fig.4.2.1). Consider a wheel in contact with a rail at the point P_j with the coordinates (x_j^*, y_j^*, z_j^*). The origin of the contact frame is located at the contact point P_j ; its vector basis is obtained from that of the wheelset-body frame $\{o^2, \bar{e}^2\}$ by the rotation $\arctan(x_j^*/z_j^*)$ around the o^2y^2 axis, *viz.* o^*y^* and $\bar{e}_2{}^2$, followed by the rotation $\mp\gamma_j$ around the axis in the direction of the base vector $\bar{e}_1{}^{Pj}$, which is the instantaneous rolling direction of the wheel. Therefore, the relation between the contact frame $\{P_j, \bar{e}^{Pj}\}$ and the wheelset-body frame $\{o^2, \bar{e}^2\}$ can be indicated by

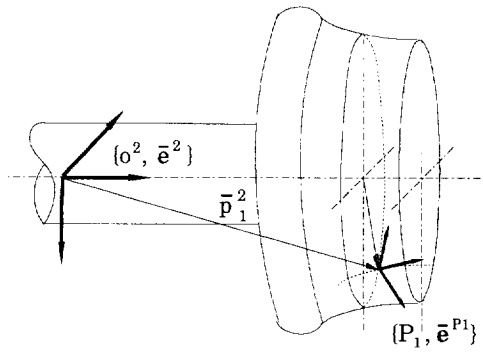

Fig.4.2.1. The contact plane

$$\bar{e}^{Pj} = \boldsymbol{G}^{Pj,2}\,\bar{e}^{2}\,, \tag{4.2.1}$$

where

$$\boldsymbol{G}^{Pj,2} = \begin{bmatrix} \dfrac{z_j^*}{r_j^*} & 0 & -\dfrac{x_j^*}{r_j^*} \\ \mp\dfrac{x_j^*}{r_j^*}\sin\gamma_j^* & \cos\gamma_j^* & \mp\dfrac{z_j^*}{r_j^*}\sin\gamma_j^* \\ \dfrac{x_j^*}{r_j^*}\cos\gamma_j^* & \pm\sin\gamma_j^* & \dfrac{z_j^*}{r_j^*}\cos\gamma_j^* \end{bmatrix}. \tag{4.2.2}$$

The longitudinal and lateral creepages are defined by the components of the relative velocity at the contact point which are taken with respect to the contact frame $\{P_j, \bar{e}^{Pj}\}$, divided by the nominal longitudinal velocity V_n of the wheelset centre. When the relative velocity at the contact point P_j is denoted by $\Delta\bar{v}(P_j)$, the creepage quantities can be found as:

$$\begin{bmatrix} \upsilon_{xj} \\ \upsilon_{yj} \\ 0 \end{bmatrix} = \frac{1}{V_n}\,\Delta v(P_j)\,, \tag{4.2.3}$$

where $\Delta v(P_j)$ is the component vector of $\Delta\bar{v}(P_j)$ with respect to $\{P_j, \bar{e}^{Pj}\}$

Another quantity, *viz.* the spin creepage υ_{spj}, is defined as the ratio between the component of the wheel angular velocity $\bar{\omega}_j$ in the normal of the surfaces at the contact point and the nominal velocity, so that

$$\upsilon_{spj} = \frac{1}{V_n}\,\bar{\omega}_j \cdot \bar{n}(P_j)\,. \tag{4.2.4}$$

4.2.2. Contact Forces[†]

The loading exerted upon the wheel at the contact point includes the normal contact force, the two tangential contact forces and the spin moment. The longitudinal

[†]In Section 4.2.2, the index j to indicate the side of rail and wheel is omitted.

tangential force $\bar{T}_x$, the lateral tangential force $\bar{T}_y$ and the spin moment $\bar{M}_z$ are defined along the directions of the vector basis $\bar{\boldsymbol{e}}^P$; by contrast, the positive normal contact force $\bar{N}$ is taken in the opposite direction of the base vector $\bar{e}_3^P$. Hence,

$$\bar{T}_x = T_x \bar{e}_1^P, \quad \bar{T}_y = T_y \bar{e}_2^P, \quad \bar{M}_z = M_z \bar{e}_3^P, \quad \bar{N} = -N \bar{e}_3^P. \tag{4.2.5}$$

The resultant of the tangential forces is defined by

$$\bar{T} = \boldsymbol{T}^T \bar{\boldsymbol{e}}^P, \tag{4.2.6}$$

with

$$\boldsymbol{T} = [\, T_x, T_y, 0 \,]^T. \tag{4.2.7}$$

This force should be limited by Coulomb's law:

$$\sqrt{T_x^2 + T_y^2} \le \mu N, \tag{4.2.8}$$

where μ is the friction coefficient.

In the three above-mentioned rolling contact theories, the contact area around the contact point, which is found in the geometric contact problem, is determined by Hertz's problem; the semi-axes a and b of the contact ellipse are functions of the normal force, the geometry and the material properties (Love, 1929). The semi-axis a is taken in the rolling direction.

In Kalker's linear theory, the formulae for the creep forces read:

$$T_x = -c^2 G C_{11} \upsilon_x, \tag{4.2.9}$$

$$T_y = -c^2 G C_{22} \upsilon_y - c^3 G C_{23} \upsilon_{sp} \tag{4.2.10}$$

and the spin moment is

$$M_z = c^3 G C_{23} \upsilon_y - c^4 G C_{33} \upsilon_{sp}. \tag{4.2.11}$$

Here G is the shear modulus of the contacting material; $c=(ab)^{1/2}$ is the average radius of the contact ellipse. The creepage and spin coefficients C_{ij} were computed and tabulated by Kalker (1967) as functions of the ratio of the semi-axes of the contact ellipse a/b and Poisson's ratio.

The creep forces are proportional to the creep quantities; the saturation effect given by Eq.(4.2.8) is not taken into account. Therefore, Kalker's linear theory is

only valid for small creepages and small spin creep. Shen, Hedrick and Elkins (1983) improved Kalker's linear theory on the basis of the Vermeulen-Johnson formulae. Shen *et al.* assume that the resultant tangential force T_R is determined by

$$T_R = \begin{cases} \mu N \left[\left(\frac{T_R^*}{\mu N}\right) - \frac{1}{3}\left(\frac{T_R^*}{\mu N}\right)^2 + \frac{1}{27}\left(\frac{T_R^*}{\mu N}\right)^3 \right], & for \quad T_R^* \le 3\mu N \\ \mu N, & for \quad T_R^* \ge 3\mu N \end{cases} \tag{4.2.12}$$

with

$$T_R^* = \sqrt{T_x^{*2} + T_y^{*2}} \,. \tag{4.2.13}$$

T_x^* and T_y^* are calculated according to Eqs.(4.2.9) and (4.2.10). Introducing the reduction coefficient $\varepsilon = T_R / T_R^*$, we obtain the creep forces

$$T_x = \varepsilon T_x^* \tag{4.2.14}$$

and

$$T_y = \varepsilon T_y^* \,. \tag{4.2.15}$$

In Kalker's simplified theory the surface displacement at a point in the contact area depends only on the surface traction at that point and the displacement is proportional to the local surface load. The boundary conditions express that at the leading edge of contact where the particles enter the contact area, the surface loads and the slip vanish. Based on the simplified theory and the saturation effect, the program FASTSIM has been developed (Kalker, 1982). Several investigators (Shen *et al.*, 1983; Fortin, 1984) have tested the accuracy of this procedure. It is reported that the results obtained by FASTSIM are always in good agreement with those determined by the exact rolling contact theory (CONTACT).

4.3. Kinematics of a Wheelset on a Track

In fact, railway vehicles travel not only along a perfect straight track but also along a curved and superelevated guideway. In the kinematic analysis, it is convenient to consider the motions of the individual bodies of a vehicle system to be composed of two parts: first the motion of the system as a whole in a nominal configuration;

secondly, the motions of the individual bodies about the nominal configuration. From the numerical analysis point of view it is also necessary to generate the equations of motion of vehicles in terms of the generalized coordinates with respect to the moving reference frame instead of those with respect to the inertial frame.

4.3.1. Kinematic Analysis of the Track Reference Frame

Consider a single wheelset moving along a track. Both when the track is tangent and when it is curved and superelevated, the motion of the wheelset relative to the inertial frame $\{o^I, \bar{e}^I\}$ can be described by the motion of the track reference frame $\{o^1, \bar{e}^1\}$ relative to the inertial frame combined with the motion of the wheelset relative to the track reference frame (see Fig.4.3.1).

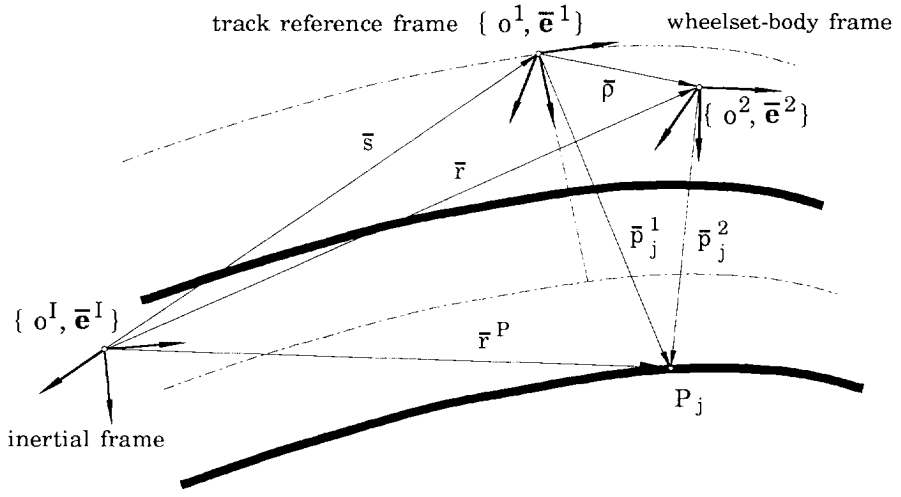

Fig.4.3.1. The coordinate systems.

The position vector of the track reference frame is denoted by $\bar{s}$. In general, we define:

$$\dot{\bar{s}} = {}^1\dot{s}^T \bar{e}^1, \quad {}^1\dot{s} = [V_n, 0, 0]^T. \tag{4.3.1}$$

Following Duffek *et al.* (1977) the orientation of the track reference frame relative to the inertial frame is here described by three consecutive rotations with the angles $(\alpha_1, \alpha_2, \alpha_3)$:

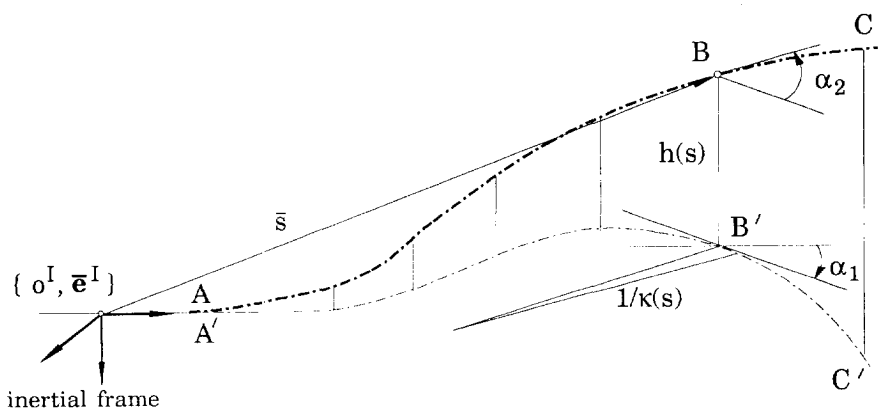

Fig.4.3.2. Definitions of the angles α_1 and α_2.

- α_1 : azimuth-angle (rotation about the base vector $\bar{e}_3^{\,I}$);
- α_2 : climb-angle (angle between the base vector $\bar{e}_1^{\,I}$ and horizontal plane);
- α_3 : cant-angle (rotation about the base vector $\bar{e}_1^{\,I}$; see Fig.C.1a).

In Fig.4.3.2, the curve $A'B'C'$ is the projection of the curve ABC on the horizontal plane. According to Appendix B, the rotation matrix $\mathbf{G}^o$ is defined by

$$\bar{e}^1 = \boldsymbol{G}^o \bar{e}^I, \quad \boldsymbol{G}^o = \boldsymbol{A}^1(\alpha_3)\boldsymbol{A}^2(\alpha_2)\boldsymbol{A}^3(\alpha_1). \tag{4.3.2}$$

The full expression of $\boldsymbol{G}^o$ is:

$$\boldsymbol{G}^o = \begin{bmatrix} \cos\alpha_2\cos\alpha_1 & \cos\alpha_2\sin\alpha_1 & -\sin\alpha_2 \\ \sin\alpha_3\sin\alpha_2\cos\alpha_1-\cos\alpha_3\sin\alpha_1 & \sin\alpha_3\sin\alpha_2\sin\alpha_1+\cos\alpha_3\cos\alpha_1 & \sin\alpha_3\cos\alpha_2 \\ \cos\alpha_3\sin\alpha_2\cos\alpha_1+\sin\alpha_3\sin\alpha_1 & \cos\alpha_3\sin\alpha_2\sin\alpha_1-\sin\alpha_3\cos\alpha_1 & \cos\alpha_3\cos\alpha_2 \end{bmatrix}. \tag{4.3.3}$$

The angular velocity $\bar{\omega}^o$ of the track reference frame reads:

$$\bar{\omega}^o = {}^1\boldsymbol{\omega}^{oT}\bar{e}^1, \quad {}^1\boldsymbol{\omega}^o = \begin{bmatrix} -\dot{\alpha}_1\sin\alpha_2+\dot{\alpha}_3 \\ \dot{\alpha}_1\sin\alpha_3\cos\alpha_2+\dot{\alpha}_2\cos\alpha_3 \\ \dot{\alpha}_1\cos\alpha_3\cos\alpha_2-\dot{\alpha}_2\sin\alpha_3 \end{bmatrix}. \tag{4.3.4}$$

It is assumed that the track is defined by the curvature κ of the curve $A'B'C'$, the

height h and the cant angle α_3; all three quantities are given as functions of the track length s. Furthermore, we have:

$$\alpha_2 = \arcsin[h'(s)], \quad d\alpha_2 = \frac{h''(s)}{\cos\alpha_2} ds \tag{4.3.5}$$

and

$$\alpha_1 = \int_0^s \kappa(s^*)\cos\alpha_2 \, ds^*, \quad d\alpha_1 = \kappa(s)\cos\alpha_2 \, ds. \tag{4.3.6}$$

In this way, for prescribed nominal forward speed $V_n=ds/dt$, the motion of the track reference frame can be completely determined.

4.3.2. Kinematic Analysis of the Wheelset

By quoting the results given in Section 2.1 and the Appendices A and B, the motion of the wheelset mass centre relative to the inertial frame $\{o^I, \bar{e}^I\}$ is expressed as follows:

$$\bar{r} = \bar{s} + \bar{\rho}, \tag{4.3.7}$$

$$\dot{\bar{r}} = \dot{\bar{s}} + \dot{\bar{\rho}} + \bar{\omega}^o \times \bar{\rho}, \tag{4.3.8}$$

and

$$\ddot{\bar{r}} = \ddot{\bar{s}} + \ddot{\bar{\rho}} + \dot{\bar{\omega}}^o \times \bar{\rho} + \bar{\omega}^o \times (\bar{\omega}^o \times \bar{\rho}) + 2\bar{\omega}^o \times \dot{\bar{\rho}}. \tag{4.3.9}$$

where $\dot{\bar{\rho}}$ and $\ddot{\bar{\rho}}$ are the velocity and the acceleration of the wheelset mass centre as seen from the track reference frame $\{o^1, \bar{e}^1\}$.

The wheelset is axisymmetric, so that the rotation of the wheelset about its axis of revolution does not affect the geometry and the complete mass distribution of the system. We define the nominal spin angle as the ratio of the vehicle travel distance s and the nominal rolling radius of the wheels; therefore, the nominal spin angular velocity is

$$\Omega_n = \frac{V_n}{r_o}. \tag{4.3.10}$$

The introduction of the nominal angular velocity Ω_n is important for the linear stability analysis.

The absolute angular velocity of the wheelset is composed of the angular velocity of the track reference frame and the angular velocity of the wheelset relative to the track reference frame:

$$\bar{\omega} = \bar{\omega}^{o} + \bar{\omega}^{21}. \tag{4.3.11}$$

The angular acceleration is then determined by

$$\dot{\bar{\omega}} = \dot{\bar{\omega}}^{o} + \dot{\bar{\omega}}^{21} + \bar{\omega}^{o} \times \bar{\omega}^{21}, \tag{4.3.12}$$

where $\dot{\bar{\omega}}^{21}$ is the angular acceleration as seen from the track reference frame. According to Appendix B, the relative angular velocity of the wheelset is

$$\bar{\omega}^{21} = \boldsymbol{\omega}^{21T}\, \bar{e}^{2} \qquad \text{with} \qquad \boldsymbol{\omega}^{21} = \boldsymbol{H}\,\dot{\boldsymbol{\theta}} - \dot{\boldsymbol{\theta}}_{n}, \tag{4.3.13}$$

where

$$\boldsymbol{H} = \begin{bmatrix} 1 & 0 & 0 \\ 0 & 1 & \sin\phi \\ 0 & 0 & \cos\phi \end{bmatrix}, \qquad \dot{\boldsymbol{\theta}} = \begin{bmatrix} \dot{\phi} \\ \dot{\chi} \\ \dot{\psi} \end{bmatrix}, \qquad \dot{\boldsymbol{\theta}}_{n} = \begin{bmatrix} 0 \\ \Omega_{n} \\ 0 \end{bmatrix}. \tag{4.3.14}$$

Here χ represents the deviation of the nominal spin rotation. Furthermore, the corresponding angular acceleration is given by:

$$\dot{\bar{\omega}}^{21} = \dot{\boldsymbol{\omega}}^{21T}\, \bar{e}^{2} \qquad \text{with} \qquad \dot{\boldsymbol{\omega}}^{21} = \boldsymbol{H}\,\ddot{\boldsymbol{\theta}} + \boldsymbol{h}_{\theta} - \ddot{\boldsymbol{\theta}}_{n}, \tag{4.3.15}$$

where

$$\boldsymbol{h}_{\theta} = \begin{bmatrix} -\dot{\psi}(-\dot{\theta}_{n} + \dot{\chi})\cos\phi \\ \dot{\phi}\,\dot{\psi}\cos\phi \\ (-\dot{\theta}_{n} + \dot{\chi})\,\dot{\phi} - \dot{\phi}\,\dot{\psi}\sin\phi \end{bmatrix}. \tag{4.3.16}$$

When the wheelset moves at the constant forward speed V_n, the nominal spin angular velocity is constant and the nominal angular acceleration vanishes.

Combining the component vector of the absolute velocity (4.3.8) and that of the absolute angular velocity (4.3.11) yields

$$\nu = \begin{bmatrix} \dot{r} \\ \omega^* \end{bmatrix}, \tag{4.3.17}$$

where

$$\bar{\dot{r}} = \dot{r}^T \bar{e}^I, \qquad \bar{\omega} = \omega^{*T} \bar{e}^2. \tag{4.3.18}$$

Similarly, we have

$$\dot{\nu} = \begin{bmatrix} \ddot{r} \\ \dot{\omega}^* \end{bmatrix}, \tag{4.3.19}$$

where the component vectors are defined by

$$\bar{\ddot{r}} = \ddot{r}^T \bar{e}^I, \qquad \bar{\dot{\omega}} = \dot{\omega}^{*T} \bar{e}^2. \tag{4.3.20}$$

Note that $\dot{\nu}$ is not the time derivative of ν because the wheelset-body frame is not embedded rigidly in the wheelset body; it is only used to designate the combination of the wheelset acceleration terms. However, ν and $\dot{\nu}$ are designated as the quasi-velocity and the quasi-acceleration of the wheelset respectively.

4.4. Kinematic Constraints between Wheelset and Track

When two bodies are in contact at a single point as shown in Fig.3.1.1, the motions of the two contacting bodies are restricted. From the kinematic point of view, the contact generates one constraint: at the contact point the normal component of the relative velocity between the two contacting bodies vanishes; as a result, the number of the degrees of freedom of the system reduces by one. The kinematic constraint equation corresponding to the contact point P can be expressed by

$$\Delta \bar{v}(P) \cdot \bar{n}(P) = 0, \tag{4.4.1}$$

where

$$\Delta \bar{v} = \bar{\dot{\rho}} + \bar{\omega}^{21} \times \bar{p}^2, \tag{4.4.2}$$

and

$$\bar{n}(P) = \bar{n}^1(P) = \bar{n}^2(P) \tag{4.4.3}$$

In Eq.(4.4.2), $\bar{\omega}^{21}$ represents the relative angular velocity between the two contacting bodies; $\dot{\bar{\rho}}$ is the velocity vector of the origin of the frame $\{o^2, \bar{e}^2\}$ as viewed from the frame $\{o^1, \bar{e}^1\}$ and $\bar{p}^2$ is the position vector of the contact point relative to the frame $\{o^2, \bar{e}^2\}$ (see Fig.3.1.1). The kinematic constraint equation (4.4.1) is linear in the generalized velocities; the coefficients of the generalized velocities are functions of the contact coordinates and the generalized coordinates. All these coordinates must satisfy the geometric constraint equations (3.1.1) and (3.1.2). Moreover, the kinematic constraint (4.4.1) is holonomic.

For the railway vehicle system the motion is shown in Fig.4.3.1. Here the motion of the wheelset is subject to the two kinematic constraints because both wheels contact their corresponding rails. Therefore, of the six generalized coordinates describing the motion of the wheelset which are the longitudinal, lateral and vertical translations u, v and w, and the rolling, spin and yaw rotations ϕ, θ and ψ (they are defined relative to the track reference frame), only four are independent. From Eq.(4.4.1) the kinematic constraints of the wheelset system are defined by

$$\Delta\bar{v}_j \cdot \bar{n}_j = 0\,, \tag{4.4.4}$$

where $\bar{n}_j$ is the normal vector of the rail (and wheel) surface at the contact point.

The track is fixed on the ground so that it does not move with respect to the inertial frame $\{o^I, \bar{e}^I\}$; therefore, the relative velocity between the wheel and the rail at the contact point is the absolute velocity of the contact point of the wheel and it is calculated by:

$$\Delta\bar{v}_j = \frac{d}{dt}(\bar{r} + \bar{p}_j^{\,2}) = \dot{\bar{r}} + \bar{\omega} \times \bar{p}_j^{\,2}\,. \tag{4.4.5}$$

Substituting (4.4.5) into Eq.(4.4.4), we obtain the kinematic constraint equations of the wheelset system:

$$\bar{n}_j \cdot (\dot{\bar{r}} + \bar{\omega} \times \bar{p}_j^{\,2}) = 0\,. \tag{4.4.6}$$

By means of the contact condition (3.2.30), Eq.(4.4.6) reduces to:

$$\boldsymbol{n}_j^T \boldsymbol{G}^o \dot{\boldsymbol{r}} - \boldsymbol{n}_j^{*T} \tilde{\boldsymbol{p}}_j^* \boldsymbol{\omega}^* = 0\,. \tag{4.4.7}$$

Using (4.3.17), we can therefore rewrite Eq.(4.4.7) in the general form (2.3.9) of a constraint equation:

$$\boldsymbol{D}\,\boldsymbol{v} + \boldsymbol{c} = \boldsymbol{0}\,, \tag{4.4.8}$$

where $\boldsymbol{c} = \boldsymbol{0}$ and

$$\boldsymbol{D} = \begin{bmatrix} \boldsymbol{n}_1^T \boldsymbol{G}^o & -\boldsymbol{n}_1^{*T} \tilde{\boldsymbol{p}}_1^* \\ \boldsymbol{n}_2^T \boldsymbol{G}^o & -\boldsymbol{n}_2^{*T} \tilde{\boldsymbol{p}}_2^* \end{bmatrix}. \tag{4.4.9}$$

In principle, the Jacobian matrix associated with the constraints may be found directly from Eq.(4.4.8). According to Eq.(4.3.8), Eq.(4.3.11) and the contact condition (3.2.25), the relative velocity (4.4.5) can be determined in terms of the motion of the track reference frame and the relative motion of the wheelset:

$$\Delta \bar{v}_j = \dot{\bar{s}} + \bar{\omega}^o \times \bar{p}_j^{\,1} + \dot{\bar{\rho}} + \bar{\omega}^{21} \times \bar{p}_j^{\,2}\,. \tag{4.4.10}$$

Substituting (4.4.10) into Eq.(4.4.6) yields:

$$\bar{n}_j \cdot (\dot{\bar{s}} + \bar{\omega}^o \times \bar{p}_j^{\,1} + \dot{\bar{\rho}} + \bar{\omega}^{21} \times \bar{p}_j^{\,2}) = 0\,. \tag{4.4.11}$$

From (3.2.10), (3.2.23) and (4.3.13), we obtain the scalar:

$$\bar{n}_j \cdot (\bar{\omega}^{21} \times \bar{p}_j^{\,2}) = \begin{vmatrix} \dfrac{x_j^*}{r_j^*}\cos\gamma_j^* & \pm\sin\gamma_j^* & \dfrac{z_j^*}{r_j^*}\cos\gamma_j^* \\ \dot{\phi} & (-\dot{\theta}_n + \dot{\chi}) + \dot{\psi}\sin\phi & \dot{\psi}\cos\phi \\ x_j^* & y_j^* & z_j^* \end{vmatrix} \tag{4.4.12}$$

$$= \cos\gamma_j^* (-x_j^* \cos\phi\, \dot{\psi} + z_j^* \dot{\phi}) (\mp \mathrm{tg}\gamma_j^* + \frac{y_j^*}{r_j^*})\,.$$

Obviously, due to the absence of the spin rotation of the wheelset in this triple product, we observe that the contact constraints are independent of the spin rotation as might be expected; only the remaining five generalized velocities are restricted by the two constraints. Therefore the spin rotation is always chosen to be one of the independent generalized coordinates.

By introducing the quantities:

$$C_j^* = \cos\gamma_j^* \left(\mp \operatorname{tg}\gamma_j^* + \frac{y_j^*}{r_j^*} \right), \tag{4.4.13}$$

and supposing that $\bar{n}_j = \boldsymbol{n}_j^T \bar{\boldsymbol{e}}^1$ with $\boldsymbol{n}_j = [n_{jx}, n_{jy}, n_{jz}]^T$, from Eq.(4.4.11) the linear relations between the six generalized velocities can be found as:

$$\begin{bmatrix} n_{1x} & n_{1y} & n_{1z} & z_1^* C_1^* & 0 & -x_1^* C_1^* \cos\phi \\ n_{2x} & n_{2y} & n_{2z} & z_2^* C_2^* & 0 & -x_2^* C_2^* \cos\phi \end{bmatrix} \begin{bmatrix} \dot{\boldsymbol{\rho}} \\ \dot{\theta} \end{bmatrix} + \boldsymbol{\xi}(t) = \mathbf{0}, \tag{4.4.14}$$

where

$$\boldsymbol{\xi}(t) = \begin{bmatrix} \bar{n}_1 \cdot (\dot{\bar{s}} + \bar{\omega}^o \times \bar{p}_1^1) \\ \bar{n}_2 \cdot (\dot{\bar{s}} + \bar{\omega}^o \times \bar{p}_2^1) \end{bmatrix}. \tag{4.4.15}$$

Eq.(4.4.15) indicates the contribution of the motion of the track reference frame, which is known as a function of the time t and the generalized coordinates (the position vectors of the contact points relative to the track reference frame). When the equations of the rail surfaces are independent of the distance s, it can be proved that $\bar{n}_j \cdot (\dot{\bar{s}} + \bar{\omega}^o \times \bar{p}_j^1)$ is equal to zero (see Appendix E). This holds, for example, for the cases of the tangent track and the track with constant radius and cant.

Usually, the longitudinal generalized coordinate u is chosen to be one of the independent generalized coordinates. Especially, when the rails in a small track segment around the origin of the track reference frame are assumed to be cylindrical, we know from Eq.(3.2.17) that n_{jx} is equal to zero. This shows that the longitudinal generalized velocity is independent of the kinematic constraints of the wheelset system. In principle, we may choose any two of the remaining four generalized coordinates to be independent. For example, when the lateral and vertical displacements v and w are chosen as the dependent generalized coordinates, it follows from Eq.(4.4.14) that their generalized velocities can be written as linear combinations of the independent generalized velocities $\dot{u}$, $\dot{\phi}$ and $\dot{\psi}$. Similarly, the generalized velocities $\dot{w}$ and $\dot{\phi}$ can be expressed as linear combinations of the independent generalized velocities $\dot{u}$, $\dot{v}$ and $\dot{\psi}$.

Generally, the generalized velocities may be expressed in terms of the independent generalized velocities:

$$\begin{bmatrix} \dot{\boldsymbol{\rho}} \\ \dot{\boldsymbol{\theta}} \end{bmatrix} = \boldsymbol{J}\,\dot{\boldsymbol{q}} + \boldsymbol{\varepsilon}(t), \tag{4.4.16}$$

where the four components of vector $\dot{\boldsymbol{q}}$ are the independent generalized velocities and the vector $\boldsymbol{\varepsilon}(t)$ is determined by the motion of the track reference frame. Because the contact constraints of the wheelset system are holonomic, Eq.(4.4.16) can in principle be integrated and $\boldsymbol{J}$ is the Jacobian matrix. Whether the lateral and vertical displacements v, w or the vertical displacement w and the rolling angle ϕ are chosen as the dependent generalized coordinates, the partial derivatives of the dependent generalized coordinates with respect to the independent ones in the Jacobian matrix $\boldsymbol{J}$ can be found from Eq.(4.4.14).

The generalized accelerations may be obtained by differentiating Eq.(4.4.16) with respect to time:

$$\begin{bmatrix} \ddot{\boldsymbol{\rho}} \\ \ddot{\boldsymbol{\theta}} \end{bmatrix} = \boldsymbol{J}\,\ddot{\boldsymbol{q}} + \dot{\boldsymbol{J}}\,\dot{\boldsymbol{q}} + \dot{\boldsymbol{\varepsilon}}(t). \tag{4.4.17}$$

The second partial derivatives implied in $\dot{\boldsymbol{J}}$ and $\dot{\boldsymbol{\varepsilon}}(t)$ can be calculated numerically or by means of a perturbation method (De Pater 1992).

Finally, from (4.3.8)-(4.3.16), (4.4.16) and (4.4.17) the quasi-velocity and the quasi-acceleration vectors defined by (4.3.17) and (4.3.19) can be expressed as functions of the independent generalized velocities and accelerations:

$$\boldsymbol{v} = \boldsymbol{A}\,\dot{\boldsymbol{q}} + \boldsymbol{b}_v, \tag{4.4.18}$$

$$\dot{\boldsymbol{v}} = \boldsymbol{A}\,\ddot{\boldsymbol{q}} + \boldsymbol{b}_a, \tag{4.4.19}$$

where

$$\boldsymbol{A} = \boldsymbol{H}^*\boldsymbol{J}, \qquad \boldsymbol{H}^* = diag[\,\boldsymbol{G}^{oT},\ \boldsymbol{H}\,], \tag{4.4.20}$$

$$\boldsymbol{b}_v = \boldsymbol{H}^*\,\boldsymbol{\varepsilon}(t) + \boldsymbol{\varepsilon}_v(t), \tag{4.4.21}$$

$$\boldsymbol{b}_a = \boldsymbol{H}^*\,(\dot{\boldsymbol{J}}\dot{\boldsymbol{q}} + \dot{\boldsymbol{\varepsilon}}) + \boldsymbol{\varepsilon}_a(t), \tag{4.4.22}$$

with

$$\boldsymbol{\varepsilon}_v(t) = \begin{bmatrix} \bar{\boldsymbol{e}}^1 \cdot \dot{\bar{s}} \\ -\dot{\boldsymbol{\theta}}_n \end{bmatrix} + \begin{bmatrix} \bar{\boldsymbol{e}}^1 \cdot \bar{\boldsymbol{\omega}}^o \times \bar{\boldsymbol{\rho}} \\ \bar{\boldsymbol{e}}^2 \cdot \bar{\boldsymbol{\omega}}^o \end{bmatrix}, \tag{4.4.23}$$

$$\boldsymbol{\varepsilon}_a(t) = \begin{bmatrix} \bar{\boldsymbol{e}}^1 \cdot \ddot{\bar{s}} \\ \boldsymbol{h}_\theta - \ddot{\boldsymbol{\theta}}_n \end{bmatrix} + \begin{bmatrix} \bar{\boldsymbol{e}}^1 \cdot \{ \dot{\bar{\boldsymbol{\omega}}}^o \times \bar{\boldsymbol{\rho}} + \bar{\boldsymbol{\omega}}^o \times (\bar{\boldsymbol{\omega}}^o \times \bar{\boldsymbol{\rho}}) + 2\bar{\boldsymbol{\omega}}^o \times \dot{\bar{\boldsymbol{\rho}}} \} \\ \bar{\boldsymbol{e}}^2 \cdot (\dot{\bar{\boldsymbol{\omega}}}^o + \bar{\boldsymbol{\omega}}^o \times \bar{\boldsymbol{\omega}}^{21}) \end{bmatrix}. \tag{4.4.24}$$

The 6×4 matrix $\boldsymbol{A}$ and the vectors $\boldsymbol{b}_v$ and $\boldsymbol{b}_a$ are only functions of the generalized coordinates and time. In the case of a tangent track, the second vectors in the right-hand sides of Eq.(4.4.23) and Eq.(4.4.24) vanish because $\bar{\boldsymbol{\omega}}^o$ is equal to zero. For the general case, Eqs.(4.4.23) and (4.4.24) can be rewritten to:

$$\boldsymbol{\varepsilon}_v(t) = \begin{bmatrix} \boldsymbol{G}^{oT}\, {}^1\dot{\boldsymbol{s}} \\ -\dot{\boldsymbol{\theta}}_n \end{bmatrix} + \begin{bmatrix} \boldsymbol{G}^{oT}\, {}^1\tilde{\boldsymbol{\omega}}^o \boldsymbol{\rho} \\ \boldsymbol{G}^{21}\, {}^1\boldsymbol{\omega}^o \end{bmatrix}, \tag{4.4.25}$$

$$\boldsymbol{\varepsilon}_a(t) = \begin{bmatrix} \boldsymbol{G}^{oT}\, {}^1\ddot{\boldsymbol{s}} \\ \boldsymbol{h}_\theta - \ddot{\boldsymbol{\theta}}_n \end{bmatrix} + \begin{bmatrix} \boldsymbol{G}^{oT}({}^1\tilde{\boldsymbol{\omega}}^o\, {}^1\dot{\boldsymbol{s}} - \tilde{\boldsymbol{\rho}}\, {}^1\dot{\boldsymbol{\omega}}^o + {}^1\tilde{\boldsymbol{\omega}}^o\, {}^1\tilde{\boldsymbol{\omega}}^o \boldsymbol{\rho} + 2\, {}^1\tilde{\boldsymbol{\omega}}^o \dot{\boldsymbol{\rho}}) \\ \boldsymbol{G}^{21}\, {}^1\dot{\boldsymbol{\omega}}^o - \tilde{\boldsymbol{\omega}}^{21} \boldsymbol{G}^{21}\, {}^1\boldsymbol{\omega}^o \end{bmatrix}. \tag{4.4.26}$$

4.5. General Equations of Motion of a Wheelset Running on an Arbitrary Track

The wheelset system is a dynamic system containing one body subject to the two contact constraints. Jourdain's principle discussed in Chapter 2 leads to the equations of motion of the wheelset system:

$$\delta \boldsymbol{v}^T (\boldsymbol{M}\dot{\boldsymbol{v}} - \boldsymbol{g} - \boldsymbol{f}) = 0, \tag{4.5.1}$$

where the components of the velocity and the virtual velocity have to satisfy the constraint equations:

$$\boldsymbol{D}\,\boldsymbol{v} + \boldsymbol{c} = \boldsymbol{0}, \qquad \boldsymbol{D}\,\delta\boldsymbol{v} = \boldsymbol{0}. \tag{4.5.2}$$

In agreement with (4.4.18) this leads to

$$\boldsymbol{v} = \boldsymbol{A}\,\dot{\boldsymbol{q}} + b_v, \qquad \delta\boldsymbol{v} = \boldsymbol{A}\,\delta\dot{\boldsymbol{q}}. \tag{4.5.3}$$

For the wheelset system, the 2×6 matrix $\boldsymbol{D}$ is given by Eq.(4.4.9), the 6×4 matrix $\boldsymbol{A}$ by Eq.(4.4.20) and

$$\boldsymbol{M} = \begin{bmatrix} m\boldsymbol{E} & \boldsymbol{0} \\ \boldsymbol{0} & \boldsymbol{I} \end{bmatrix}, \qquad \boldsymbol{g} = \begin{bmatrix} \boldsymbol{0} \\ -\tilde{\boldsymbol{\omega}}^{*}\boldsymbol{I}\,\boldsymbol{\omega}^{*} \end{bmatrix}. \tag{4.5.4}$$

Here m represents the mass of the wheelset and $\boldsymbol{I}$ the inertia matrix of the wheelset; $\boldsymbol{f}$ contains the resultant force and the resultant torque applied at the system.

Due to the constraint (4.5.2) this system has only four degrees of freedom. In general, the spin angle χ and the longitudinal displacement u are always chosen as independent generalized coordinates; the other two are chosen from the remaining four generalized coordinates which are the lateral and vertical displacements v, w, and the rolling and yaw angles ϕ, ψ. Therefore, the general equations of motion of a single wheelset on an arbitrary track can be written in terms of the independent generalized coordinates:

$$\boldsymbol{M}_A\,\ddot{\boldsymbol{q}} - \boldsymbol{A}^T(\boldsymbol{f}_g + \boldsymbol{f}) = \boldsymbol{0}, \tag{4.5.5}$$

where

$$\boldsymbol{M}_A = \boldsymbol{A}^T\boldsymbol{M}\,\boldsymbol{A}, \qquad \boldsymbol{f}_g = -\boldsymbol{M}\,\boldsymbol{b}_a + \boldsymbol{g}. \tag{4.5.6}$$

The vector $\boldsymbol{q}$ contains the four independent generalized coordinates; the vector $\boldsymbol{b}_a$ is given by (4.4.22). The 4×1 vector $\boldsymbol{A}^{\mathrm{T}}\boldsymbol{f}_g$ describes the generalized gyroscopic forces and the 4×1 vector $\boldsymbol{A}^{\mathrm{T}}\boldsymbol{f}$ includes the generalized applied forces.

The resultant impressed force and torque $\boldsymbol{f}$ applied at the wheelset system can be separated into two parts: $\boldsymbol{f} = \boldsymbol{f}_{\mathrm{e}} + \boldsymbol{f}_{\mathrm{C}}$. The first part $\boldsymbol{f}_{\mathrm{e}}$ contains the components of the impressed forces and the components of the impressed torques with the exception of the contribution of the contact forces and the contact spin moments. The gravity force of the wheelset is incorporated in $\boldsymbol{f}_{\mathrm{e}}$. The second part $\boldsymbol{f}_{\mathrm{C}}$ is due to the forces and the torques in the contact patches. We know that the normal contact forces are constraint forces and therefore, $\boldsymbol{f}_{\mathrm{C}}$ comprises only the tangential contact forces and the spin moments which are considered as impressed forces and torques respectively.

According to (4.2.5), the resultant impressed force due to the contacts at both

sides of the wheelset system reads

$$\bar{f}_{tCT} = \bar{T}_1 + \bar{T}_2 = f_T^T [\, G^{oT} G^{12} G^{2,P1},\ G^{oT} G^{12} G^{2,P2} \,]^T \bar{e}^I , \tag{4.5.7}$$

where

$$f_T = [\, T_{x1},\ T_{y1},\ 0,\ T_{x2},\ T_{y2},\ 0 \,]^T . \tag{4.5.8}$$

The resultant torque due to the contacts is

$$\begin{aligned} \bar{f}_{rCM} &= \sum_{j=1}^{2} (\bar{M}_{zj} + \bar{p}_j^2 \times \bar{T}_j) \\ &= f_M^T [\, n_1^*,\ n_2^* \,]^T \bar{e}^2 + f_T^T [\, \tilde{p}_1^* G^{2,P1},\ \tilde{p}_2^* G^{2,P2} \,]^T \bar{e}^2 , \end{aligned} \tag{4.5.9}$$

where

$$f_M = [\, M_{z1},\ M_{z2} \,]^T , \tag{4.5.10}$$

Therefore, combining (4.5.7) and (4.5.9) yields

$$f_C = U_T f_T + U_M f_M . \tag{4.5.11}$$

Obviously, the first three components of f_C, which are taken with respect to the inertial frame, represent the total contact force; the remaining three components represent the total torque due to the contacts and they are taken with respect to the wheelset-body frame. The matrices in Eq.(4.5.11) are

$$U_T = \begin{bmatrix} G^{oT} G^{12} G^{2,P1} & G^{oT} G^{12} G^{2,P2} \\ \tilde{p}_1^* G^{2,P1} & \tilde{p}_2^* G^{2,P2} \end{bmatrix} \tag{4.5.12}$$

and

$$U_M = \begin{bmatrix} \mathbf{0} & \mathbf{0} \\ n_1^* & n_2^* \end{bmatrix} . \tag{4.5.13}$$

As discussed in Section 4.2, the tangential contact forces and the spin moments are functions of the creepages and the spin creeps. By means of (4.2.3), (4.2.4), (4.3.11) and (4.4.10), we find for the creep quantities:

$$\begin{bmatrix} \upsilon_{xj} \\ \upsilon_{yj} \\ 0 \end{bmatrix} = \frac{1}{V_n} \boldsymbol{G}^{Pj,2} \left\{ \boldsymbol{G}^{21} \left({}^{1}\dot{\boldsymbol{s}} + {}^{1}\tilde{\boldsymbol{\omega}}^{o} \boldsymbol{p}_j \right) + \boldsymbol{G}^{21} \dot{\boldsymbol{\rho}} + \tilde{\boldsymbol{\omega}}^{21} \boldsymbol{p}_j^{*} \right\}, \tag{4.5.14}$$

and

$$\upsilon_{spj} = \frac{1}{V_n} \left(\boldsymbol{n}_j^{T} {}^{1}\boldsymbol{\omega}^{o} + \boldsymbol{n}_j^{*T} \boldsymbol{\omega}^{21} \right). \tag{4.5.15}$$

On the other hand, the tangential contact forces and the spin moments are also functions of the normal contact forces, which are the constraint forces corresponding to the kinematic constraints (4.5.2), so that the normal contact forces need to be determined. Corresponding to the constraints (4.5.2), Eq.(2.3.17) gives the vector of the Lagrangian multipliers $\boldsymbol{\lambda}$,

$$\boldsymbol{\lambda} = -(\boldsymbol{D}\boldsymbol{M}^{-1}\boldsymbol{D}^{T})^{-1}\boldsymbol{D}\boldsymbol{M}^{-1}(\boldsymbol{f}_g + \boldsymbol{f}). \tag{4.5.16}$$

To check the physical interpretation of these Lagrangian multipliers, *i.e.* the relationship between the multipliers and the normal contact forces, we have to know the so-called distribution matrix of the normal contact forces. The formula for the resultant constraint forces applied at the wheelset body reads:

$$\bar{f}_{tCN} = \bar{N}_1 + \bar{N}_2 = -\boldsymbol{f}_N^{T} [\, \boldsymbol{G}^{oT} \boldsymbol{n}_1 \,,\, \boldsymbol{G}^{oT} \boldsymbol{n}_2 \,]^{T} \bar{\boldsymbol{e}}^{I}, \tag{4.5.17}$$

where $\boldsymbol{f}_N = [\, N_1 \,,\, N_2 \,]^{T}$. The resultant constraint torque is:

$$\bar{f}_{rCN} = \bar{p}_1^{2} \times \bar{N}_1 + \bar{p}_2^{2} \times \bar{N}_2 = -\boldsymbol{f}_N^{T} [\, \tilde{\boldsymbol{p}}_1^{*} \boldsymbol{n}_1^{*} \,,\, \tilde{\boldsymbol{p}}_2^{*} \boldsymbol{n}_2^{*} \,]^{T} \bar{\boldsymbol{e}}^{2}. \tag{4.5.18}$$

Combining (4.5.17) and (4.5.18) yields:

$$\boldsymbol{f}_{CN} = \boldsymbol{U}_N \boldsymbol{f}_N, \tag{4.5.19}$$

where the 6×2 matrix $\boldsymbol{U}_N$ is the distribution matrix of the normal contact forces and is determined by:

$$\boldsymbol{U}_N = -\begin{bmatrix} \boldsymbol{G}^{oT} \boldsymbol{n}_1 & \boldsymbol{G}^{oT} \boldsymbol{n}_2 \\ \tilde{\boldsymbol{p}}_1^{*} \boldsymbol{n}_1^{*} & \tilde{\boldsymbol{p}}_2^{*} \boldsymbol{n}_2^{*} \end{bmatrix}. \tag{4.5.20}$$

Comparing (4.5.20) and (4.4.9), we find $\boldsymbol{U}_N = -\boldsymbol{D}^{T}$. Therefore, the vector $\boldsymbol{f}_N$ of

the normal contact forces is equal to $-\boldsymbol{\lambda}$, *viz.*

$$\boldsymbol{f}_N = (\boldsymbol{D}\boldsymbol{M}^{-1}\boldsymbol{D}^T)^{-1}\boldsymbol{D}\boldsymbol{M}^{-1}(\boldsymbol{f}_g + \boldsymbol{f}). \tag{4.5.21}$$

Meanwhile, we verify that the distribution matrix $\boldsymbol{U}_N$ is orthogonal to the transpose of the matrix $\boldsymbol{A}$, in agreement with Eq.(2.3.11).

Because the normal contact forces are incorporated in the general reduced equations of motion of the wheelset, Eqs.(4.5.5) and (4.5.21) are coupled; therefore, they must be solved simultaneously. During a numerical integration, good approximations for the normal contact forces are available from the preceding integration step. Thus, only a few iterations, possibly just one, are required to generate the solution. When we start the integration of Eq.(4.5.5), the normal contact forces often have to be determined in the absence of good starting values.

4.6. Equations of Motion of a Wheelset on a Tangent Track

For the tangent track, the vector basis of the track reference frame $\{o^1, \bar{\boldsymbol{e}}^1\}$ remains parallel to that of the inertial frame $\{o^I, \bar{\boldsymbol{e}}^I\}$; this implies that many terms comprised in the general equations of motion (4.5.5) will be simplified considerably. First of all, the angular velocity of the track reference frame vanishes and the rotation matrix $\boldsymbol{G}^o$ is the 3×3 unit matrix:

$$\bar{\omega}^o = 0, \quad \boldsymbol{G}^o = \boldsymbol{E}, \tag{4.6.1}$$

so that according to Eq.(4.3.8) the component vector of the absolute velocity of the wheelset mass centre with respect to the inertial frame is determined by

$$\dot{\boldsymbol{r}} = \dot{\boldsymbol{s}} + \dot{\boldsymbol{\rho}}. \tag{4.6.2}$$

According to Eq.(4.3.11) the component vector of the absolute angular velocity of the wheelset with respect to the wheelset-body frame reduces to

$$\boldsymbol{\omega}^* = \boldsymbol{\omega}^{21}. \tag{4.6.3}$$

The normal vector of the contact plane with respect to the track reference frame is given in (3.2.17):

$$\bar{n}_j = \boldsymbol{n}_j^T \bar{\boldsymbol{e}}^1, \quad \boldsymbol{n}_j = [\,n_{jx},\, n_{jy},\, n_{jz}\,]^T = [\,0,\, \pm\sin\gamma_j,\, \cos\gamma_j\,]^T. \tag{4.6.4}$$

From Eq.(4.4.14) we know that the displacement u is independent of the kinematic

constraints in the case of a tangent track. Moreover, substituting (4.6.1) and (4.6.4) into Eq.(4.4.15), we find that $\boldsymbol{\xi}(t) = \mathbf{0}$. As a result, the dependent generalized coordinates are independent of the displacement u and time t.

In literature the equations of motion of the wheelset are often derived in terms of the lateral displacement v and the yaw angle ψ; the vertical displacement w and the rolling angle ϕ are then the dependent generalized coordinates. In this case the vector of the independent generalized coordinates reads:

$$\boldsymbol{q} = [\, u,\ v,\ \chi,\ \psi \,]^T. \tag{4.6.5}$$

As stated before, the dependent generalized coordinates are functions of only two independent generalized coordinates: the lateral displacement v and the yaw angle ψ. In general, these functions cannot be expressed explicitly; they can only be found numerically from the equations based on the geometric compatibility conditions of two bodies in contact. By contrast, once the contact coordinates are attained, the kinematic constraint equations can be explicitly written in terms of the linear generalized velocities, *viz.* Eq.(4.4.14). Therefore, the Jacobian matrix, which corresponds to the geometric contact constraints, can be determined from the kinematic constraint equations. As a result, we obtain

$$\boldsymbol{J} = \begin{bmatrix} 1 & 0 & 0 & 0 \\ 0 & 1 & 0 & 0 \\ 0 & w_{,v} & 0 & w_{,\psi} \\ 0 & \phi_{,v} & 0 & \phi_{,\psi} \\ 0 & 0 & 1 & 0 \\ 0 & 0 & 0 & 1 \end{bmatrix}. \tag{4.6.6}$$

Solving Eq.(4.4.14) for the dependent generalized velocities, we find the first partial derivatives in the matrix $\boldsymbol{J}$:

$$\phi_{,v} = \frac{1}{z_1^* C_1 - z_2^* C_2}, \tag{4.6.7}$$

$$\phi_{,\psi} = \frac{(x_1^* C_1 - x_2^* C_2)\cos\phi}{z_1^* C_1 - z_2^* C_2} \tag{4.6.8}$$

and

$$w_{,v} = \frac{z_1^* \,\mathrm{tg}\gamma_2 C_1 + z_2^* \,\mathrm{tg}\gamma_1 C_2}{z_1^* C_1 - z_2^* C_2}, \tag{4.6.9}$$

$$w_{,\psi} = \frac{(x_1^* z_2^* - x_2^* z_1^*) C_1 C_2 (\mathrm{tg}\gamma_1 + \mathrm{tg}\gamma_2)\cos\phi}{z_1^* C_1 - z_2^* C_2}. \tag{4.6.10}$$

where

$$C_j = -\frac{1}{\mathrm{tg}\gamma_1 + \mathrm{tg}\gamma_2} \frac{\cos\gamma_j^*}{\cos\gamma_j} \left(\mp \mathrm{tg}\gamma_j + \frac{y_j^*}{r_j^*} \right). \tag{4.6.11}$$

Moreover, the vectors $\boldsymbol{b}_v$ and $\boldsymbol{b}_a$ in Eqs.(4.4.21)-(4.4.22) reduce to:

$$\boldsymbol{b}_v = \boldsymbol{\varepsilon}_v = \left[V_n,\ 0,\ 0,\ 0,\ -\Omega_n,\ 0 \right]^T \tag{4.6.12}$$

and

$$\boldsymbol{b}_a = \dot{\boldsymbol{J}}\dot{\boldsymbol{q}} + \begin{bmatrix} \boldsymbol{0} \\ \boldsymbol{h}_\theta \end{bmatrix} + \dot{\boldsymbol{\varepsilon}}_v. \tag{4.6.13}$$

Here the acceleration terms in $\boldsymbol{b}_a$ vanish for the constant nominal speed.

The determination of the creep forces has been discussed in the previous section. For this case $\boldsymbol{f}_g$ in the equations of motion (4.5.5) is:

$$\boldsymbol{f}_g = -\boldsymbol{M}(\dot{\boldsymbol{J}}\dot{\boldsymbol{q}} + \dot{\boldsymbol{\varepsilon}}_v) - \begin{bmatrix} \boldsymbol{0} \\ \tilde{\boldsymbol{\omega}}^{21} \boldsymbol{I}\, \boldsymbol{\omega}^{21} + \boldsymbol{I}\, \boldsymbol{h}_\theta \end{bmatrix}. \tag{4.6.14}$$

The normal contact forces are still calculated by Eq.(4.5.21).

Both the matrix $\boldsymbol{M}_A$ in Eq.(4.5.6) and the product $\boldsymbol{D}\boldsymbol{M}^{-1}\boldsymbol{D}^T$ in Eq.(4.5.21) are positive definite. Furthermore, we have

$$\boldsymbol{M}_A = \begin{bmatrix} m & 0 & 0 & 0 \\ 0 & m+(mw_{,v}^2+I_x\phi_{,v}^2) & 0 & mw_{,v}w_{,\psi}+I_x\phi_{,v}\phi_{,\psi} \\ 0 & 0 & I_y & I_y\sin\phi \\ 0 & mw_{,v}w_{,\psi}+I_x\phi_{,v}\phi_{,\psi} & I_y\sin\phi & I_z\cos^2\phi+I_y\sin^2\phi+(mw_{,\psi}^2+I_x\phi_{,\psi}^2) \end{bmatrix}. \tag{4.6.15}$$

When the rolling and yaw angles are chosen as the independent generalized coordinates, the equations of motion can be derived in a similar way (Yang and De

Pater 1991). In the subsequent analyses, we only consider the cases that the lateral displacement v and the yaw angle ψ are the independent generalized coordinates.

4.7. Discussions on the Equations of Motion of a Wheelset on a Curved Track

When the surface equations of the rails which are given with respect to the track reference frame $\{o^1, \bar{e}^1\}$, are independent of the distance s, it can be proved (see Appendix E) that the following equation holds :

$$\bar{n}_j \cdot (\dot{\bar{s}} + \bar{\omega}^o \times \bar{p}_j^1) = 0 . \tag{4.7.1}$$

Therefore, in this case the kinematic constraint (4.4.11) reduces to

$$\bar{n}_j \cdot (\dot{\bar{\rho}} + \bar{\omega}^{21} \times \bar{p}_j^2) = 0 . \tag{4.7.2}$$

Obviously, Eq.(4.7.2) is independent of the motion of the track reference frame. Correspondingly, we find that the vectors $\boldsymbol{\xi}(t)$ and $\boldsymbol{\varepsilon}(t)$ defined in (4.4.15) and (4.4.16) are equal to zero. For the tangent track and the track with constant radius of curvature, constant cant and zero climb-angle, Eq.(4.7.1) can be proved easily.

When the radius of curvature of the track, the cant angle or the climb-angle varies with the distance s, even when the cross-sections of the rails are assumed to remain constant, it is very difficulty to derive the exact equations of the rail surfaces. Fortunately, the instantaneous geometric contact between the track and the wheelset is only related to a small track segment. As stated in Section 3.2.1 and Appendix C, this small segment of the curved track can usually be assumed as a tangent track or, which is even better, as a track with constant radius and cant angle when the track radius is small. In these cases the real surface equations of the rails can be approximated by equations which are independent of the distance s. Based on this postulate, the exact kinematic constraint equations (4.4.11) are replaced by (4.7.2) for the curved track.

Now we consider the case in which the small segment of the curved track under consideration is assumed to be cylindrical and perpendicular to the plane of the cross-section. Because the normal vector of the contact plane with respect to the track reference frame is still given by (3.2.17), the kinematic constraint equations (4.7.2) are independent of the longitudinal displacement u. As a result, the Jacobian

matrix $\boldsymbol{J}$ and the matrix $\boldsymbol{M}_A$ are the same as those for the tangent track. Despite we have $\xi(t)=0$ and $\varepsilon(t)=0$, as compared with the case of the tangent track, the vectors $\boldsymbol{b}_v$ and $\boldsymbol{b}_a$ in Eqs.(4.4.21) and (4.4.22) are much more complicated. As shown in (4.4.25) and (4.4.26), they strongly depend on the motion of the track reference frame and thus on the geometric configuration of the whole curved track.

As an example, we consider the simplest curved track whose radius and cant angle are constant and whose climb-angle is equal to zero. According to Section (4.3.1), the rotation matrix $\boldsymbol{G}^o$ in (4.3.3) reduces to

$$\boldsymbol{G}^o = \begin{bmatrix} \cos\alpha & \sin\alpha & 0 \\ -\cos\beta\sin\alpha & \cos\beta\cos\alpha & \sin\beta \\ \sin\beta\sin\alpha & -\sin\beta\cos\alpha & \cos\beta \end{bmatrix}, \tag{4.7.3}$$

where we use α and β tc replace the angle α_1 and the cant angle α_3, which are defined in Section (4.3.1), respectively. By means of Eq.(4.3.6), we obtain:

$$\alpha = \frac{s}{R_0}, \qquad \dot{\alpha} = \frac{V_n}{R_0}. \tag{4.7.4}$$

where R_0 is the radius of curvature of the track. The components of the angular velocity of the track reference frame $\bar{\omega}^o$ are therefore given by:

$${}^1\boldsymbol{\omega}^o = [\ 0,\ \frac{V_n}{R_0}\sin\beta,\ \frac{V_n}{R_0}\cos\beta\ ]^T. \tag{4.7.5}$$

For a prescribed nominal speed $V_n=ds/dt$, the motion of the track reference frame can be completely determined.

4.8. A Method to Treat the Case of a Tangent Track with Irregularities

In investigations on tracks with irregularities it is a common practice to assume that the rail profiles remain the same along the track. The irregularities of the track geometry, as shown in Fig.4.8.1, are defined in terms of four parameters: the deviations of the track gauge, the lateral alignment, the cross level and the vertical alignment (Garg and Dukkipati, 1984).

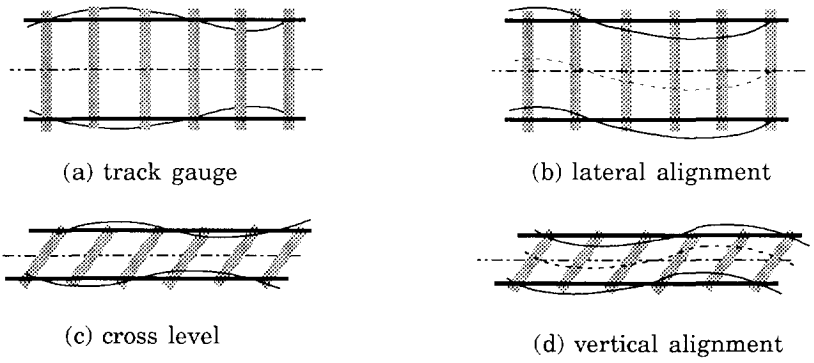

(a) track gauge (b) lateral alignment

(c) cross level (d) vertical alignment

Fig 4.8.1. Definitions of track irregularities

In order to take into account the influences of the irregularities on the contact geometry, according to section 3.4.2 we may rewrite the first-order equations as $\boldsymbol{g}(\boldsymbol{x}, \boldsymbol{\lambda}) = \mathbf{0}$. Here $\boldsymbol{x}$ contains the four lateral contact coordinates; the parameters are

$$\boldsymbol{\lambda} = [\ \phi,\ \psi,\ b,\ \Delta b,\ r,\ \Delta r,\ b^*,\ \Delta b^*,\ r^*,\ \Delta r^*\ ]^T. \tag{4.8.1}$$

Here, the deviations of the four track parameters: b, Δb, Δr and r can represent the irregularities of the track. We denote these deviations by δb, $\delta\Delta b$, $\delta\Delta r$ and δr respectively, where

δb	is the variation of track gauge;
$0.5\delta\Delta b$	the lateral alignment;
$0.5\delta\Delta r$	the cross level;
δr	the vertical alignment.

Furthermore, by means of Eqs.(3.4.43)-(3.4.48) we find that both $\delta\Delta b$ and δr do not affect the lateral contact coordinates; they only change the lateral and vertical displacements to $v+0.5\delta\Delta b$ and $w+\delta r$ respectively. Only the deviations δb and $\delta\Delta r$ influence the lateral contact coordinates.

The following assumptions are made in the dynamic simulations when the track irregularities are taken into account:

(1) The track reference frame moves with the lateral and vertical track alignment but its vector basis remains parallel to the inertial frame;

(2) A small track segment is cylindrical in the track reference frame;

(3) Eqs.(4.7.1) and (4.7.2) hold for the case of a track with irregularities.

On the basis of these assumptions, the deviations of the lateral and vertical

alignments are incorporated in the motion of the track reference frame.

The quasi-velocity and quasi-acceleration vectors for such a track-wheelset system are still expressed in the general forms of (4.4.18) and (4.4.19):

$$\boldsymbol{v} = \boldsymbol{A}\,\dot{\boldsymbol{q}} + \boldsymbol{b}_v\,, \qquad \dot{\boldsymbol{v}} = \boldsymbol{A}\,\ddot{\boldsymbol{q}} + \boldsymbol{b}_a\,, \tag{4.8.2}$$

Here the vectors $\boldsymbol{b}_v$ and $\boldsymbol{b}_a$ are given by

$$\boldsymbol{b}_v = [\,V_n,\ \delta\dot{v},\ \delta\dot{w},\ 0,\ -\Omega_n,\ 0\,]^T\,, \tag{4.8.3}$$

$$\boldsymbol{b}_a = \boldsymbol{H}^*\dot{\boldsymbol{J}}\dot{\boldsymbol{q}} + [\boldsymbol{0}^T,\ \boldsymbol{h}_\theta^T\,]^T + [\,\dot{V}_n,\ \delta\ddot{v},\ \delta\ddot{w},\ 0,\ -\dot{\Omega}_n,\ 0\,]^T \tag{4.8.4}$$

with

$$\delta v = 0.5\delta\Delta b\,, \qquad \delta w = \delta r\,. \tag{4.8.5}$$

The matrix $\boldsymbol{J}$ is identical with (4.6.6), which has been derived for a perfect tangent track. The influences of the deviations of the track gauge and the cross level are incorporated in the determination of the contact coordinates.

4.9. Linearized Equations of Motion for Stability Analysis

When a railway vehicle moves along a tangent track at low speed, the whole vehicle system may perform a stable stationary motion. The stability of this motion can be concluded from the eigenvalues of the equations of motion of the system which is obtained by linearizing the equations of motion (4.5.5) around the stationary motion. By considering small deviations, the linearized equations of motion may, in general, be written as:

$$\boldsymbol{A}_0^T\boldsymbol{M}\boldsymbol{A}_0\,\Delta\ddot{\boldsymbol{q}} - \boldsymbol{A}_0^T(\,\Delta\boldsymbol{f}_g + \Delta\boldsymbol{f}) - \Delta\boldsymbol{A}^T(\boldsymbol{f}_{g0} + \boldsymbol{f}_0) = \boldsymbol{0}\,. \tag{4.9.1}$$

where the index 0 refers to the stationary motion; the operator Δ indicates the deviations of the corresponding terms. When the constraint forces given by (4.5.21) are incorporated in the reduced equations of motion (4.5.5) due to the friction forces, the deviation of the constraint forces must also be taken into account:

$$\Delta\boldsymbol{\lambda} = -\Delta\boldsymbol{D}_\lambda(\boldsymbol{f}_{g0} + \boldsymbol{f}_0) + \boldsymbol{D}_{\lambda 0}(\,\Delta\boldsymbol{f}_g + \Delta\boldsymbol{f})\,, \tag{4.9.2}$$

where $\boldsymbol{\lambda}$ contains the Lagrangian multipliers and

$$\boldsymbol{D}_{\lambda} = (\boldsymbol{D}\boldsymbol{M}^{-1}\boldsymbol{D}^{T})^{-1}\boldsymbol{D}\boldsymbol{M}^{-1} \tag{4.9.3}$$

Due to the fact that there exists spin creep even in the stationary motion and that the contact geometry is strongly nonlinear, the linearization process is very complicated. De Pater (1979, 1987, 1992) has done comprehensive research work on this subject. He has expressed the parts of the profiles which are near the contact points by polynomials of second order in terms of the lateral contact coordinates and then the contact geometric quantities such as the contact angles can be found as functions of the independent generalized coordinates. He has also considered the influence of the fact that in the stationary motion, the lateral tangential forces are unequal to zero and the influence of the deviation of Kalker's creep coefficient f_{23} which is due to the deviation of the normal contact force. In certain cases, these two factors, which are overlooked by many investigators, may play an important role in determining the critical speed of the vehicle.

In order to simplify the linear stability analysis, we consider the motion of a symmetric wheelset system moving stationarily along the centre of the track. Because the lateral motion, which is described by the lateral displacement v and the yaw angle ψ, uncouples from the symmetric motion (with u and χ), only the lateral motion is considered in the linearizing process. In this case, we denote the contact coordinates by $\boldsymbol{p}_j^{*}=[0, \pm b_0, r_0]^{\mathrm{T}}$ and in the following analysis we replace $\Delta\boldsymbol{q}$ by $\boldsymbol{q}$, so $\boldsymbol{q}=[v, \psi]^{\mathrm{T}}$.

From either Eqs.(4.6.20)-(4.6.23) or the following relations between the generalized coordinates given by De Pater (1988):

$$\phi = -\frac{\mathrm{tg}\gamma_0}{b_0 - r_0\,\mathrm{tg}\gamma_0}\,v, \tag{4.9.4}$$

$$w = -\left(\frac{\mathrm{tg}\gamma}{b-r\,\mathrm{tg}\gamma} + \frac{(b+R\sin\gamma)(b+R^{*}\sin\gamma)}{(R^{*}-R)(b-r\mathrm{tg}\gamma)^2\cos^3\gamma}\right)_0 \frac{v^2}{2} + (b_0 - r_0\mathrm{tg}\gamma_0)\mathrm{tg}\gamma_0\,\frac{\psi^2}{2}, \tag{4.9.5}$$

we find that $\phi_{,\psi}$, $\phi_{,vv}$, $\phi_{,v\psi}$ and $w_{,v\psi}$ vanish and that $w_{,v}$ and $w_{,\psi}$ are small quantities of order one. Here, R_0^{*} and R_0 are the radii of curvature of the wheel and rail profiles in the lateral direction. Therefore, by means of Eq(4.6.6), we have;

$$\boldsymbol{A}_0 = \begin{bmatrix} 0 & 1 & 0 & \phi_{,v} & 0 & 0 \\ 0 & 0 & 0 & 0 & 0 & 1 \end{bmatrix}^{T}, \quad \Delta\boldsymbol{A} = \begin{bmatrix} 0 & 0 & w_{,vv}v & 0 & 0 & 0 \\ 0 & 0 & w_{,\psi\psi}\psi & 0 & \phi_{,v}v & 0 \end{bmatrix}^{T}. \tag{4.9.6}$$

where the partial derivatives are determined by Eqs.(4.9.4) and (4.9.5).

According to section (4.5) the resultant impressed force and torque may be given by $\boldsymbol{f}_e = [\, f_{ex},\ 0,\ mg,\ 0,\ 0,\ 0\,]^T$. From Eqs.(4.6.16) and (4.9.6) we see that the linearizing process implies that $\Delta \boldsymbol{A}^{\mathrm{T}} \boldsymbol{f}_{\mathrm{g}0}$ and $\boldsymbol{A}_0^{\mathrm{T}} \Delta \boldsymbol{f}_e$ are equal to zero and that

$$\Delta \boldsymbol{A}^T \boldsymbol{f}_{e0} = \begin{bmatrix} mg\, w_{,vv} & 0 \\ 0 & mg\, w_{,\psi\psi} \end{bmatrix} \begin{bmatrix} v \\ \psi \end{bmatrix}, \tag{4.9.7}$$

and

$$\boldsymbol{A}_0^T \Delta \boldsymbol{f}_g = -\begin{bmatrix} 0 & I_y \Omega_n \phi_{,v} \\ -I_y \Omega_n \phi_{,v} & 0 \end{bmatrix} \begin{bmatrix} \dot{v} \\ \dot{\psi} \end{bmatrix}. \tag{4.9.8}$$

For Kalker's linear creep law, we use f_{11}, f_{22} and f_{23} to denote the coefficients of the creepages and the spin creep υ_{xj}, υ_{yj} and υ_{spj} in Eqs.(4.2.9) and (4.2.10), and use f_{33} to denote the coefficient of υ_{spj} in Eq.(4.2.11). We introduce

$$\boldsymbol{\upsilon} = [\, \boldsymbol{\upsilon}_1^T,\ \boldsymbol{\upsilon}_2^T \,]^T, \qquad \boldsymbol{\upsilon}_j = [\, \upsilon_{xj},\ \upsilon_{yj},\ \upsilon_{spj} \,]^T, \tag{4.9.9}$$

so the linear creep law is

$$\boldsymbol{T}_j = \boldsymbol{K}_{Tj} \boldsymbol{\upsilon}_j = \begin{bmatrix} -f_{11} & 0 & 0 \\ 0 & -f_{22} & -f_{23} \\ 0 & 0 & 0 \end{bmatrix} \boldsymbol{\upsilon}_j, \quad \boldsymbol{M}_{zj} = \boldsymbol{K}_{Mj} \boldsymbol{\upsilon}_j = \begin{bmatrix} 0 \\ f_{23} \\ -f_{33} \end{bmatrix}^T \boldsymbol{\upsilon}_j. \tag{4.9.10}$$

This leads to

$$\boldsymbol{f}_T = \boldsymbol{K}_T \boldsymbol{\upsilon}, \qquad \boldsymbol{f}_M = \boldsymbol{K}_M \boldsymbol{\upsilon}, \tag{4.9.11}$$

where

$$\boldsymbol{K}_T = \begin{bmatrix} \boldsymbol{K}_{T1} & 0 \\ 0 & \boldsymbol{K}_{T2} \end{bmatrix}, \qquad \boldsymbol{K}_M = \begin{bmatrix} \boldsymbol{K}_{M1} & 0 \\ 0 & \boldsymbol{K}_{M2} \end{bmatrix}. \tag{4.9.12}$$

A difficulty arises due to the linearization associated with the tangential forces and the spin moments. Because the spin creep contains a term of order zero, as pointed out by De Pater (1992), we have to take into account the change of the coefficients f_{23} and f_{33}. The linearization of the creep quantities leads to

$$\boldsymbol{\upsilon}_j = \boldsymbol{\upsilon}_{0j} + \Delta \boldsymbol{\upsilon}_j. \tag{4.9.13}$$

We may also introduce the following linearizations:

$$\gamma_j \approx \gamma_0 \pm \Delta\gamma_j, \quad z_j \approx r_j \approx r_0 \pm \Delta r_j, \tag{4.9.14}$$

where

$$\Delta\gamma_j = \frac{\varepsilon v}{b_0}, \quad \Delta r_j = \lambda v. \tag{4.9.15}$$

The effective conicity λ and the contact angle parameter ε derived by De Pater (1979) are

$$\lambda = \frac{R_0^* \mathrm{tg}\gamma_0}{R_0^* - R_0}\left(\frac{b_0 + R_0 \sin\gamma_0}{b_0 - r_0 \mathrm{tg}\gamma_0}\right), \quad \varepsilon = \frac{b_0^* \cos^{-3}\gamma_0}{R_0^* - R_0}\left(\frac{b_0 + R_0 \sin\gamma_0}{b_0 - r_0 \mathrm{tg}\gamma_0}\right). \tag{4.9.16}$$

It is clear that from (4.5.14) and (4.5.15) we have

$$\boldsymbol{\upsilon}_{0j} = [\ 0,\ 0,\ \mp\frac{\sin\gamma_0}{r_0}\ ]^T, \tag{4.9.17}$$

and

$$\Delta\boldsymbol{\upsilon}_j = [\ \mp\frac{b_0}{V_n}\dot{\psi} \mp \frac{\lambda}{r_0}v,\ \frac{c_v}{V_n}\dot{v} - \psi\cos\gamma_0,\ \frac{\cos\gamma_0}{V_n}\dot{\psi} - \frac{\varepsilon}{b_0 r_0}v\ ]^T. \tag{4.9.18}$$

where the coefficient c_v is given by

$$c_v = \frac{b_0}{(b_0 - r_0 \mathrm{tg}\gamma_0)\cos\gamma_0}. \tag{4.9.19}$$

By introducing the quantity $T_0 = f_{23}\sin\gamma_0/r_0$, the creep forces and torques due to the stationary motion are

$$\boldsymbol{f}_{C0} = \boldsymbol{U}_{T0}\boldsymbol{f}_{T0} + \boldsymbol{U}_{M0}\boldsymbol{f}_{M0} = [0,\ 0,\ -2T_0\sin\gamma_0,\ 0,\ 2f_{33}\frac{\sin^2\gamma_0}{r_0},\ 0]^T \tag{4.9.20}$$

and the deviations of the creep forces and torques are determined by:

$$\Delta\boldsymbol{f}_C = \Delta\boldsymbol{U}_T\boldsymbol{f}_{T0} + \Delta\boldsymbol{U}_M\boldsymbol{f}_{M0} + \boldsymbol{U}_{T0}\Delta\boldsymbol{f}_T + \boldsymbol{U}_{M0}\Delta\boldsymbol{f}_M, \tag{4.9.21}$$

or

$$\Delta f_C = \Delta U_T K_{T0} \upsilon_0 + \Delta U_M K_{M0} \upsilon_0 + U_{T0} \Delta K_T \upsilon_0 + U_{M0} \Delta K_M \upsilon_0 + U_{T0} K_{T0} \Delta \upsilon + U_{M0} K_{M0} \Delta \upsilon \quad (4.9.22)$$

In the following analysis, the second and fourth terms of the right-hand member of the last equation are neglected. From Eqs.(4.9.12) and (4.9.17), we have,

$$\Delta K_T \upsilon_0 = \left[0, \ \frac{\sin\gamma_0}{r_0}(\Delta f_{23})_1, \ 0, \ \ 0, \ -\frac{\sin\gamma_0}{r_0}(\Delta f_{23})_2, \ 0 \right]^T . \quad (4.9.23)$$

By means of De Pater's analysis(1987), the non-zero components of (4.9.23) are

$$\pm\frac{\sin\gamma_0}{r_0}(\Delta f_{23})_j = \pm\frac{f_{23}}{N_0}\frac{\sin\gamma_0}{r_0}\Delta N_j = \pm\frac{T_0}{N_0}\Delta N_j , \quad (4.9.24)$$

where

$$N_0 = \frac{mg}{2\cos\gamma_0} - T_0 \operatorname{tg}\gamma_0 . \quad (4.9.25)$$

The deviations of the normal contact forces may be determined by Eq.(4.9.2) and they are given by

$$\Delta N_j = \pm N_0 \operatorname{tg}\gamma_0 \frac{\varepsilon}{b_0} v \pm I_y \Omega_n c_n \dot{\psi} \mp c_n^* \operatorname{ctg}\gamma_0 \left(f_{22}\left(\frac{c_v}{V_n}\dot{v} - \psi\cos\gamma_0\right) + f_{23}\left(\frac{\cos\gamma_0}{V_n}\dot{\psi} - \frac{\varepsilon}{b_0 r_0} v\right)\right), \quad (4.9.26)$$

where

$$c_n = \frac{m(b\cos\gamma_0 - r_0\sin\gamma_0)}{I_x \sin^2\gamma_0 + m(b\cos\gamma_0 - r_0\sin\gamma_0)^2}, \qquad c_n^* = \left(1 - \frac{b_0 c_n}{\cos\gamma_0}\right)\operatorname{ctg}\gamma_0 . \quad (4.9.27)$$

Finally, substituting these analytical results into Eq.(4.9.1), we can obtain the following set of linear homogeneous differential equations:

$$M_L \ddot{q} + C_L \dot{q} + K_L q = 0 , \quad (4.9.28)$$

where

$$\boldsymbol{M}_L = \begin{bmatrix} m + I\phi_{,v}^2 & 0 \\ 0 & I \end{bmatrix}, \tag{4.9.29}$$

$$\boldsymbol{C}_L = \begin{bmatrix} 2f_{22}\dfrac{c_v^2}{V_n} & I_y\Omega_n\phi_{,v} + 2f_{23}c_v\dfrac{\cos\gamma_0}{V_n} \\ -I_y\Omega_n\phi_{,v} - 2f_{23}\dfrac{c_v}{V_n} & 2f_{11}\dfrac{b^2}{V_n} + 2f_{33}\dfrac{\cos\gamma_0}{V_n} \end{bmatrix} + \begin{bmatrix} 2c_n^* f_{22}\dfrac{T_0 c_v^2}{N_0 V_n} & 2c_n^* f_{23}\dfrac{T_0 c_v\cos\gamma_0}{N_0 V_n} - 2I_y\Omega_n c_n\dfrac{T_0 c_v}{N_0} \\ 0 & 0 \end{bmatrix} \tag{4.9.30}$$

$$\boldsymbol{K}_L = \begin{bmatrix} -(mg - 2T_0\sin\gamma_0)w_{,vv} - 2f_{23}\dfrac{\varepsilon c_v}{b_0 r_0} & -2f_{22}c_v\cos\gamma_0 \\ 2f_{11}\dfrac{\lambda b_0}{r_0} - 2f_{33}\dfrac{\varepsilon\cos\gamma_0}{b_0 r_0} & -(mg - 2T_0\sin\gamma_0)w_{,\psi\psi} + 2f_{23}\cos^2\gamma_0 \end{bmatrix} + \begin{bmatrix} -2T_0(\phi_{,v}\sin\gamma_0 + \mathrm{tg}\gamma_0\dfrac{\varepsilon c_v}{b_0}) - 2c_n^* f_{23}\dfrac{T_0\varepsilon c_v}{N_0 b_0 r_0} & -2c_n^* f_{22}\dfrac{T_0 c_v}{N_0}\cos\gamma_0 \\ -2f_{33}\phi_v\dfrac{\sin^2\gamma_0}{r_0} & 0 \end{bmatrix}. \tag{4.9.31}$$

When the contact angle γ_0 is assumed to be small, the deviations of the normal contact forces can be neglected and the stationary tangential force T_0 can also be treated as a small quantity as compared with N_0. In this case the matrices $\boldsymbol{C}_L$ and $\boldsymbol{K}_L$ may be simplified considerably.

When the stationary wheelset position is not in the central plane of the track, the normal contact forces of both sides have different values and so do the contact angles and Kalker's linear creep coefficients. To avoid these difficulties in the linearization, we may approximate the solution by substituting the average values of the parameters of the asymmetric system into (4.9.29) to (4.9.31).

Chapter 5

Dynamic Models of a Single Wheelset with Independently Rotating Wheels

The literature concerned with independently rotating wheel (IRW) systems for railway vehicles is comprehensively reviewed by Dukkipati *et al.* (1991); they discuss various methods of providing the guidance capability to railway vehicles with IRW. In this chapter, a wheelset system with independently rotating wheels is studied as a system with five degrees of freedom: the longitudinal and lateral displacements of the mass centre of the wheelset system, the yaw angle of the system and the two spin rotations of the wheels around the system axis of revolution. The equations of motion of such a system are derived and they are compared with the equations of motion for the conventional wheelset.

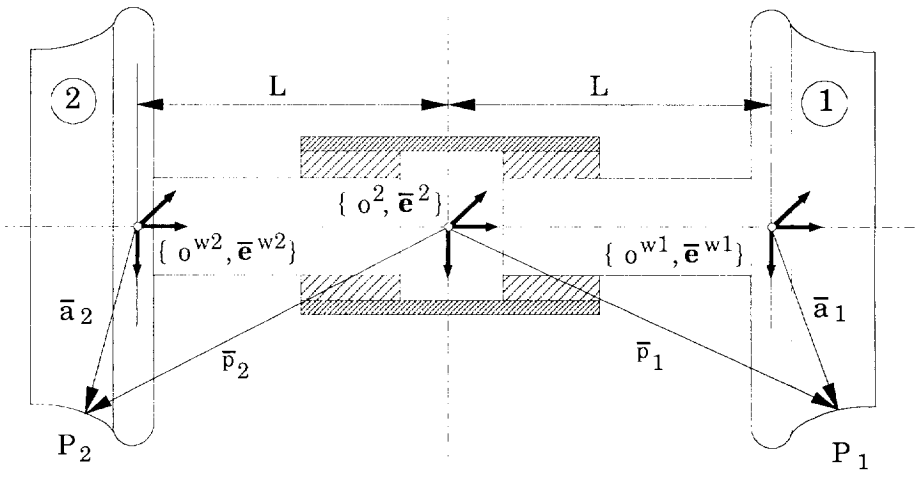

Fig. 5.1. An independently rotating wheel system.

An IRW system is shown in Fig.5.1. The frame $\{o^2, \bar{e}^2\}$, which is still

called the wheelset-body frame, is located at the mass centre of the IRW system. Similar to the conventional wheelset system, the position vector of its origin relative to the inertial frame is denoted by $\bar{r}$ and $\bar{\rho}$ is the position vector relative to the track reference frame $\{o^1, \bar{e}^1\}$; the absolute velocity and acceleration of the origin are determined by Eqs.(4.3.8) and (4.3.9). As shown in Fig 5.1, the right-hand wheel is identified as body 1 and the left-hand wheel as body 2. The wheel-body frame $\{o^{wj}, \bar{e}^{wj}\}$ is situated at the mass centre of wheel j; its base vectors are always parallel to those of the wheelset-body frame. The position vector of the origin of the wheel-body frame relative to the origin of the wheelset-body frame is denoted by the constant vector $\pm\bar{l}$, where

$$\bar{l} = \boldsymbol{l}^T \bar{\boldsymbol{e}}^2, \qquad \boldsymbol{l} = [0, L, 0]^T. \tag{5.1}$$

In agreement with Chapter 2, we use $\bar{r}_j$ to denote the position vector of the origin of the wheel-body frame relative to the inertial frame and $\bar{\omega}_j$ to denote the absolute angular velocity of the wheel-body frame. The position vectors of the contact points are shown in Fig.5.1.

The interaction between two wheels is due to the revolute joint, which gives rise to five constraint equations. Therefore, together with the two contact constraints, the system is subjected to seven kinematic constraints, which are represented by the following constraint equations:

$$\dot{\bar{r}}_2 = \dot{\bar{r}}_1 + \bar{\omega}_1 \times (-2\bar{l}), \tag{5.2}$$

$$\bar{e}_1^2 \cdot (\bar{\omega}_1 - \bar{\omega}_2) = 0, \tag{5.3}$$

$$\bar{e}_3^2 \cdot (\bar{\omega}_1 - \bar{\omega}_2) = 0, \tag{5.4}$$

$$\bar{n}_j \cdot (\dot{\bar{r}}_j + \bar{\omega}_j \times \bar{a}_j) = 0. \tag{5.5}$$

Combining Eqs.(5.2)-(5.5) yields the general form of the constraint equations:

$$\boldsymbol{D}\boldsymbol{v} + \boldsymbol{c} = \boldsymbol{0}. \tag{5.6}$$

In this case the vector $\boldsymbol{c}$ with seven components is equal to zero and

$$v = \begin{bmatrix} \dot{r}_1 \\ \dot{r}_2 \\ \omega_1^* \\ \omega_2^* \end{bmatrix}, \quad D = \begin{bmatrix} E & -E & 2G\tilde{l} & 0 \\ 0 & 0 & Q & -Q \\ n_1^T G^o & 0 & -n_1^{*T}\tilde{a}_1^* & 0 \\ 0 & n_2^T G^o & 0 & -n_2^{*T}\tilde{a}_2^* \end{bmatrix}, \quad Q = \begin{bmatrix} 1 & 0 & 0 \\ 0 & 0 & 1 \end{bmatrix}. \tag{5.7}$$

On the other hand, because the wheelset system with IRW is axisymmetric and the mass centres of the system and the wheels are located in the axis of revolution of the system, the quasi-velocity vector discussed in Chapter 2 can easily be expressed as:

$$v = A_1 v_1, \tag{5.8}$$

where

$$A_1 = \begin{bmatrix} E & -G\tilde{l} & 0 \\ E & G\tilde{l} & 0 \\ 0 & E & 0 \\ 0 & E & d_\chi \end{bmatrix}, \quad v_1 = \begin{bmatrix} \dot{r} \\ \omega_1^* \\ \dot{\chi}_{21} \end{bmatrix}, \quad d_\chi = \begin{bmatrix} 0 \\ 1 \\ 0 \end{bmatrix}. \tag{5.9}$$

The matrix G is the rotation matrix of the wheelset-body frame relative to the inertial frame and χ_{21} represents the relative spin angle between the wheels. The spin rotations do not affect the contact constraints between rails and wheels and we choose the longitudinal and lateral displacements of the mass centre of the wheelset system u and v, the yaw angle ψ, the spin angle χ_1 of the right-hand wheel and the relative spin angle χ_{21} as the independent generalized coordinates of the system:

$$q = [\, u,\ v,\ \chi_1,\ \psi,\ \chi_{21} \,]^T. \tag{5.10}$$

In this way we can write

$$v_1 = A_2 \dot{q} + \begin{bmatrix} \varepsilon_v(t) \\ 0 \end{bmatrix}, \tag{5.11}$$

where

$$A_2 = H_2^* J_2, \qquad H_2^* = diag[\, H^*,\ 1 \,], \qquad J_2 = diag[\, J, 1 \,]. \tag{5.12}$$

The 7×5 matrix $\boldsymbol{J}_2$ is the Jacobian matrix of the IRW system due to the contact constraints. The matrices $\boldsymbol{H}^*$ and $\boldsymbol{J}$ are defined by (4.4.20) and the vector $\boldsymbol{\varepsilon}_v(t)$ by (4.4.25); they refer to the conventional wheelset. Substituting (5.11) into Eq.(5.8) yields

$$\boldsymbol{v} = \boldsymbol{A}\,\dot{\boldsymbol{q}} + \boldsymbol{b}_v . \tag{5.13}$$

with

$$\boldsymbol{A} = \boldsymbol{A}_1\boldsymbol{A}_2 , \quad \boldsymbol{b}_v = \boldsymbol{A}_1 \begin{bmatrix} \boldsymbol{\varepsilon}_v(t) \\ 0 \end{bmatrix}, \tag{5.14}$$

Correspondingly, the quasi-accelerations are:

$$\dot{\boldsymbol{v}} = \boldsymbol{A}\,\ddot{\boldsymbol{q}} + \boldsymbol{b}_a . \tag{5.15}$$

where

$$\boldsymbol{b}_a = \boldsymbol{A}_1 (\boldsymbol{H}_2^* \dot{\boldsymbol{J}}_2 \dot{\boldsymbol{q}} + [\boldsymbol{\varepsilon}_a^T , 0]^T) + \boldsymbol{b}_{IRW} . \tag{5.16}$$

See Appendix F. Here the vector $\boldsymbol{\varepsilon}_a(t)$ is determined by Eq.(4.4.26) and

$$\boldsymbol{b}_{IRW} = \begin{bmatrix} \boldsymbol{G}\tilde{\omega}_1\tilde{\omega}_1\boldsymbol{l} \\ -\boldsymbol{G}\tilde{\omega}_1\tilde{\omega}_1\boldsymbol{l} \\ \boldsymbol{0} \\ \boldsymbol{h}_{\theta 21} \end{bmatrix}, \quad \boldsymbol{h}_{\theta 21} = \begin{bmatrix} -\dot{\chi}_{21}\,\omega_{13} \\ 0 \\ \dot{\chi}_{21}\,\omega_{11} \end{bmatrix}. \tag{5.17}$$

Now, the creepages and the spin creep can be calculated by

$$\left[\upsilon_{xj},\ \upsilon_{yj},\ 0 \right]^T = \frac{1}{V_n}\,\bar{\boldsymbol{e}}^{Pj} \cdot (\dot{\bar{r}}_j + \bar{\omega}_j \times \bar{a}_j) = \frac{1}{V_n}\,\boldsymbol{G}^{Pj,2} (\boldsymbol{G}^T \dot{\boldsymbol{r}} + \tilde{\boldsymbol{\omega}}_j^* \boldsymbol{p}_j^*) , \tag{5.18}$$

and

$$\upsilon_{spj} = \frac{1}{V_n}\,\bar{n}_j \cdot \bar{\omega}_j = \frac{1}{V_n}\,\boldsymbol{n}_j^{*T}\,\boldsymbol{\omega}_j^* . \tag{5.19}$$

The tangential contact forces and the spin moment for each wheel can be determined by means of the definitions of (4.2.3)-(4.2.6) and the creep laws.

Therefore, the equations of motion of an IRW system can be written as Eq.(2.3.14) together with Eq.(2.3.17). For the IRW system, f includes the tangential contact forces and the spin moments. The vector $\boldsymbol{\lambda}$ contains seven Lagrangian multipliers which correspond to the interaction forces due to the revolute joint and the normal contact forces.

In general, the constraint forces due to the revolute joint need not to be determined; by contrast, the normal contact forces are required because they directly influence the friction forces. In order to determine the normal contact forces and to compare the equations of motion with those of the conventional wheelset, we rewrite the equations of motion Eq.(2.3.14) of an IRW system as:

$$\boldsymbol{A}_2^T \boldsymbol{M}_{IRW} \boldsymbol{A}_2 \ddot{\boldsymbol{q}} - \boldsymbol{A}_2^T (\boldsymbol{f}_{gIRW} + \boldsymbol{f}_{IRW}) = \boldsymbol{0} \tag{5.20}$$

and the normal contact forces are determined by

$$f_N = (\boldsymbol{D}_{IRW} \boldsymbol{M}_{IRW}^{-1} \boldsymbol{D}_{IRW}^T)^{-1} \boldsymbol{D}_{IRW} \boldsymbol{M}_{IRW}^{-1} (\boldsymbol{f}_{gIRW} + \boldsymbol{f}_{IRW}), \tag{5.21}$$

where

$$\boldsymbol{M}_{IRW} = \boldsymbol{A}_1^T \boldsymbol{M} \boldsymbol{A}_1, \quad \boldsymbol{f}_{gIRW} = \boldsymbol{A}_1^T \boldsymbol{f}_g, \quad \boldsymbol{f}_{IRW} = \boldsymbol{A}_1^T \boldsymbol{f}, \quad \boldsymbol{D}_{IRW} = [-\boldsymbol{U}_N^T, \boldsymbol{0}]. \tag{5.22}$$

$\boldsymbol{D}_{\mathrm{IRW}}$ is a 2×7 matrix whose submatrix $\boldsymbol{U}_{\mathrm{N}}$ was derived for the conventional wheelset; see Eq.(4.5.20). The first three components of the vector $\boldsymbol{f}_{\mathrm{IRW}}$ represent the components of the resultant impressed force applied at the IRW system; they certainly include the tangential forces. The following three components represent the components of the resultant torque and the last component is the spin torque applied at the left-hand wheel. In more detail, we have

$$\boldsymbol{M}_{IRW} = \begin{bmatrix} m\boldsymbol{E} & \boldsymbol{0} & \boldsymbol{0} \\ \boldsymbol{0} & \boldsymbol{I} & I_{wy} \boldsymbol{d}_\chi \\ \boldsymbol{0} & I_{wy} \boldsymbol{d}_\chi^T & I_{wy} \end{bmatrix}, \tag{5.23}$$

$$\boldsymbol{f}_{gIRW} = -\boldsymbol{M}_{IRW} (\boldsymbol{H}_2^* \dot{\boldsymbol{J}}_2 \dot{\boldsymbol{q}} + \begin{bmatrix} \boldsymbol{\varepsilon}_a(t) \\ 0 \end{bmatrix}) - \begin{bmatrix} \boldsymbol{0} \\ \tilde{\boldsymbol{\omega}}_1 \boldsymbol{I} \boldsymbol{\omega}_1 + I_{wy} h_{\theta 21} \\ 0 \end{bmatrix} \tag{5.24}$$

and

$$(f_{IRW})_{CONT} = \begin{bmatrix} \boldsymbol{U}_T f_T + \boldsymbol{U}_M f_M \\ -\sin\gamma_2^* M_{z2} + T_{x2} r_2^* \end{bmatrix}. \tag{5.25}$$

Here m is the mass of the whole wheelset system; the diagonal 3×3 matrix $\boldsymbol{I}$ represents the inertia matrix of the whole system with respect to the wheelset mass centre and I_{wy} is the moment of inertia of the wheel about the axis of revolution. $\boldsymbol{h}_{\theta 1}$ is defined by (4.3.16). f_T, f_M, $\boldsymbol{U}_T$ and $\boldsymbol{U}_M$ are defined by (4.5.8), (4.5.10), (4.5.12) and (4.5.13) for the conventional wheelset system and r_2^* is the instantaneous rolling radius of the left-hand wheel. Moreover, it can be shown that Eq.(5.22) reduces to:

$$f_N = -(\boldsymbol{U}_N^T \boldsymbol{M}^{-1} \boldsymbol{U}_N)^{-1} \boldsymbol{U}_N^T \boldsymbol{M}^{-1} f' \tag{5.26}$$

Note that here $\boldsymbol{M}$=diag[mE, $\boldsymbol{I}$] and that f' contains only the first six components of $(f_{gIRW} + f_{IRW})$.

Chapter 6

Applications in Railway Vehicle Dynamics

The need to economically and effectively qualify new designs of railway vehicles has led to rapid developments of more reliable and accurate computer simulation codes (Kortüm, Sharp and De Pater, 1991). On the basis of the theoretical analyses presented in the previous chapters, a computer simulation program, RyVehSim, has been developed for the investigation of the dynamic behaviour of railway vehicles.

In this chapter, RyVehSim is briefly introduced. In order to validate this simulation code, first a single conventional wheelset is studied; for Pascal's benchmark (Kortüm, 1991) the results given by RyVehSim are in good agreement with those given by MEDYNA, VOCO (Pascal, 1990) and Robotran (Fisette, 1991b). Subsequently, Kik's benchmark (Kik and Pascal, 1991) is considered. The dynamic analysis is also carried out for this vehicle model moving along tracks with asymmetric profiles: the *CTO-Measured-Profiles* and *ORE-Benchmark-Profiles*. As compared with conventional vehicles, the results in Section 6.4 show that vehicles equipped with IRW have a completely different dynamic behaviour. Ultimately, the influence of the track irregularities is demonstrated.

6.1. RyVehSim for Railway Vehicle Dynamic Simulation

RyVehSim has been developed to predict the dynamic behaviour of railway vehicles. It can be employed to study a single wheelset, a complete vehicle system and even a train with several vehicles. The vehicle may be equipped with a number of conventional wheelsets or wheelsets with independently rotating wheels (IRW). For vehicles with both conventional wheelsets and IRW, the sequence of the wheelsets and IRW can be chosen arbitrarily.

The motion of a body in the vehicle system is described by the small relative motion combined with the large motion of the moving reference frame. As discussed in Section 4.3, the motion of the reference frame is prescribed by the given nominal speed of the vehicle and the track route.

The vehicle systems handled by RyVehSim are assumed to be assembled by various kinds of suspension elements (springs and dampers). Obviously, the

interactions between bodies due to these suspensions do not give rise to geometric or kinematic constraints; therefore, such suspensions do not reduce the number of degrees of freedom of the vehicle system. In RyVehSim, a wheelset, as discussed in Chapter 4, has four degrees of freedom; a bogie has full six degrees of freedom which are represented by the three displacements of the body mass centre and the three rotation angles that are defined in Appendix B. However, for a carbody the longitudinal motion is often considered as a kinematic excitation, so that it has only five degrees of freedom which are the lateral and vertical displacements of the mass centre and the three rotation angles. For a vehicle with one carbody and two two-axle bogies, the system has altogether 33 degrees of freedom.

The interaction force or torque due to a suspension element mostly depends only on the relative motion between its connecting bodies. Once the motion of the body mass centre and the body rotation are given, the position and velocity of a node attached to the suspension can easily be calculated by means of Eqs.(2.1.1) and (2.1.2). Thus, the suspension force and torque can be determined. The suspension elements available in RyVehSim are springs with linear stiffness and dampers with linear characteristics; they are listed as follows:

- spring;
- bending spring;
- damper;
- a combination of a spring and a damper in parallel;
- a combination of a spring and a damper in series.

The nonlinear suspensions such as the bump stop and the Coulomb ("dry") friction damper can be introduced by users. Associated with the geometric and kinematic information of the nodes, RyVehSim provides a special subroutine in which the users are able to define a large number of nonlinear suspension elements as a library for various railway vehicles. Impressed forces or torques, which are constants or time functions, can be defined in a similar way.

The numerical analysis of the vehicle system is carried out through the time integration of the nonlinear equations of motion. RyVehSim can record any desired information such as the displacements and accelerations of points of the bodies, the suspension forces and torques, the creepages and the spin creep, and the normal and tangential contact forces. All these data may be used in a post-processor. In RyVehSim, each integration step includes the following items:

- the geometric contact between track and wheelset;
- the contact mechanics;
- the integration of the equations of motion;
- the determination of the constraint forces (the normal contact forces).

In the geometric contact problem, the independent generalized coordinates of the wheelset, usually the lateral displacement and the yaw angle, are the input arguments. By means of the first-order theory, this problem is solved on-line in terms of the independent generalized coordinates. On the other hand, in order to overcome the numerical difficulties due to double contact, the jump positions of the contact points have to be determined in advance with the aid of GeoCont discussed in Chapter 3. Then by making use of this information, the program RyVehSim can judge in which range of the profiles the contact takes place during the simulation. As a result, we obtain the contact coordinates, the radii of curvature of the rail and wheel profiles at the contact points, the contact angles, the dependent generalized coordinates (the vertical displacement and the rolling angle) as well as components of the Jacobian matrix of the track-wheelset subsystem.

With increasing vehicle speed, flange contact tends to occur. At this moment, RyVehSim is incapable of dealing with the flange contact appropriately. When the lateral displacement of the wheelset exceeds a limit given by the user, the program halts or enforces the displacement to remain equal to the limit value.

The creepages and the spin creep are calculated by means of the definitions (4.2.3) and (4.2.4). Using the normal contact forces obtained from the preceding integration step and the geometric parameters at the contact points, we determine the contact areas by means of Hertz's theory. Therefore, during the simulation, the instantaneous values of the ratio of the semi-axes of the contact ellipse and the lengths of the semi-axes are calculated. The tangential contact forces obey the creep laws. RyVehSim provides three options: Kalker's linear law, the Shen-Hedrick-Elkins law and Kalker's simplified theory incorporated in FASTSIM.

The Runge-Kutta-Fehlberg 45 method (which has a variable stepsize) is adopted to integrate the nonlinear equations of motion. On the basis of the integration results, the normal contact forces are amended by Eq.(4.4.23). If desired, the accuracy can be improved through an iteration procedure.

All numerical results presented in this chapter have been obtained by using RyVehSim with FASTSIM. The default mash number required by FASTSIM is 10×10; Poisson's ratio is chosen to be 0.28 and the shear modulus 8.1×10^{10} N/m^2.

6.2. A Single Conventional Wheelset

A single wheelset problem proposed by Pascal (Kortüm 1991) is regarded as one of the benchmarks for comparing the various simulation codes used by railway engineers. The wheelset shown in Fig. 6.2.1 moves at the constant speed of 30 m/s

and it is loaded by a lateral force applied at the wheelset at the track level and a constant vertical force (F_z=154715 N) at the wheelset mass centre. Only the mass of the wheelset is provided and is equal to 1887kg. It is expected that the yaw angle of the wheelset remains small because of a stiff torsional spring with the stiffness $K_{qz}=8.16\cdot10^7$ Nm/rad, which yields a restoring moment about a vertical axis and keeps the wheelset almost orthogonal to the track. The lateral displacement of the wheelset is only bounded by the wheel flanges. The profiles of the rails and the wheelset are the *UIC60-S1002-Standard* profiles. Only the first of the three exercises required in the benchmark is presented here.

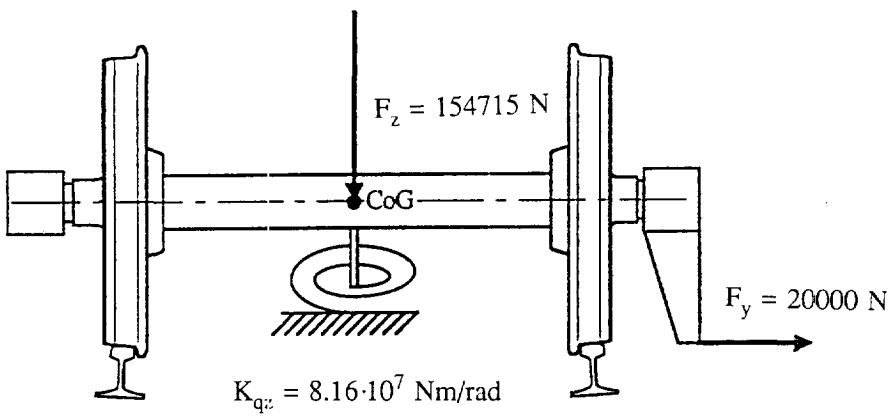

Fig.6.2.1 Wheelset benchmark proposed by Pascal.

Pascal's benchmark								
μ=0.3	v(mm)	ψ(mrad)	N_1 (kN)	N_2 (kN)	T_{x1} (kN)	T_{x2} (kN)	T_{y1} (kN)	T_{y2} (kN)
MEDYNA	4.888	-0.422	90.0	84.1	23.2	-23.2	11.4	-3.30
Robotran	5.193	-0.421	90.32	84.11	23.29	-23.49	9.95	-2.88
VOCO	5.214	-0.422	89.85	84.45	23	-23	10.0	-2.91
RyVehSim	4.930	-0.427	90.21	84.14	23.40	-23.61	9.65	-3.45

Table 6.2.1. Survey of the stationary results for Pascal's benchmark.

In this analysis, the stationary wheelset motion as well as the contact forces are determined as functions of the friction coefficient μ in the case that the lateral impressed force is a step loading of 20 kN. The solutions are determined by integrating the nonlinear equations of motion. The detailed solutions indicate that for μ=0.1 and 0.2, the contact point at the right-hand side oscillates around the second

jump position (v=4.823mm, see Fig.3.5.4) so that no stationary solution is obtained. The results for these values of μ are the mean values. Tables 6.2.1 and 6.2.2 show that the results found by RyVehSim are in good agreement with those obtained by some other simulation codes (Pascal, 1990; Fisette, 1991b).

Pascal's benchmark								
VOCO results								
fric. coeff.	v(mm)	ψ(mrad)	N_1 (kN)	N_2 (kN)	T_{x1} (kN)	T_{x2} (kN)	T_{y1} (kN)	T_{y2} (kN)
0.1	4.96	-0.157	90.91	84.45	8.475	-8.475	1.576	-0.64
0.2	5.047	-0.298	90.53	84.45	16.3	-16.3	4.964	-1.787
0.3	5.214	-0.422	89.85	84.45	23	-23	10.0	-2.91
0.4	5.4	-0.526	88.6	84.45	28.6	-28.6	15.8	-4.02
RyVehSim results								
0.1	4.830	-0.151	90.82	84.46	8.247	-8.321	1.484	-1.053
0.2	4.830	-0.281	90.18	84.64	15.52	-15.57	4.252	-2.557
0.3	4.93	-0.427	90.21	84.14	23.40	-23.61	9.65	-3.45
0.4	5.434	-0.546	89.49	84.04	29.88	-30.16	14.11	-4.60

Table 6.2.2. Comparison of the results found by VOCO and RyVehSim

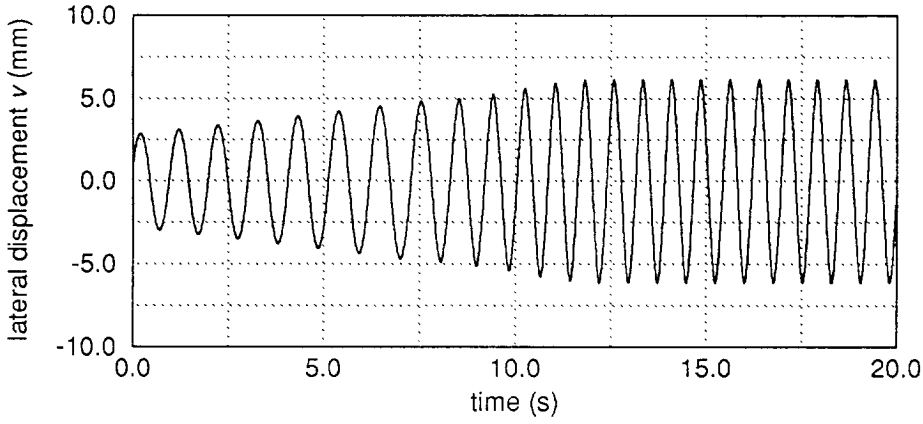

Fig.6.2.2. The time history of the lateral displacement at 9 m/s.

The second example concerns the nonlinear behaviour of a single wheelset without mounting any suspension element. The profiles are also *UIC60-S1002-Standard*. The inertia properties are: m=1500 kg, I_x=I_z=1000 kgm^2 and I_y=100 kgm^2; the friction coefficient μ=0.3. Fig.6.2.2 shows the time history of the lateral

displacement of the wheelset mass centre when the wheelset moves along a tangent track at a constant speed of 9 m/s; the relation between the lateral displacement and the yaw angle is shown in Fig.6.2.3. With initial values of the lateral displacement v=1mm and the yaw angle ψ=2mrad, the lateral displacement approaches the stable limit cycle after about 12 seconds. The wave length of the limit cycle of the lateral displacement is about 6.84m; its amplitude is about 6.14mm. The amplitude of the yaw angle is equal to 5.37 mrad.

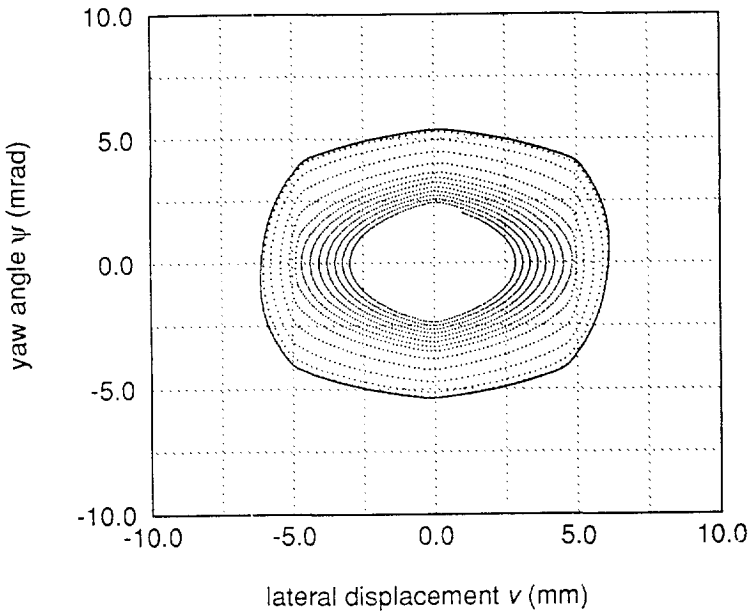

Fig.6.2.3. The relation between the lateral displacement and the yaw angle during the transient motion at 9m/s.

The third example demonstrates the dynamic response of a wheelset passing a track with an imperfection (see Fig.6.2.4) as given in the ORE benchmark (ORE, 1991). Just as in the second example, no suspension restricts the motion of the wheelset, but the profiles are now the *ORE-Benchmark-Profiles*. The inertia properties slightly change to: m=1503 kg, I_x=I_z=810 kgm^2 and I_y=112 kgm^2. The integration is carried out at a constant speed of 10 m/s and with zero initial values of the lateral displacement and the yaw angle. The lateral displacement and the yaw angle shown in Fig.6.2.5 are given relative to the track reference frame. Due to the track perturbation, the trajectory of the wheelset changes significantly. Between the travelling distances of 5.0 and 5.1 m, the yaw angle becomes almost equal to the

very large value of −50 mrad and the lateral displacement sharply changes from −1.4mm to −1.75mm.

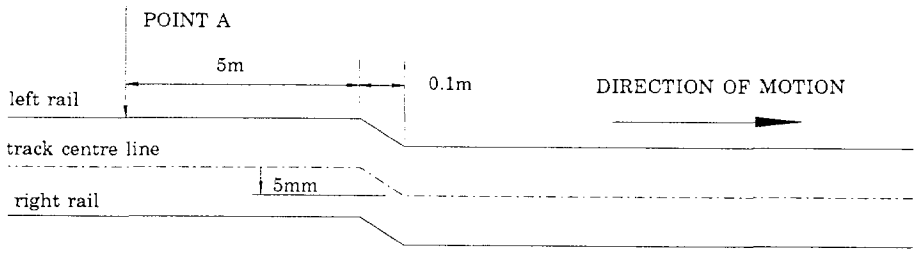

Fig.6.2.4. Track alignment input for ORE Benchmark.

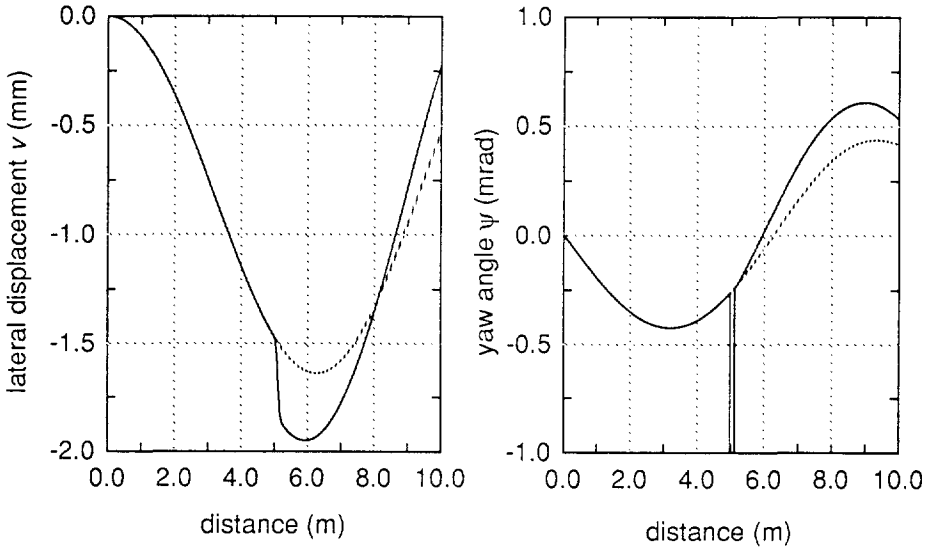

Fig.6.2.5. The response of the wheelset (the dot line for the perfect tangent track and the solid line for the track defined in Fig.6.2.4).

6.3. Complete Vehicle System

Besides the above-mentioned single wheelset benchmark proposed by Pascal, another railway vehicle benchmark was submitted by Kik in the workshop of the Interna-

tional Association of Vehicle System Dynamics (IAVSD) in Herbertov and later on it was revised by Kik and Pascal (1991). In this benchmark a passenger car with two-axle bogies is specified. The combination of the profiles is also *UIC60-S1002 Standard*. With the exception of the bump stop, the suspensions are linear. The locations of the nodes to which the suspensions are attached, are shown in Fig.6.3.1. The mass centre of the carbody has an excentricity of 0.2m to the right-hand side relative to the geometric centre of the carbody. The geometric configuration of the whole system refers to the equilibrium position in case the carbody mass centre coincides with its geometric centre.

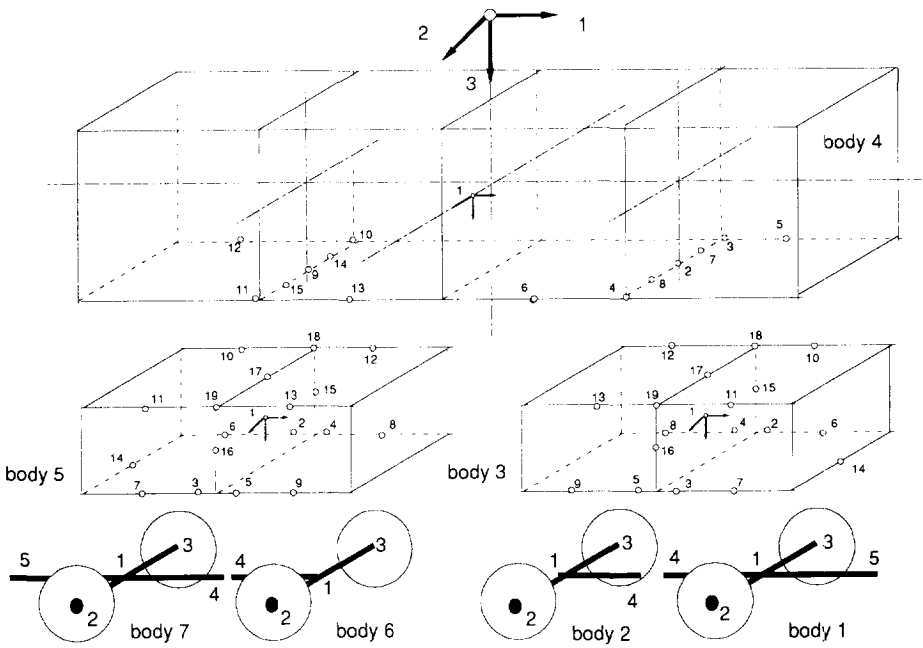

Fig.6.3.1. Kik's benchmark vehicle: a cross bracing spring is mounted between node 4 of body 1 and node 4 of body 2; an axle-bracing spring is mounted between node 5 of body 1 and node 14 of body 3; for the trailing bogie we have a similar situation.

First of all, the generalized coordinates in the stationary motion are found by integrating the nonlinear equations of motion. The lateral displacement of the mass centre and the rolling angle of the carbody are equal to 0.23 m and 0.0610 rad, respectively; all the four wheelsets are almost in the track central plane. But the

normal contact forces applied at the wheels are quite different; at a right-hand wheel it is about 62.05kN and at a left-hand side wheel it is about 40.93kN. This difference is due to the excentricity of the carbody mass centre.

Corresponding to the stability analysis requested in the benchmark, the simulation is carried out at a speed of 170m/s, however, with different initial values as compared to those of the benchmark. The carbody and the bogies are placed in the positions which coincide with their geometric configurations in the stationary motion. An initial lateral velocity of 0.01m/s is assigned to the two bogies and the first, second and third wheelsets. In addition, the first wheelset has an initial lateral displacement of 0.001m, whereas the three other wheelsets are in the central position.

In order to understand the creep law generated by the FASTSIM algorithm, the normalized creepage τ and normalized creep force σ, which are defined by:

$$\sigma = \frac{\sqrt{T_x^2+T_y^2}}{\mu N}, \qquad \tau = \frac{abG}{3\mu N}\sqrt{(C_{11}\upsilon_x)^2+(C_{22}\upsilon_y+C_{23}\sqrt{ab}\,\upsilon_{sp})^2}, \tag{6.3.1}$$

are recorded point by point in each integration step (see Fig.6.3.2). During the motion, the contact ellipse for each contact point is determined from the normal contact force and the radii of curvature of the profiles at that instant. This illustrates the importance of a good algorithm for the creep law: it is not enough to use just a simple formulae.

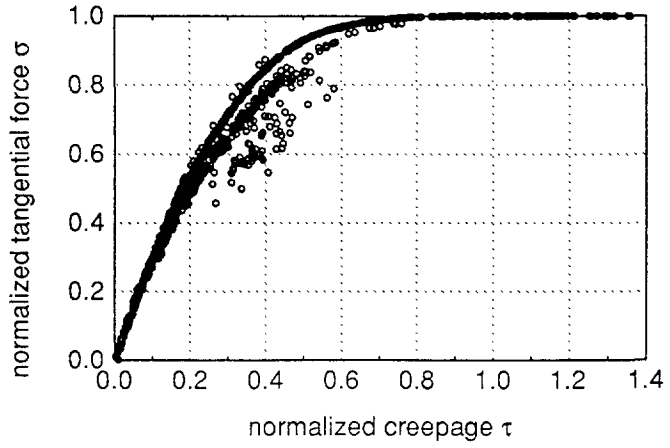

Fig.6.3.2. The results of FASTSIM.

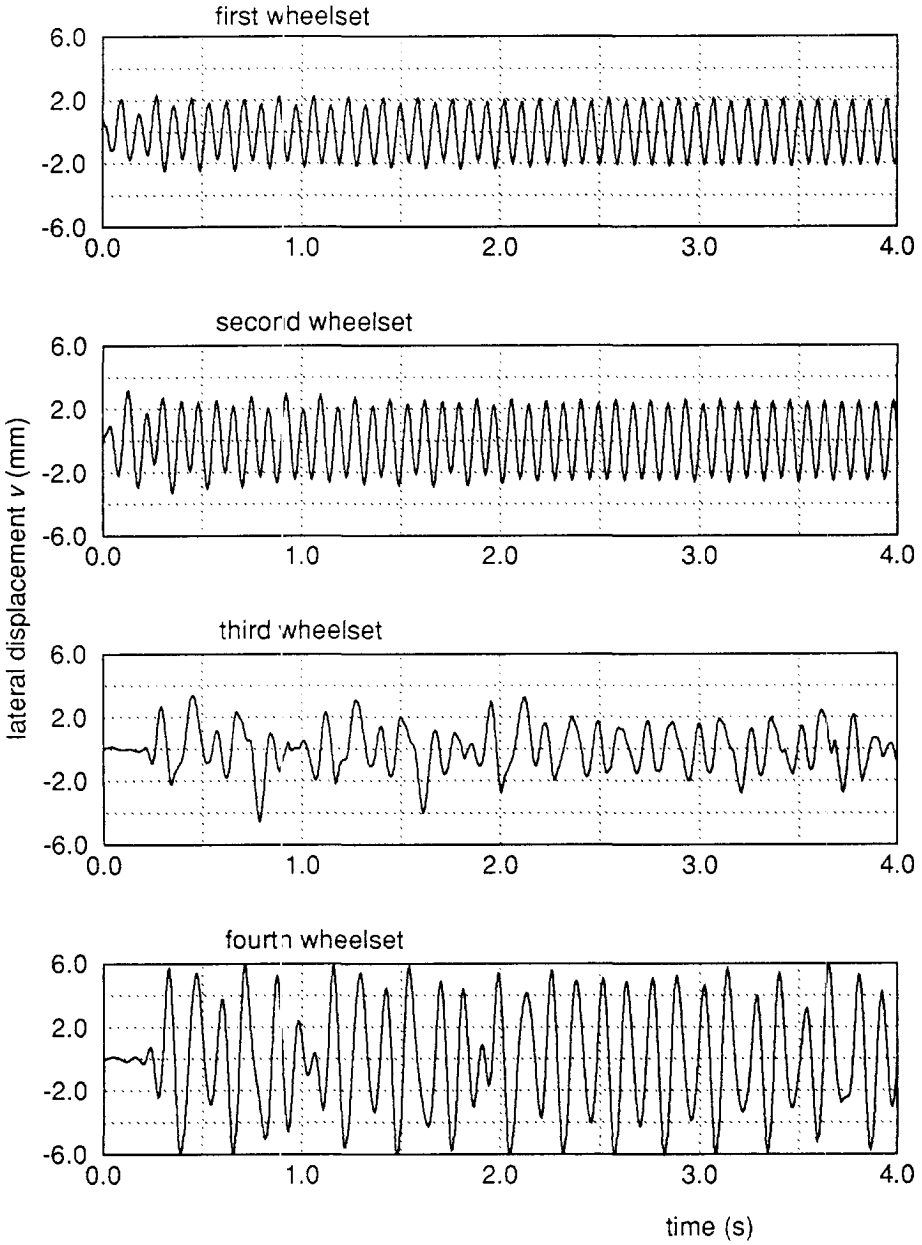

Fig.6.3.3. The lateral response of the wheelsets.

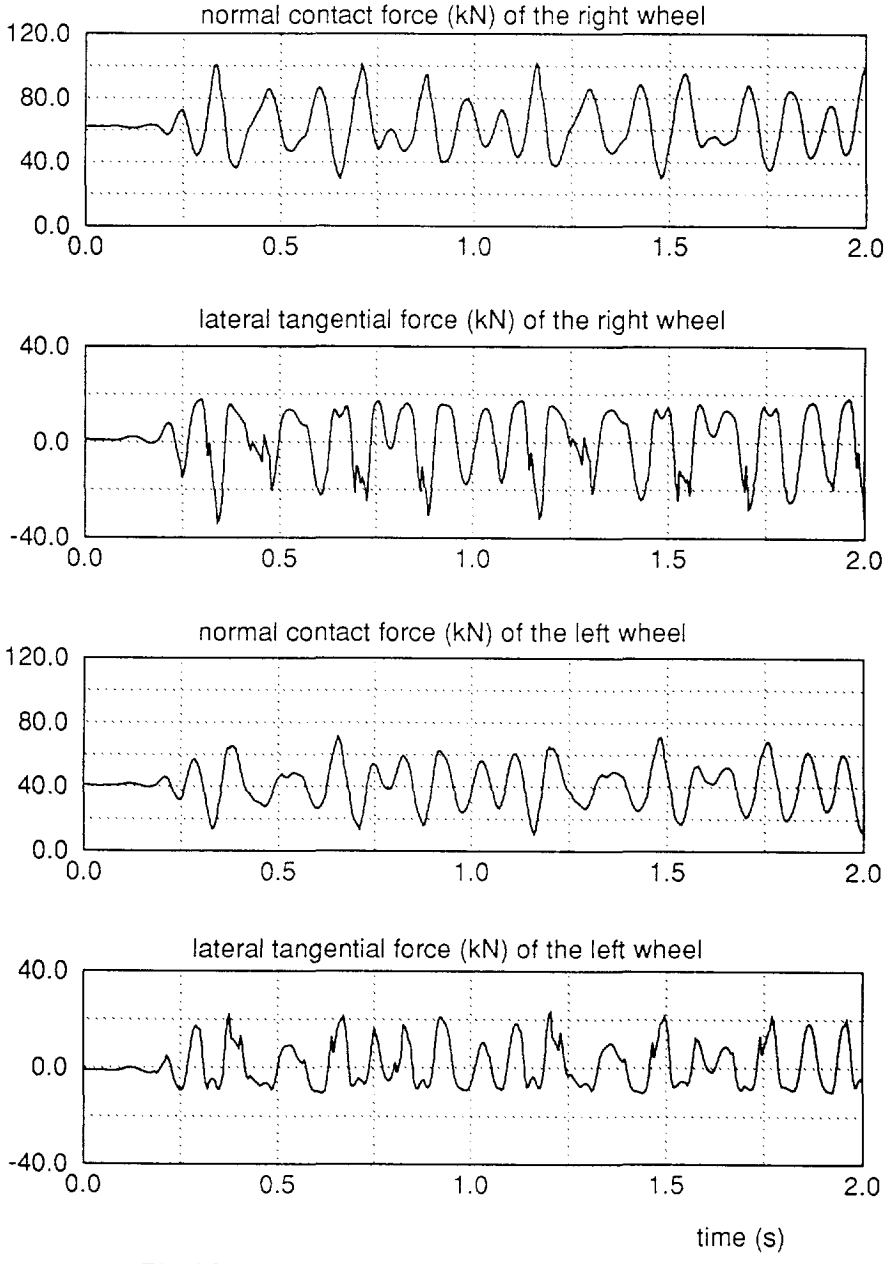

Fig.6.3.4. The contact forces of the fourth wheelset.

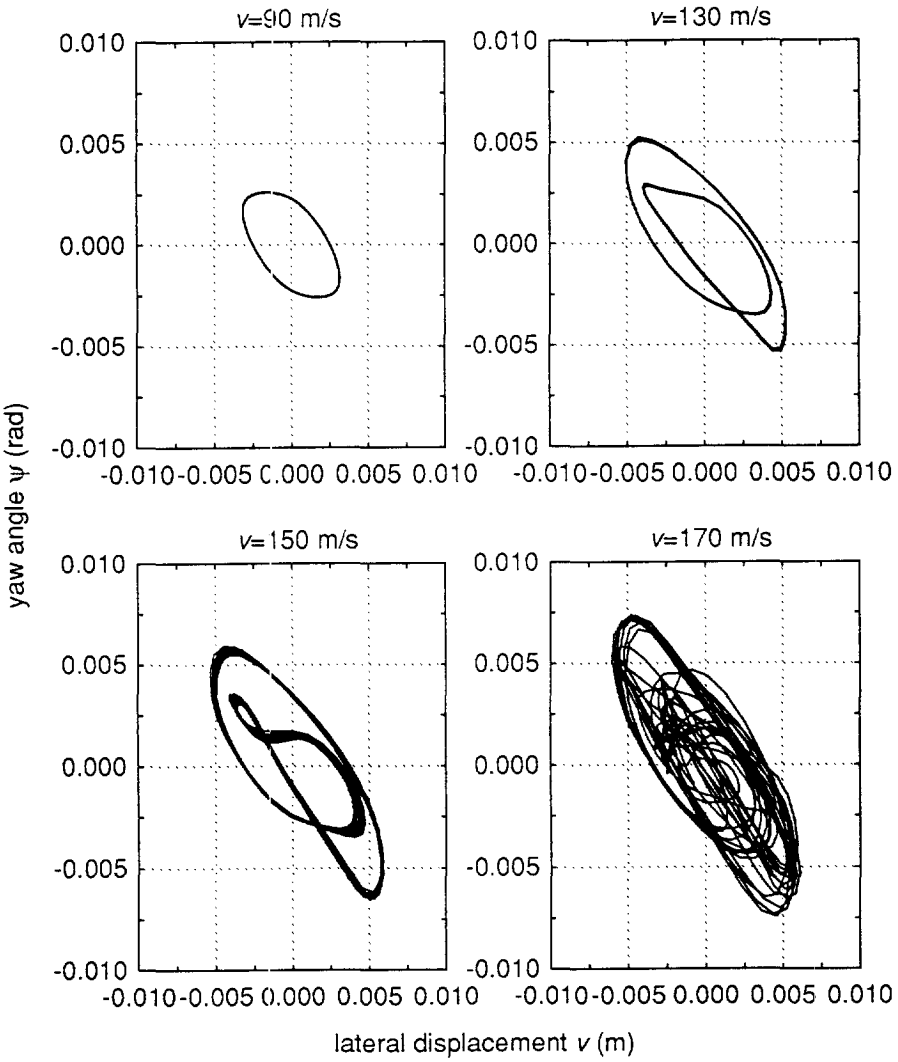

Fig.6.3.5. The relation between the lateral displacement and the yaw angle for the fourth wheelset.

The lateral responses of the wheelsets are shown in Fig.6.3.3. Under the aforementioned initial conditions, the 1st and 2nd wheelsets soon achieve limit cycles; the other two perform chaotic motions. The lateral amplitudes of the first three wheelsets

are at the same level of about 2mm; but the dynamic response of the 4th wheelset is critical. Its lateral amplitude is about 6.1mm and thus it is much larger than those of the other wheelsets. Fig.6.3.4 indicates the influence of the excentricity of the carbody mass centre on the contact forces of the 4th wheelset; the amplitudes of the contact forces applied at the right-hand wheel are larger than those at the left-hand wheel; the mean values of the normal forces approach the stationary values.

The simulations have also been carried out for the vehicle running at other speeds. Fig.6.3.5 demonstrates the influence of the vehicle speed. With the increase of the speed, the amplitudes increase and the limit cycle of the lateral motion of the 4th wheelset becomes chaotic at high speed.

The influence of the profiles is studied by comparing the dynamic responses of the vehicle moving along the three kinds of the tracks which are *UIC60-S1002 Standard*, *CTO-Measured-Profiles*, *ORE-Benchmark-Profiles*. The detailed investigations indicate that the *ORE-Benchmark-Profiles* provide the best dynamic properties. Below 150m/s the lateral motion quickly tends to the stationary motion. Because of the asymmetry of the profiles, the wheelset mass centre moves away from the track centre to stay at the position where v=-0.81mm corresponding to the zero difference of the rolling radii (see Fig.6.3.6). At 170 m/s, the wheelsets of the trailing bogie hunt with very small amplitudes: 0.5mm at the leading wheelset and 1mm at the trailing wheelset, whereas the wheelsets of the leading bogie are stationary. Between 210 and 220 m/s, the trailing wheelset of the leading bogie starts moving laterally, resulting even in flange contact.

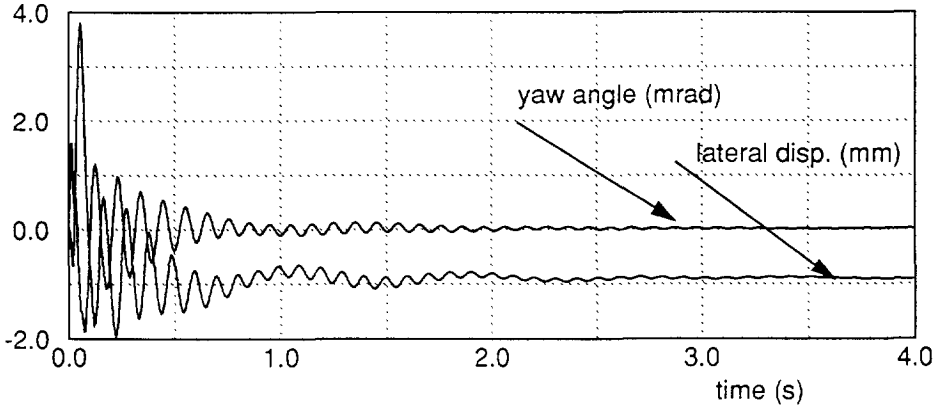

Fig.6.3.6. The response of the 4th wheelset of Kik's vehicle model with ORE-Benchmark-Profiles at 150 m/s.

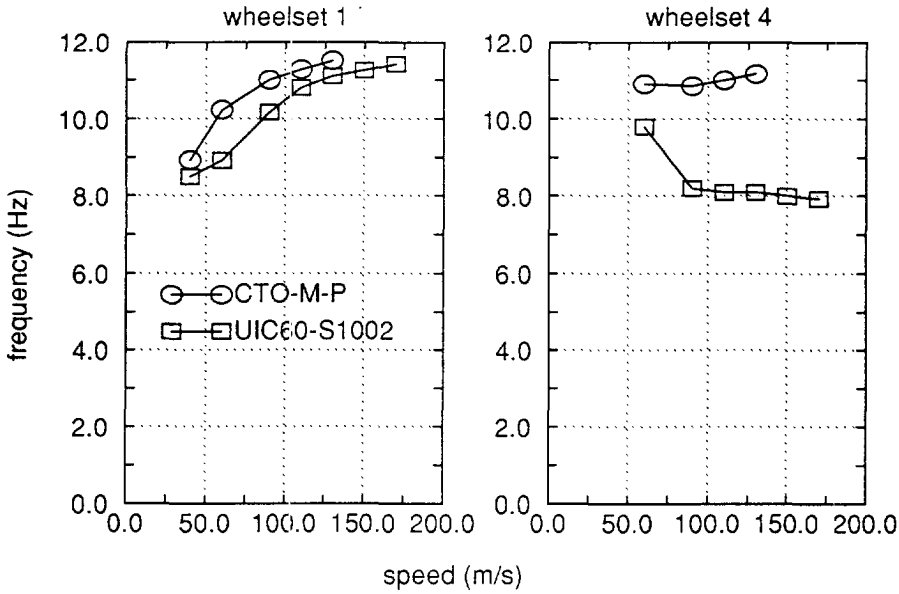

Fig.6.3.7. The relation between the frequency and the velocity.

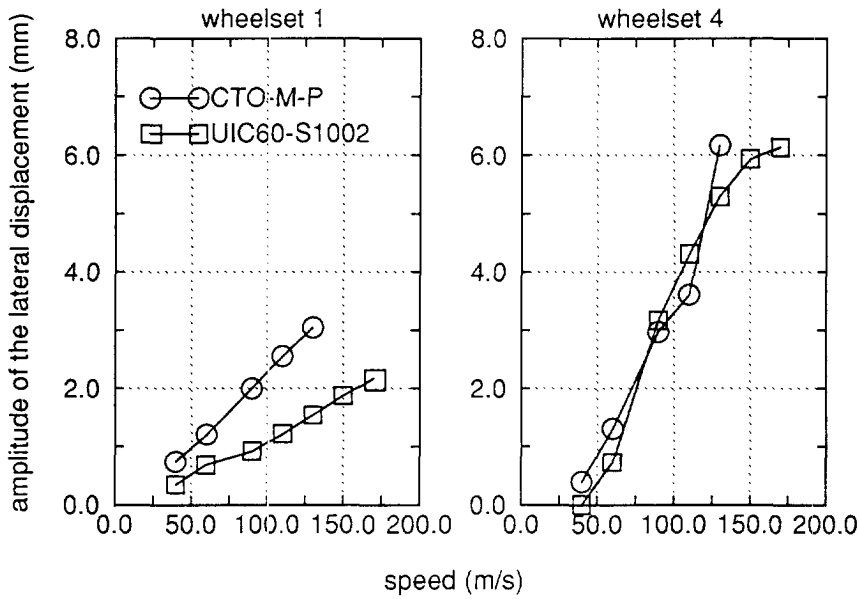

Fig.6.3.8 The relation between the lateral displacement and the velocity.

For the other two combinations of the profiles, the results are compared in Figs.6.3.7-6.3.8. By contrast to the situation with *ORE-Benchmark-Profiles*, these two

combinations show that the flange contact tends to occur at the 4th wheelset. The critical speeds of flange contact are also lower: for *UIC60-S1002 Standard* it is in the range of 170m/s-180m/s and for *CTO-Measured-Profiles* it is in the range of 130m/s-140m/s. For the 1st wheelset the hunting frequency changes significantly with speed . Above a certain speed the frequency of the 4th wheelset remains around 8 Hz for *UIC60-S1002 Standard.* For *CTO-Measured-Profiles* the frequency of that wheelset is always around 11 Hz. These simulation results signify that the dynamic behaviour of the vehicle with the *UIC60-S1002 Standard* profiles is better than that of the vehicle with *CTO-Measured-Profiles.*

The analysis confirms that the contact geometry plays a very important role in railway vehicle dynamics. A jump of the contact point occurring even at small lateral displacements induces the hunting motion.

6.4. Vehicles with Independently Rotating Wheels

First the conventional single wheelset model defined in the second example in Section 6.2 is modified into an IRW system. The dynamic response of the IRW system is shown in Fig.6.4.1. By contrast to the situation for the conventional wheelset, at a speed of 9m/s both the lateral motion and the yaw motion of the IRW system slowly converge to a stationary motion; the average wave length for the IRW is equal to 16.75m, which is much longer than that for the conventional wheelset. It is seen that releasing the spin rotation constraint between the two wheels may improve the dynamic behaviour of the single wheelset system.

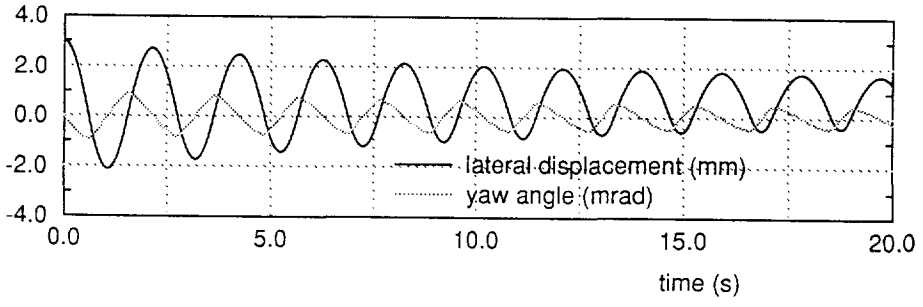

Fig.6.4.1. The response of the wheelset with IRW at 9m/s

Secondly, we compare two kinds of two-axle bogies, one with conventional

wheelsets and the other with independently rotating wheels. The inertia properties of the systems as well as the geometric configurations are selected from Kik's benchmark; but the suspensions are modified by removing the longitudinal cross bracing and the two axle bracing, and by reducing stiffness of the primary longitudinal and lateral springs from $4.0 \cdot 10^6$ to $8.0 \cdot 10^5$ N/m. Fig.6.4.2 shows the dynamic responses of the lateral displacement and the yaw angle of the wheelset at a speed of 35m/s.

For the conventional bogie we now observe a hunting motion. The amplitudes of its trailing wheelset are slightly larger than those of the leading wheelset and the wave lengths are almost equal (10.5m). As compared to the motion of the conventional bogie, the motion of the bogie with IRW is quite stationary. The yaw angles of the wheelsets with IRW vanish; but the wheelset centres shift about 4.2mm to the left-hand side of the track. In spite of the large lateral displacement, the longitudinal tangential contact forces vanish as expected. The reason is that the difference of rolling radii no longer generates a sufficiently large tangential force which tends to move the wheelsets to the central position for the symmetric profiles or to a position where the difference of the rolling radii is near to zero for the asymmetric profiles.

The third example is to study the influence of the sequence of the IRW wheelset by comparing three vehicles which are modifications of Kik's benchmark. In the first vehicle model all four conventional wheelsets are replaced by wheelsets with IRW; in the second model only the trailing bogie is equipped with two unconventional wheelsets; in the third model the wheelsets of the leading bogie are replaced by IRW systems. The results shown in Figs.6.4.3 to 6.4.5 refer to the same speed: 40m/s. In agreement with the remark in Section 6.1, we see that in Figs.6.4.3 and 6.4.4, the results are unreliable after a certain lapse of time.

The responses of the wheelset of the leading bogie for the first and third vehicles are similar. The yaw angles vanish; the wheelsets first run off the track centre about 5mm and then slowly go down to 4mm. The motions of the trailing bogies of the first and second vehicles are unstable; the flange contacts first occur at the leading wheelset (third wheelset). Among the three vehicles only the third one may be considered as stable. A detailed investigation shows that the first wheelset achieves flange contact at a speed in between 90m/s and 110m/s.

Evidently, as compared with the conventional vehicle discussed in the preceding section, these three vehicles are unacceptable. To implement the IRW technique in the railway vehicles needs further comprehensive investigations.

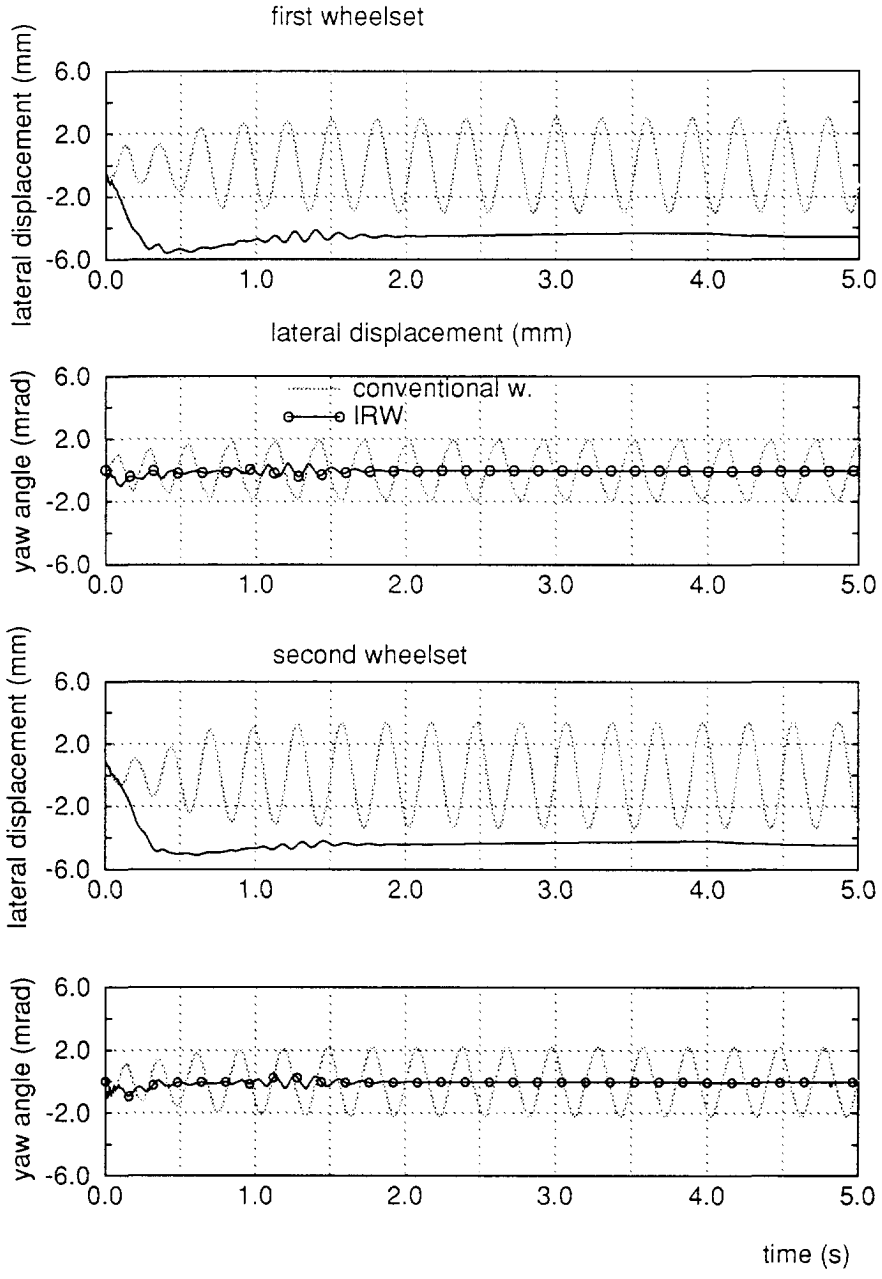

Fig.6.4.2. The response of the bogie models.

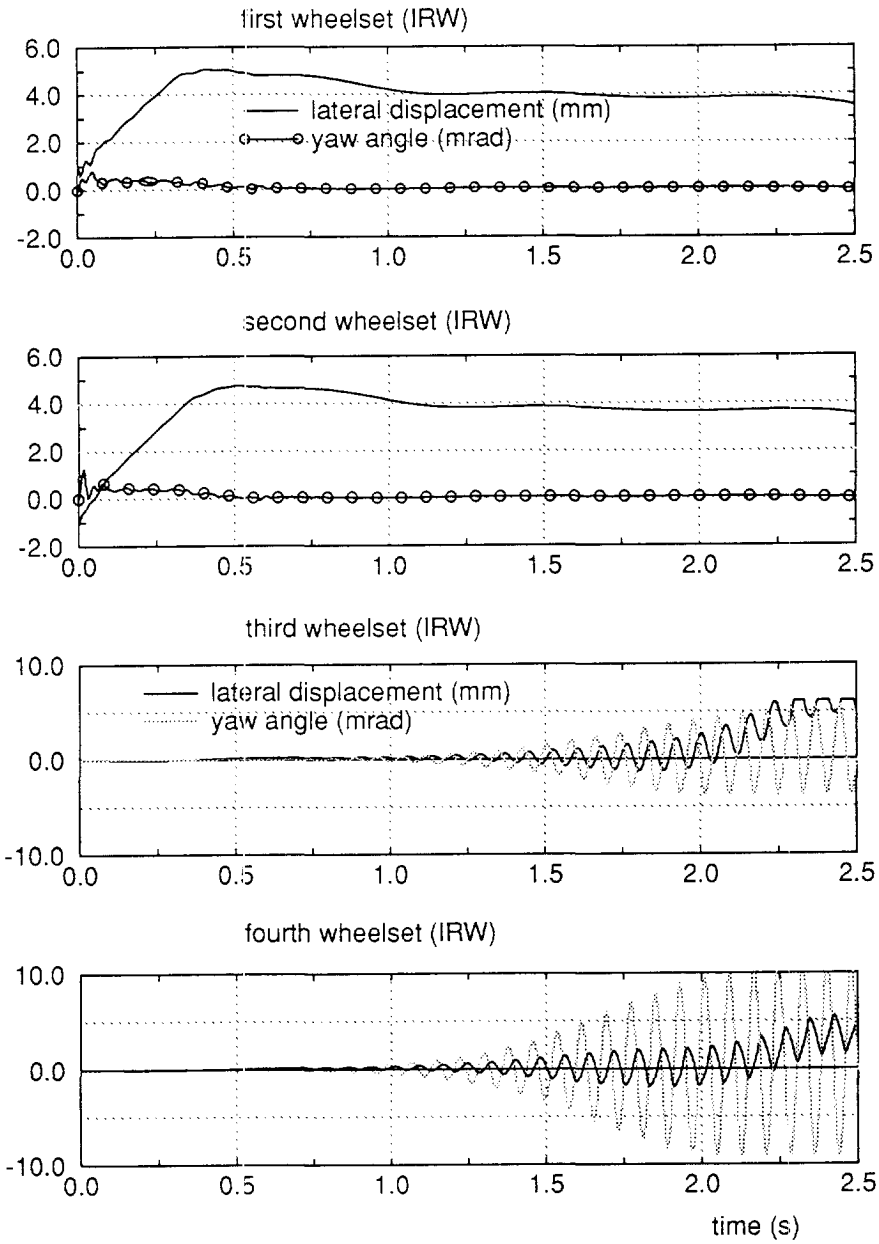

Fig.6.4.3. The response of the first vehicle model at 40m/s.

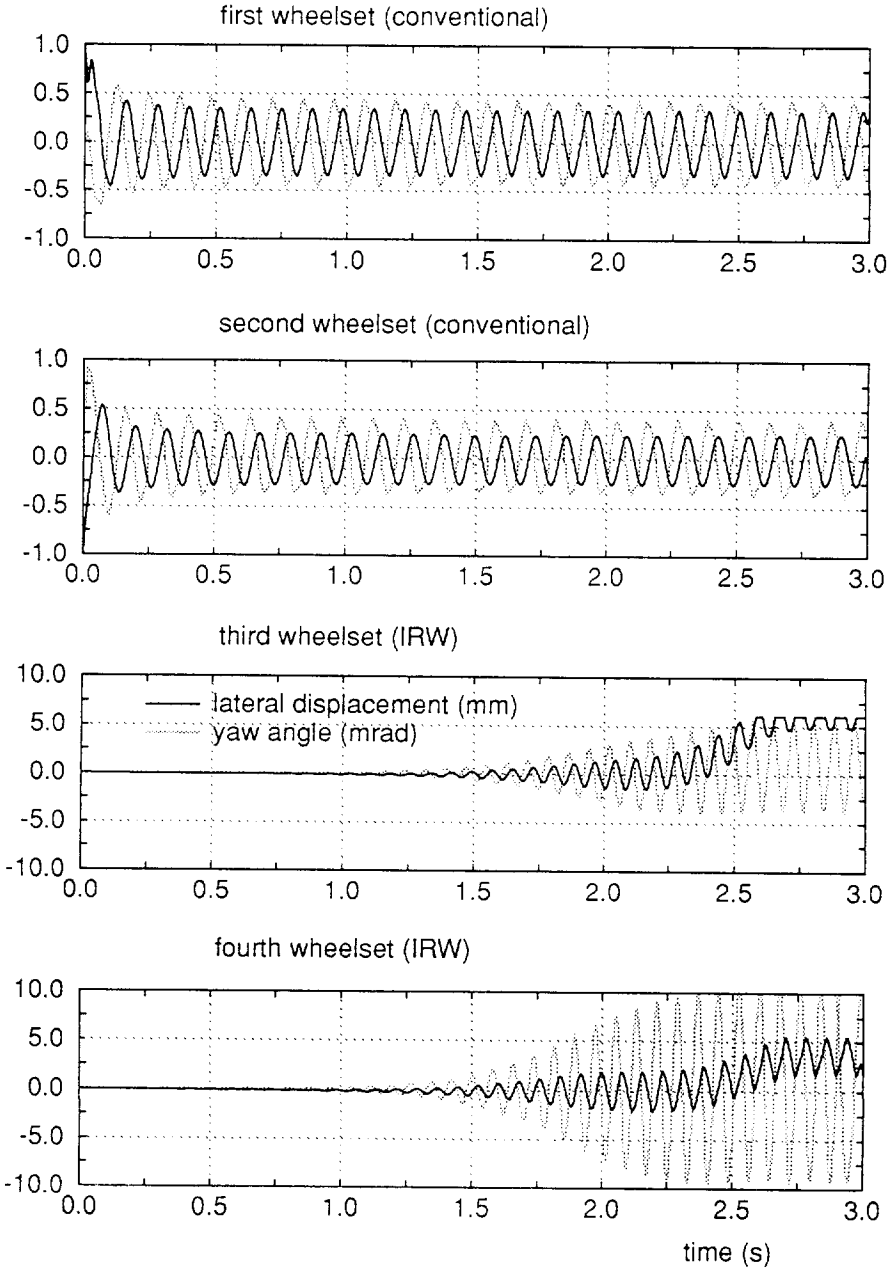

Fig.6.4.4. The response of the second vehicle model at 40m/s.

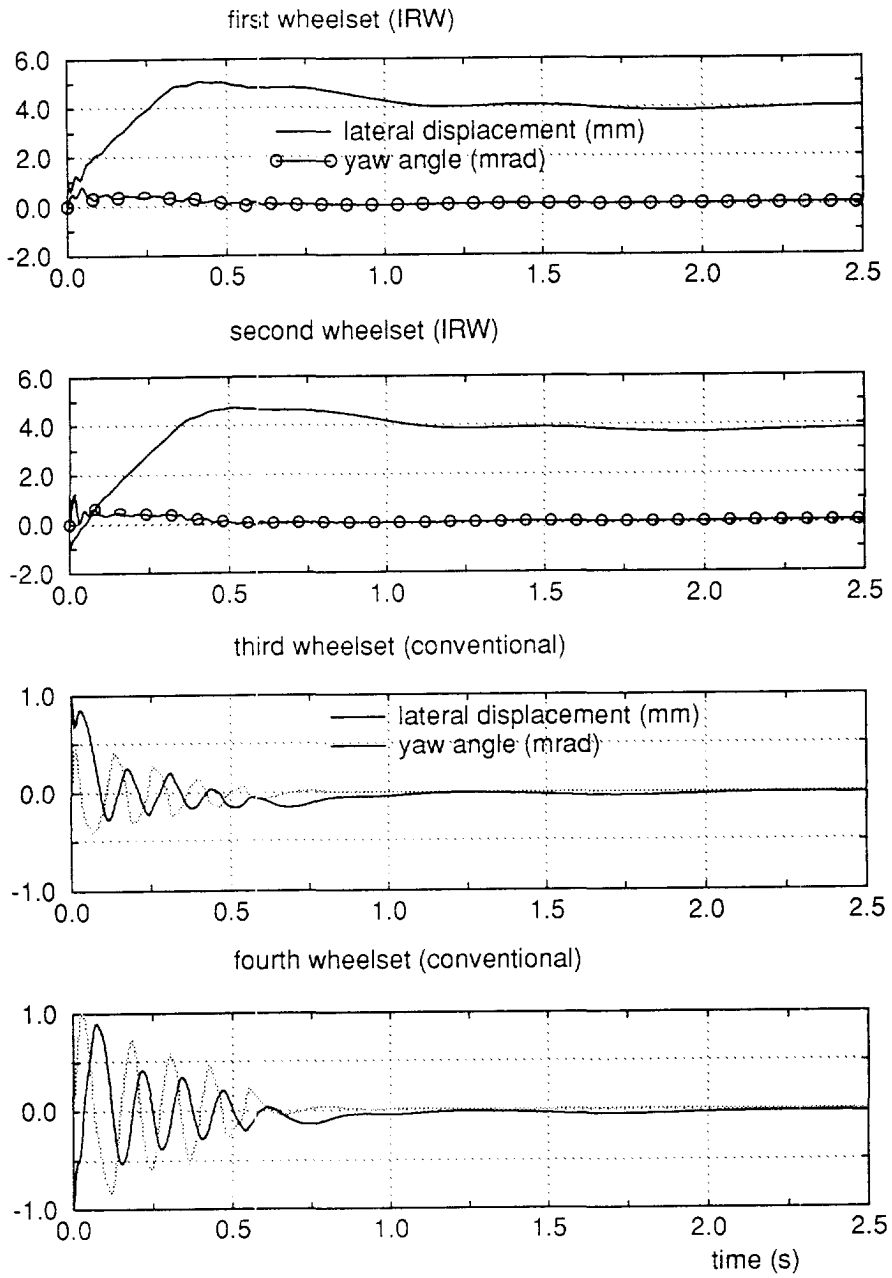

Fig.6.4.5. The response of the third vehicle model at 40m/s.

6.5. Influence of track irregularities

The track irregularities are, in general, discussed in Section 4.8. According to the numerical results shown in Section 3.5.3, the variation of the track gauge shifts the double-contact position, for instance, in the case of the well-known profile combination of *UIC60-S1002*. When the track irregularities are taken into account in the dynamic simulation, in order to avoid the difficulty in the online determination of the geometric contact position, the rail and wheel profiles, (*UIC60-S1002-Standard*) of the vehicle required in Kik's benchmark are replaced by the combination of *ORE-Benchmark-Profiles*. As shown in Section 6.3, among the three analyzed vehicles the one equipped with *ORE-Benchmark-Profiles* provides the best dynamic behaviour; its critical speed of the hunting motion is higher than 150m/s.

All four kinds of track irregularities can be handled in the dynamic simulations but no attempt is made to use recorded real track irregularities. Sinusoidal excitations are easily arranged and can be used here without loss of generality. As an example, the variation of the track gauge and the cross level are represented only by the first harmonic and the lateral and vertical alignment by the first and third harmonics; they are given as follows:

- the variation of the track gauge:

$$\delta b = 0.001 \sin\left(\frac{2\pi s}{40}\right), \tag{6.5.1}$$

- the lateral alignment:

$$\delta \Delta b = 0.002 \sin\left(\frac{2\pi s}{40}\right) + 0.001 \sin\left(\frac{6\pi s}{40}\right), \tag{6.5.2}$$

- the cross level:

$$\delta \Delta r = 0.001 \sin\left(\frac{2\pi s}{25}\right), \tag{6.5.3}$$

- the vertical alignment:

$$\delta r = 0.002 \sin\left(\frac{2\pi s}{25}\right) + 0.001 \sin\left(\frac{6\pi s}{25}\right). \tag{6.5.4}$$

The wave lengths of the lateral and vertical alignments are equal to 25m and 40m respectively. At a speed of 60m/s they correspond to excitation frequency of 2.4Hz and 1.5Hz respectively and at 90m/s they correspond to 3.6Hz and 2.25Hz. Due to the irregularities, the hunting motion arises. As shown in Fig.6.5.1, the accelerations are most sensitive to the third harmonic of both wave lengths. The information

gained will be of great value for understanding the influence of the track irregularities on the railway vehicle dynamics.

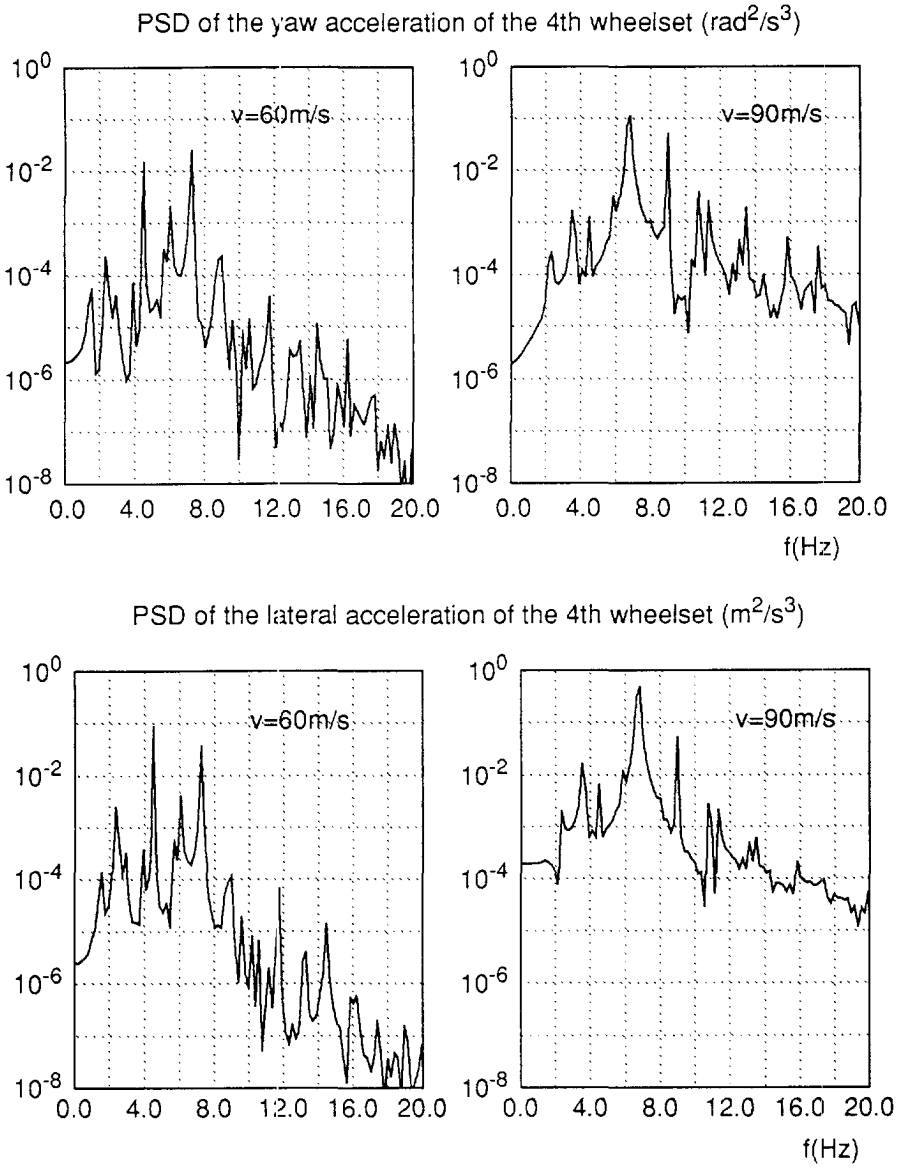

Fig.6.5.1 The influence of the track irregularities (power spectral density).

Chapter 7

Conclusions and Recommendations for Future Research

Our objective to develop a reliable and highly accurate computer-aided analysis tool based on the multibody system method to predict and evaluate the dynamic behaviour of railway vehicle systems has been reached to a great extent. The equations of motion of the vehicle system have been derived in terms of the independent generalized coordinates, which represent the motion of the bodies relative to the nominal motion of the vehicle. The geometrical and physical nonlinearities due to the contact between rail and wheel have been incorporated in the vehicle models and are handled accurately. The nonlinearities of suspension characteristics can also be taken into account in the vehicle models.

We realize that the geometric contact constraints between track and wheelset depend only on the small segment around the nominal position of the wheelset. In case of a curved track it is in general sufficient to replace the actual curved track by the tangent along the track curve in determining the constraints. Hence, in the curving studies we can directly make use of the numerical methods for the tangent track discussed in Chapter 3.

When the motion of the track reference frame is defined properly, it is shown that this motion is independent of the contact constraints in the wheelset system (for the case of a transition curved track, this is an approximation). If so, the generalized coordinates are restricted by the constraints which are both holonomic and scleronomic. Then the analytical expressions for the components of the Jacobian matrix associated with the contact constraints are obtained as functions of the generalized coordinates, the contact coordinates and the contact angles. Using these analytical expressions leads to an improvement of the accuracy of the integrating process.

In the derivation of the general equations of motion of a single wheelset moving along an arbitrary track, the traditional and still extensively used methods. in which parameters such as the difference of rolling radii, the equivalent conicity and the gravitational stiffness (Garg 1984) are applied, have been completely abandoned. Meanwhile, the longitudinal translation and the spin rotation were no

longer assumed to be constant in contradistinction to what most investigators do, and they were chosen as independent generalized coordinates in the equations of motion. Moreover, the whole vehicle system was fully described in three dimensions.

In the literature about establishing the equations of motion of a wheelset equipped with independently rotating wheels, it is often assumed a priori that the longitudinal creepages of both wheels vanish. But the consequence of this (incorrect) assumption would be that it gives rise to two additional nonholonomic constraints to ensure zero longitudinal creepages. As shown in Chapter 5, once the relative spin rotation between the two wheels is fixed, the equations of motion of the subsystem reduce to those for the conventional wheelset, as it would be expected.

In certain combinations of rail and wheel profiles there are double-contacts even for small lateral displacements. These double-contacts divide the profiles into several sections and it is of interest to know that the edges of the sections remain almost the same when the track gauge and the yaw angle vary. This enables us to set up a method to judge accurately the contact region during online determination of the geometric contact constraints in the dynamic simulations. Moreover, the online calculation of the geometric contact position makes it possible to consider the irregularities of the track more properly.

These double-contacts destabilize the motion of the vehicles. Hence, in the design of new combinations of rail and wheel profiles, such double-contacts should be avoided. Moreover, the phenomenon of double-contact existing in service lines needs to be investigated in more detail in order to know whether this occurs already for new wheels or starts after wear in service.

The maximum normal force exerted at the contact patch comprises the static and dynamic loads. A direct method to reduce the contact forces seems to be lowering the weight of the whole vehicle system by using new materials and by optimizing the structure of the vehicle. In order to minimize the dynamic normal load and the tangential contact forces, the vehicle should be operated at a speed for which the parasitic motion is absent. Consequently, in order to increase the vehicle speed, it is necessary to investigate the relation between the design parameters and the stability of the stationary motion.

Despite the fact that the lateral responses of the single wheelset with independently rotating wheels and the bogie equipped with IRW show better dynamic behaviour as compared to the conventional wheelset and bogie, the complete vehicle equipped with IRW behaves in a quite different manner. Therefore, it is inappropriate to eliminate the spin constraint between the two wheels completely. However, making use of advantages of the IRW technology, for instance, by installing elastic and damping devices or controlled actuators between

the two wheels to adjust the longitudinal contact force and to avoid large stationary lateral shift as well as to deliver sufficient guidance, may provide railway engineers with a good opportunity to achieve a more optimal design. More simulations and theoretical analyses are required with the now available tools to evaluate such devices.

The simulation subroutines for a vehicle negotiating a curved track will be accomplished in the near future. Special attention is to be paid to the transition curve, in which flange contact often occurs. The dynamic behaviour of the vehicles with advanced IRW devices passing through a curve is also of interest to be studied.

The wheel flange plays an extremely important role in the safety aspect of the vehicle. The flange operates as a limiting device to the lateral displacement and the corresponding forces. To study the vehicle derailment, an appropriate simulation of the flange contact requires more accurate considerations of the geometric contact between the track and wheelset system. Meanwhile, due to the large lateral force applied at the rail in this case, it would be better also to incorporate the displacement and the rotation of the rail in the investigations.

Besides passive suspension systems, active-controlled suspension systems and mechanism linkage systems are more and more applied in railway vehicle design. Both the kinematic and the dynamic analysis methods have to be extended in order to be able to analyse such systems.

Appendices

A. Geometric and Algebraic Representations in Kinematics

The position of an object in the three-dimensional Euclidean space is commonly specified with respect to a Cartesian coordinate system. A Cartesian frame is characterized by the location of its origin o and its three orthogonal base vectors $\bar{e}_i$ (i=1,2,3). We restrict ourselves to orthogonal bases. The frame is simply designated by the notation $\{o, \bar{\boldsymbol{e}}\}$. The symbol $\bar{\boldsymbol{e}}$ denotes the vector basis of the coordinate system and reads

$$\bar{\boldsymbol{e}} = \left[\bar{e}_1, \ \bar{e}_2, \ \bar{e}_3 \right]^T . \tag{A.1}$$

A directed line segment from one point in space to another one is called a geometric vector or simply a vector. If a geometric vector is denoted by $\bar{a}$ and the components of it with respect to three axes of the frame $\{o, \bar{\boldsymbol{e}}\}$ are a_1, a_2 and a_3 respectively, $\bar{a}$ can be expressed by

$$\bar{a} = \bar{\boldsymbol{e}}^T \boldsymbol{a} = \boldsymbol{a}^T \bar{\boldsymbol{e}} \tag{A.2}$$

with

$$\boldsymbol{a} = [\, a_1, \ a_2, \ a_3 \,]^T . \tag{A.3}$$

$\boldsymbol{a}$ is called an algebraic vector with three components.

In general, we have used overlining such as $\bar{a}$ for the geometric description (in which a quantity is independent of the definition of a coordinate system), and a bold font such as $\boldsymbol{a}$ for the algebraic description (in which a quantity is taken with respect to a certain coordinate system).

The scalar product and the vector product of two arbitrary vectors in space are determined by

$$\bar{a} \cdot \bar{b} = \boldsymbol{a}^T \boldsymbol{b} = \boldsymbol{b}^T \boldsymbol{a} \tag{A.4}$$

and

$$\bar{a} \times \bar{b} = \bar{c}, \qquad \tilde{\boldsymbol{a}}\, \boldsymbol{b} = \boldsymbol{c}, \tag{A.5}$$

where the tilde operator "~" generates a 3×3 skew-symmetric matrix $\tilde{\boldsymbol{a}}$ from an

algebraic vector $\boldsymbol{a}$ in such a way that

$$\tilde{\boldsymbol{a}} = \begin{bmatrix} 0 & -a_3 & a_2 \\ a_3 & 0 & -a_1 \\ -a_2 & a_1 & 0 \end{bmatrix}. \tag{A.6}$$

Note that the algebraic vectors $\boldsymbol{a}$, $\boldsymbol{b}$ and $\boldsymbol{c}$ in Eqs.(A.4) and (A.5), corresponding to the geometric vectors $\bar{a}$, $\bar{b}$ and $\bar{c}$ respectively, are taken with respect to the same orthogonal frame, e.g., the frame $\{o, \bar{\boldsymbol{e}}\}$.

The relation between two frames in space is determined by the position vector linking their origins and the 3×3 matrix for the rotation from one frame to the other. We denote the two frames by $\{o^i, \bar{\boldsymbol{e}}^i\}$ and $\{o^j, \bar{\boldsymbol{e}}^j\}$ respectively. The rotation matrix $\boldsymbol{G}^{ji}$ carrying $\{o^i, \bar{\boldsymbol{e}}^i\}$ to $\{o^j, \bar{\boldsymbol{e}}^j\}$ is defined by

$$\bar{\boldsymbol{e}}^j = \boldsymbol{G}^{ji}\,\bar{\boldsymbol{e}}^i. \tag{A.7}$$

The rotation matrix $\boldsymbol{G}^{ji}$ is an orthogonal matrix, which implies that

$$\boldsymbol{G}^{ij} = [\boldsymbol{G}^{ji}]^{-1} = [\boldsymbol{G}^{ji}]^T, \tag{A.8}$$

where $\boldsymbol{G}^{ij}$ is the rotation matrix from $\{o^j, \bar{\boldsymbol{e}}^j\}$ to $\{o^i, \bar{\boldsymbol{e}}^i\}$.

A quantity relating two frames such as the rotation matrix $\boldsymbol{G}^{ji}$ is generally indicated by two superscripts. Additionally, if necessary, an algebraic vector with respect to a frame is indicated by a left superscript, e.g., ${}^j\boldsymbol{a}$ represents the components of geometric vector $\bar{a}$ with respect to the frame $\{o^j, \bar{\boldsymbol{e}}^j\}$. These notational rules are taken from Roberson and Schwertassek (1989).

As we know, the components of $\bar{a}$ can be given either in the frame $\{o^i, \bar{\boldsymbol{e}}^i\}$ or in the frame $\{o^j, \bar{\boldsymbol{e}}^j\}$, thus,

$$\bar{a} = \bar{\boldsymbol{e}}^{iT}\,{}^i\boldsymbol{a} = \bar{\boldsymbol{e}}^{jT}\,{}^j\boldsymbol{a}. \tag{A.9}$$

Using Eq.(A.7) leads to

$${}^j\boldsymbol{a} = \boldsymbol{G}^{ji}\,{}^i\boldsymbol{a}. \tag{A.10}$$

More details of the vector algebra and the transformations of the coordinate systems are given in Bowen and Wang (1980).

We designate the position vector of the origin o^j relative to $\{o^i, \bar{\boldsymbol{e}}^i\}$ by $\bar{s}$. The relation between the rotation matrix $\boldsymbol{G}^{ji}$ and the angular velocity vector $\bar{\omega}^{ji}$ of the frame $\{o^j, \bar{\boldsymbol{e}}^j\}$ relative to the frame $\{o^i, \bar{\boldsymbol{e}}^i\}$ is (Roberson and Schwertassek, 1989)

$$\frac{d\boldsymbol{G}^{ji}}{dt} = -{}^j\tilde{\boldsymbol{\omega}}^{ji}\,\boldsymbol{G}^{ji}, \tag{A.11}$$

where ${}^{j}\boldsymbol{\omega}^{ji}$ represents the algebraic vector of the angular velocity taken with respect to the frame $\{o^j, \bar{e}^j\}$

$$\bar{\omega}^{ji} = \bar{e}^{jT}\, {}^{j}\boldsymbol{\omega}^{ji}. \tag{A.12}$$

We consider a particle P. Its position vector relative to $\{o^j, \bar{e}^j\}$ is denoted by $\bar{\rho}$ (see Fig.A.1) and the vector relative to $\{o^i, \bar{e}^i\}$ by $\bar{r}$; then

$$\bar{r} = \bar{s} + \bar{\rho}. \tag{A.13}$$

Differentiating both sides of the last equation, we obtain the velocity vector and the acceleration vector of the particle P as viewed from the frame $\{o^i, \bar{e}^i\}$:

$$\dot{\bar{r}} = \dot{\bar{s}} + \dot{\bar{\rho}} + \bar{\omega} \times \bar{\rho} \tag{A.14}$$

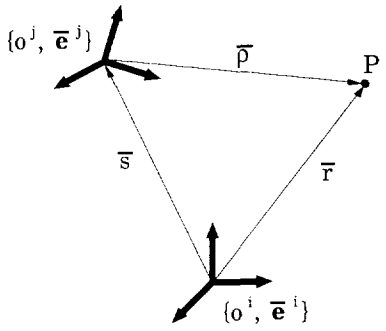

Fig. A1. The position of point P.

and

$$\ddot{\bar{r}} = \ddot{\bar{s}} + \ddot{\bar{\rho}} + \dot{\bar{\omega}} \times \bar{\rho} + \bar{\omega} \times (\bar{\omega} \times \bar{\rho}) + 2\bar{\omega} \times \dot{\bar{\rho}}, \tag{A.15}$$

where we notice that $\dot{\bar{\rho}}$ and $\ddot{\bar{\rho}}$ represent the velocity and acceleration vectors of the particle as viewed from the frame $\{o^j, \bar{e}^j\}$.

The algebraic descriptions corresponding to Eqs.(A.13)-(A.15) are taken with respect to the frame $\{o^i, \bar{e}^i\}$. So we have:

$$\boldsymbol{r} = \boldsymbol{s} + \boldsymbol{G}^{ij}\, {}^{j}\boldsymbol{\rho}, \tag{A.16}$$

$$\dot{\boldsymbol{r}} = \dot{\boldsymbol{s}} + \boldsymbol{G}^{ij}\, {}^{j}\dot{\boldsymbol{\rho}} + \boldsymbol{G}^{ij}\, {}^{j}\tilde{\boldsymbol{\omega}}\, {}^{j}\boldsymbol{\rho} \tag{A.17}$$

and

$$\ddot{\boldsymbol{r}} = \ddot{\boldsymbol{s}} + \boldsymbol{G}^{ij}\, {}^{j}\ddot{\boldsymbol{\rho}} + \boldsymbol{G}^{ij}\, {}^{j}\dot{\tilde{\boldsymbol{\omega}}}\, {}^{j}\tilde{\boldsymbol{\rho}} + \boldsymbol{G}^{ij}\, {}^{j}\tilde{\boldsymbol{\omega}}\, {}^{j}\tilde{\boldsymbol{\omega}}\, {}^{j}\boldsymbol{\rho} + 2\boldsymbol{G}^{ij}\, {}^{j}\tilde{\boldsymbol{\omega}}\, {}^{j}\dot{\boldsymbol{\rho}} \tag{A.18}$$

The algebraic vectors ${}^{j}\boldsymbol{\rho}$, ${}^{j}\dot{\boldsymbol{\rho}}$ and ${}^{j}\ddot{\boldsymbol{\rho}}$ correspond to the geometric vectors $\bar{\rho}$, $\dot{\bar{\rho}}$ and $\ddot{\bar{\rho}}$ respectively and are taken with respect to the frame $\{o^j, \bar{e}^j\}$.

B. General Representation of Rotation

The rotation of a body in space is a motion with three degrees of freedom. We can use either the four Euler parameters, only three of which are independent, or three independent angles to represent the rotation. Here we give a general definition of these angles and also determine the corresponding angular velocity and acceleration.

We utilise the symbols o-i (i=1,2,3) to indicate the three axes of the body-fixed frame $\{o, \bar{e}\}$. Without loss of generality, we suppose that the body-fixed frame $\{o, \bar{e}\}$ is coinciding with a frame $\{o, \bar{e}^1\}$ at the beginning of the rotations and that the final position of the body-fixed frame is obtained by the following sequence of operations: a rotation θ_1 about the o-l axis, followed by a rotation θ_2 about the o-m axis and followed by a rotation θ_3 about the o-n axis. The index l is one of the integers 1, 2 and 3; so are the indices m and n. These indices must satisfy the conditions: m is equal to neither l nor n.

The angles to represent the rotation of a frame are θ_1, θ_2 and θ_3. We introduce three auxiliary frames $\{o, \bar{e}^2\}$, $\{o, \bar{e}^3\}$ and $\{o, \bar{e}^4\}$. These frames coincide respectively with the three positions of the body-fixed frame after each rotation; the final position of the body-fixed frame is identical with the frame $\{o, \bar{e}^4\}$. Thus, we use G^{41}, G^{42} and G^{43} to indicate the rotation matrices from the frames $\{o, \bar{e}^1\}$, $\{o, \bar{e}^2\}$ and $\{o, \bar{e}^3\}$ to the final frame $\{o, \bar{e}^4\}$, respectively. We obtain

$$G^{41} = A^n(\theta_3)A^m(\theta_2)A^l(\theta_1), \quad G^{42} = A^n(\theta_3)A^m(\theta_2), \quad G^{43} = A^n(\theta_3), \qquad \text{(B.1)}$$

where the matrices A^l, A^m and A^n, given by Roberson (1989 p69-70), represent the rotation matrices between two adjacent frames, e.g., the rotation matrix from the frame $\{o, \bar{e}^2\}$ to the frame $\{o, \bar{e}^3\}$ is denoted by the notation A^m, which may be one of the following matrices

$$A^1(\alpha)=\begin{bmatrix} 1 & 0 & 0 \\ 0 & \cos\alpha & \sin\alpha \\ 0 & -\sin\alpha & \cos\alpha \end{bmatrix}, \quad A^2(\alpha)=\begin{bmatrix} \cos\alpha & 0 & -\sin\alpha \\ 0 & 1 & 0 \\ \sin\alpha & 0 & \cos\alpha \end{bmatrix}, \quad A^3(\alpha)=\begin{bmatrix} \cos\alpha & \sin\alpha & 0 \\ -\sin\alpha & \cos\alpha & 0 \\ 0 & 0 & 1 \end{bmatrix}. \qquad \text{(B.2)}$$

The angular velocity of the body relative to the frame $\{o, \bar{e}^1\}$ contains three relative angular velocities which are associated with the three rotations. We write

$$\bar{\omega} = \bar{\omega}^{21} + \bar{\omega}^{32} + \bar{\omega}^{43} \qquad \text{(B.3)}$$

with

$$\bar{\omega}^{21} = \bar{e}^{1T} \boldsymbol{\lambda}^{l}(\theta_1), \qquad \bar{\omega}^{32} = \bar{e}^{2T} \boldsymbol{\lambda}^{m}(\theta_2), \qquad \bar{\omega}^{43} = \bar{e}^{3T} \boldsymbol{\lambda}^{n}(\theta_3), \tag{B.4}$$

where $\boldsymbol{\lambda}^{i}(\alpha)$ $(i=1,2,3)$ is defined in such a way that the *k-th* $(k=1,2,3)$ component of it is equal to zero for $i \neq k$ or $\dot{\alpha}$ for $i=k$,

$$\boldsymbol{\lambda}^{1}(\alpha) = \begin{bmatrix} \dot{\alpha} \\ 0 \\ 0 \end{bmatrix}, \quad \boldsymbol{\lambda}^{2}(\alpha) = \begin{bmatrix} 0 \\ \dot{\alpha} \\ 0 \end{bmatrix}, \quad \boldsymbol{\lambda}^{3}(\alpha) = \begin{bmatrix} 0 \\ 0 \\ \dot{\alpha} \end{bmatrix}. \tag{B.5}$$

It is easy to show that

$$\boldsymbol{A}^{i}(\alpha)\boldsymbol{\lambda}^{i}(\alpha) = \boldsymbol{\lambda}^{i}(\alpha). \tag{B.6}$$

The algebraic vector of the angular velocity with respect to the body-fixed frame can be expressed as

$${}^{4}\boldsymbol{\omega} = {}^{4}\boldsymbol{\omega}^{21} + {}^{4}\boldsymbol{\omega}^{32} + {}^{4}\boldsymbol{\omega}^{43} \tag{B.7}$$

with

$${}^{4}\boldsymbol{\omega}^{21} = \boldsymbol{G}^{41}\boldsymbol{\lambda}^{l}(\theta_1), \qquad {}^{4}\boldsymbol{\omega}^{32} = \boldsymbol{G}^{42}\boldsymbol{\lambda}^{m}(\theta_2), \qquad {}^{4}\boldsymbol{\omega}^{43} = \boldsymbol{G}^{43}\boldsymbol{\lambda}^{n}(\theta_3). \tag{B.8}$$

We use notation $\boldsymbol{C}_{*,j}$ to represent the column j of matrix $\boldsymbol{C}$, i.e.,

$$\boldsymbol{C}_{*,j} = [\boldsymbol{C}_{1j}, \boldsymbol{C}_{2j}, \ \ldots \ , \boldsymbol{C}_{kj}]^{T}. \tag{B.9}$$

Eq.(B.7) reduces to

$${}^{4}\boldsymbol{\omega} = \boldsymbol{H}\dot{\boldsymbol{\theta}}, \tag{B.10}$$

where the coefficient matrix $\boldsymbol{H}$ of the angular velocity is determined by

$$\boldsymbol{H} = [\boldsymbol{G}^{41}_{*,l}, \boldsymbol{G}^{42}_{*,m}, \boldsymbol{G}^{43}_{*,n}]. \tag{B.11}$$

The components of the matrix $\boldsymbol{H}$ are only functions of the rotation angles.

Because the cross product of two identical vectors vanishes, the angular acceleration with respect to the body-fixed frame can be determined by differentiating both sides of Eq.(B.10)

$${}^{4}\dot{\boldsymbol{\omega}} = \boldsymbol{H}\ddot{\boldsymbol{\theta}} + \dot{\boldsymbol{H}}\dot{\boldsymbol{\theta}}. \tag{B.12}$$

The corresponding angular acceleration vector is

$$\dot{\bar{\omega}} = \bar{e}^{4T}\,{}^4\dot{\boldsymbol{\omega}}\,. \tag{B.13}$$

The classical choice of angles is $l = 3$, $m = 1$ and $n = 3$. The angles are universally known as the Euler angles. The rotation matrix for this case is

$$\boldsymbol{G}^{41} = \boldsymbol{A}^3(\theta_3)\boldsymbol{A}^1(\theta_2)\boldsymbol{A}^3(\theta_1). \tag{B.14}$$

In railway vehicle dynamics, the rotations are usually described by the yaw, rolling and pitch angles, i.e., l=3, m=1 and n=2. The yaw axis is the vertical axis of the vehicle (pointing downward), the rolling axis is about the forward axis and the pitch axis is about the remaining (lateral) axis. These angles are called Tait-Bryan angles in Roberson and Schwertassek (1989). When the three angles are denoted by

$$\theta_1 = \psi, \qquad \theta_2 = \phi, \qquad \theta_3 = \chi, \tag{B.15}$$

the rotation matrix can be written as

$$\boldsymbol{G}^{41} = \boldsymbol{A}^2(\chi)\boldsymbol{A}^1(\phi)\boldsymbol{A}^3(\psi). \tag{B.16}$$

The full expression of the rotation matrix given in the last equation is

$$\boldsymbol{G}^{41} = \begin{bmatrix} \cos\chi\cos\psi - \sin\phi\sin\chi\sin\psi & \cos\chi\sin\psi + \sin\phi\sin\chi\cos\psi & -\cos\phi\sin\chi \\ -\cos\phi\sin\psi & \cos\phi\cos\psi & \sin\phi \\ \sin\phi\cos\chi\sin\psi + \sin\chi\cos\psi & \sin\chi\sin\psi - \sin\phi\cos\chi\cos\psi & \cos\phi\cos\chi \end{bmatrix}. \tag{B.17}$$

The angular velocity given by Eq.(B.10) reduces to

$${}^4\boldsymbol{\omega} = \begin{bmatrix} \cos\chi & 0 & -\cos\phi\sin\chi \\ 0 & 1 & \sin\phi \\ \sin\chi & 0 & \cos\phi\cos\chi \end{bmatrix} \begin{bmatrix} \dot{\phi} \\ \dot{\chi} \\ \dot{\psi} \end{bmatrix} \tag{B.18}$$

and the angular acceleration given in Eq.(B.12) to

$${}^4\dot{\boldsymbol{\omega}} = \begin{bmatrix} \cos\theta & 0 & -\cos\phi\sin\theta \\ 0 & 1 & \sin\phi \\ \sin\chi & 0 & \cos\phi\cos\chi \end{bmatrix} \begin{bmatrix} \ddot{\phi} \\ \ddot{\chi} \\ \ddot{\psi} \end{bmatrix} + \begin{bmatrix} -\dot{\chi}\sin\chi & 0 & \dot{\phi}\sin\phi\sin\chi - \dot{\chi}\cos\phi\cos\chi \\ 0 & 0 & \dot{\phi}\cos\phi \\ \dot{\chi}\cos\chi & 0 & -\dot{\phi}\sin\phi\cos\chi - \dot{\chi}\cos\phi\sin\chi \end{bmatrix} \begin{bmatrix} \dot{\phi} \\ \dot{\chi} \\ \dot{\psi} \end{bmatrix} \tag{B.19}$$

Note that the component sequence in the vector $[\dot{\phi},\ \dot{\chi},\ \dot{\psi}]^T$ corresponds with the

indices of the frame vector basis. The 3x3 matrix on the right-hand side of Eq.(B.18) is still called the coefficient matrix of the angular velocity.

When the algebraic vectors of the angular velocity and acceleration vectors $\bar{\omega}$ and $\dot{\bar{\omega}}$ are taken with respect to an auxiliary frame, e.g., $\{o, \bar{e}^3\}$, we have

$$\bar{\omega} = e^{3T}\,{}^3\boldsymbol{\omega}\,, \qquad \dot{\bar{\omega}} = e^{3T}\,{}^3\dot{\boldsymbol{\omega}} \tag{B.20}$$

with

$${}^3\boldsymbol{\omega} = \boldsymbol{G}^{43T}\,{}^4\boldsymbol{\omega}\,, \qquad {}^3\dot{\boldsymbol{\omega}} = \boldsymbol{G}^{43T}\,{}^4\dot{\boldsymbol{\omega}}\,. \tag{B.21}$$

Using Eqs.(B.1), (B.15), (B.18) and (B.19), we obtain, with l=3, m=1 and n=2:

$${}^3\boldsymbol{\omega} = \begin{bmatrix} 1 & 0 & 0 \\ 0 & 1 & \sin\phi \\ 0 & 0 & \cos\phi \end{bmatrix} \begin{bmatrix} \dot{\phi} \\ \dot{\chi} \\ \dot{\psi} \end{bmatrix} \tag{B.22}$$

and the angular acceleration

$${}^3\dot{\boldsymbol{\omega}} = \begin{bmatrix} 1 & 0 & 0 \\ 0 & 1 & \sin\phi \\ 0 & 0 & \cos\phi \end{bmatrix} \begin{bmatrix} \ddot{\phi} \\ \ddot{\chi} \\ \ddot{\psi} \end{bmatrix} + \begin{bmatrix} 0 & 0 & -\dot{\chi}\cos\phi \\ 0 & 0 & \dot{\phi}\cos\phi \\ \dot{\chi} & 0 & -\dot{\phi}\sin\phi \end{bmatrix} \begin{bmatrix} \dot{\phi} \\ \dot{\chi} \\ \dot{\psi} \end{bmatrix}. \tag{B.23}$$

C. Contact between Curved Track and Wheelset

With respect to the geometric contact for a curved track with very small radius of curvature, for example when the radius of curvature is of the same order of magnitude as the track gauge, we may not assume that in a small track segment the track is cylindrical. We restrict ourselves to the case that the curved track has a constant radius of curvature and a constant superelevation (the "cant" angle β). When the radius of curvature and the cant angle vary with the distance along the curve, we still can consider them to be constant in a small segment of the curve in the neighbourhood of the wheelset (see Fig. C.1). De Pater (1981) presented the general theory of the motion of a single wheelset moving through a curve with constant radius and cant.

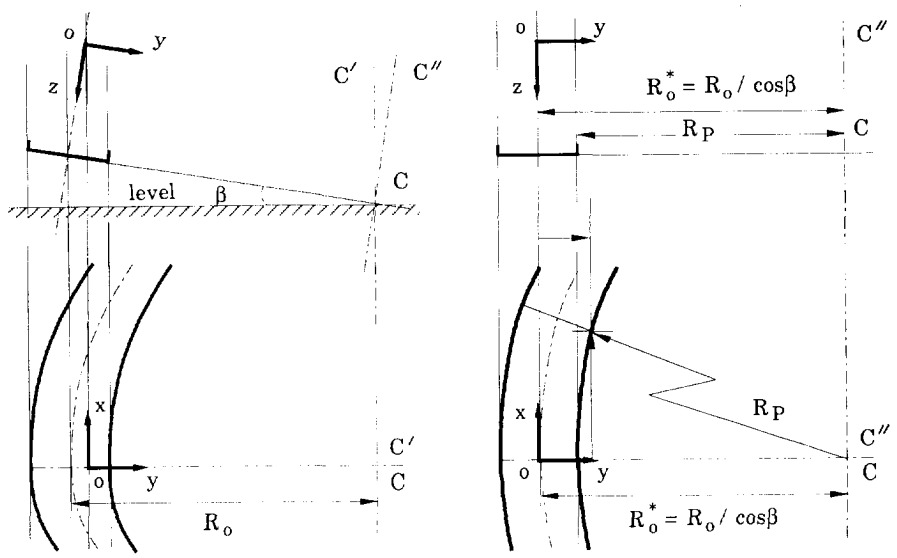

(a). As viewed from the vertical line CC′. (b). As viewed from the line CC″.

Fig. C.1. A curved track.

The restriction means that the trajectory of the track gauge centre is a circle. Moreover, the inner rail and the outer rail of the track are concentric toroids about *CC′*. In this case, the z-axis of the track reference frame is still perpendicular to the top line of the rails; the x-axis is the tangent line of the track central trajectory at the frame origin; the y-axis is therefore perpendicular to *CC″*. In addition, the rotation of the y-axis around the axis *CC′* forms a circular conical surface with the conicity ($\pi/2$ - tgβ); the x-y-plane is a tangent plane of the surface. The rails lay on a similar conical surface. However, for a small longitudinal displacement u, the rails may be replaced by ones that lay on the plane parallel to the x-y-plane. Therefore, the influence of the cant angle β may be represented by the modified curve radius which is measured along the rail tops; in other words, the radius of the track centre trajectory indicated by R_C in Fig.C1a is modified by $R_0^*=R_0/\cos\beta$ in Fig.C1b. The other effects of the cant angle, which are taken into account by De Pater (1981), may be neglected when the geometric contact is determined with respect to the track reference frame for small longitudinal displacements and we shall consider the track as circular in Fig.C1b.

Using a cylindrical coordinate system we can easily draw up the surface equation of the track segment. The origin of the cylindrical coordinate system is

located at the circle centre of the rails C and its vertical axis is parallel to the vertical axis o-z of the track reference frame (o, x, y, z). The surface equation of the track segment can be written as:

$$z - f_j(R) = 0, \tag{C.1}$$

with

$$R = R_0^* - R_P. \tag{C.2}$$

Because the geometric constraints are investigated in the track reference frame, we have to convert the quantities in the cylindrical coordinates system to the track reference frame. Doing so we obtain

$$R_p = \sqrt{x^2 + (y - R_0^*)^2} \tag{C.3}$$

If the surface equation of the track segment is designated as $F_j(x, y, z)=0$, its partial derivatives with respect to the coordinates x, y, z can be expressed as

$$\frac{\partial F_j}{\partial x} = f_j'(R)\frac{x}{R_p}, \quad \frac{\partial F_j}{\partial y} = f_j'(R)\frac{y - R_0^*}{R_p}, \quad \frac{\partial F_j}{\partial z} = 1. \tag{C.4}$$

where $f_j'(R)$ represents the partial derivative of the rail profile function with respect to the argument R; it depends only on the profile function itself.

Because the inner normal vector of the rail is defined to be positive, the unit normal vector of the rail at a point (x, y, z) reads

$$\bar{n}_j = \boldsymbol{n}_j^T \bar{\boldsymbol{e}}^1 \tag{C.5}$$

with

$$\boldsymbol{n}_j = \frac{1}{\sqrt{1 + f_j'^2}}\left[f_j'\frac{x}{R_p}, \; f_j'\frac{(y - R_0^*)}{R_p}, \; 1\right]^T. \tag{C.6}$$

Using the notation given in Eqs.(3.2.12)-(3.2.14), Eq.(C.6) can be written as

$$\boldsymbol{n}_j = \left[\mp\frac{x}{R_p}\sin\gamma_j, \; \mp\frac{(y - R_0^*)}{R_P}\sin\gamma_j, \; \cos\gamma_j\right]^T. \tag{C.7}$$

Obviously, in a tangent track the radius of curvature of the track is infinite; thus, Eq.(3.2.17) can be considered as a special case of Eq.(C.7).

When the coordinates of the contact points lying in the rail surfaces are designated by $(x_j,\ y_j,\ z_j)$ and when we substitute (3.2.5), (3.2.18) and (C.7) into Eq.(3.2.29), we obtain the expression

$$\begin{bmatrix} \frac{x_j^*}{r_j^*}\cos\gamma_j^* \\ \pm\sin\gamma_j^* \\ \frac{z_j^*}{r_j^*}\cos\gamma_j^* \end{bmatrix} = \begin{bmatrix} \cos\psi & \sin\psi & 0 \\ -\cos\phi\sin\psi & \cos\phi\cos\psi & \sin\phi \\ \sin\phi\sin\psi & -\sin\phi\cos\psi & \cos\phi \end{bmatrix} \begin{bmatrix} \mp\frac{x_j}{R_{Pj}}\sin\gamma_j \\ \mp\frac{(y_j - R_0^*)}{R_{Pj}}\sin\gamma_j \\ \cos\gamma_j \end{bmatrix} \quad \text{(C.8)}$$

Only two equations in (C.8) are independent.

The equations associated with the first contact condition are still valid in this case; they are given by Eqs.(3.2.27)-(3.2.29). Therefore, the geometric contact conditions together with the body surface equations and Eqs.(C.2), give rise to the following set of 16 equations for the 19 variables which include the two auxiliary variables R_j:

$$(y_1-y_2)-[\,(x_1^*-x_2^*)\sin\psi-(y_1^*-y_2^*)\cos\psi\cos\phi-(z_1^*-z_2^*)\cos\psi\sin\phi\,] = 0, \quad \text{(C.9)}$$

$$[\,z_1-z_2\,]-[\,(y_1^*-y_2^*)\sin\phi+(z_1^*-z_2^*)\cos\phi\,] = 0, \quad \text{(C.10)}$$

$$R_j - R_0^* + \sqrt{x_j^2 + (y_j - R_0^*)^2} = 0, \quad \text{(C.11)}$$

$$z_j - f_j(R_j) = 0, \quad \text{(C.12)}$$

$$\sqrt{x_j^{*2} + z_j^{*2}} - f_j^*(y_j^*) = 0, \quad \text{(C.13)}$$

$$\frac{x_j^*}{r_j^*}\cos\gamma_j^* \pm \frac{x_j}{R_0^* - R_j}\sin\gamma_j\cos\psi \pm \frac{(y_j - R_0^*)}{R_0^* - R_j}\sin\gamma_j\sin\psi = 0, \quad \text{(C.14)}$$

$$\pm\sin\gamma_j^* \mp \frac{x_j}{R_0^* - R_j}\sin\gamma_j\cos\phi\sin\psi \pm \frac{(y_j - R_0^*)}{R_0^* - R_j}\sin\gamma_j\cos\phi\cos\psi - \cos\gamma_j\sin\phi = 0, \tag{C.15}$$

$$x_j - \left\{u + x_j^*\cos\psi - y_j^*\sin\psi\cos\phi + z_j^*\sin\phi\sin\psi\right\} = 0. \tag{C.16}$$

$$v - \frac{1}{2}\left\{(y_1+y_2) - [(x_1^*+x_2^*)\sin\psi + (y_1^*+y_2^*)\cos\phi\cos\psi - (z_1^*+z_2^*)\sin\phi\cos\psi]\right\} = 0, \tag{C.17}$$

$$w - \frac{1}{2}\left\{[f_1(y_1)+f_2(y_2)] - [(y_1^*+y_2^*)\sin\phi + (z_1^*+z_2^*)\cos\phi]\right\} = 0, \tag{C.18}$$

In order to solve this set of equations, three of the 19 variables have to be chosen as independent parameters.

D. Profiles of the Rails and Wheels in the Examples

Besides the circular cylindrical rails and the conical wheels, three combinations of the rail and wheel profiles are treated in various examples of the numerical computations. One is the symmetrical system of the UIC60 rails and the S1002 wheels; this well-known combination is often used in testing and comparing the software. Another combination called *CTO-Measured-Profiles* is asymmetric; it is provided by "Centrum Technisch Onderzoek" (CTO) of Netherlands Railways; these profiles result from measurements on worn out rails and wheels. Because the wheels are turned off periodically, the wheelset in this system is considered to be symmetrical and the wheel profiles are obtained by averaging the experimental data of both wheels; the rails have different profiles and they have been measured at 27.9 km in the line between Venlo and Eindhoven. This measured track-wheelset system has 1435 mm track gauge and 1360mm wheelset gauge. The third combination given in the ORE benchmark, is designated as *ORE-Benchmark-Profiles*; in this asymmetrical system, the track gauge is equal to 1434.07mm and the wheelset gauge is 1359.9mm

For the two asymmetrical systems, the original data are first transformed to the local coordinate systems. The origins of the local coordinate systems for the rails may not rest on the surface of the rails, as shown for instance in Fig.D1. The *CTO-Measured-Rail* has been measured in the polar coordinate system (o_M, ρ, θ). Point *A* is the reference point for the *CTO* instrument; its coordinates with respect to the

polar coordinate system are (34mm,0). By means of this point the original experimental data listed in Table.D1 can be corrected; moreover, the coordinates of point *A* are (34mm, 31.5mm) with respect to the local coordinate system. For the *ORE-Benchmark-Rail*, the coordinates of the origins o_{0j} for the rails are (±750mm, 33mm) with respect to the original coordinate system (o_M, y_M, z_M) and those for the wheels are (±749.95mm, 0). Furthermore, the transformed profiles are smoothed by means of a least square method. The original data of the profiles are listed at the end of this Appendix. For the theoretical rail profile UIC60, the origin of the local coordinate system is always chosen at the point where the rail profile curve intersects the axis of symmetry of the rail.

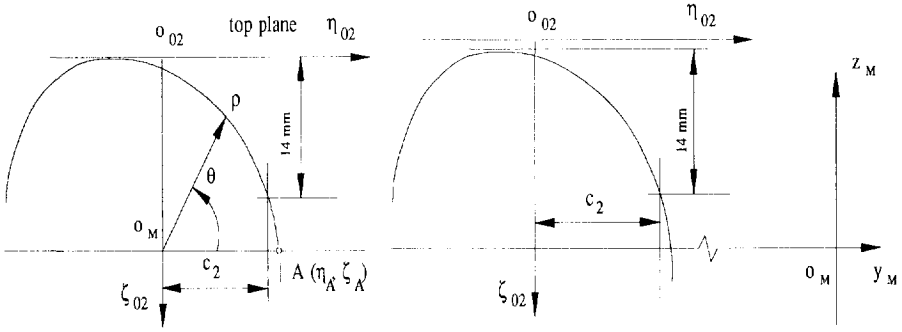

Fig.D1. The local coordinate system of the rails. The left-hand figure refers to *CTO-Measured-Rail* and the right-hand figure to *ORE-Benchmark-Rail.*

(mm)	UIC60 1/40	UIC60 1/20	ORE-Benchmark-Rail	CTO-Measured-Rails
c_1	35.988	35.021	32.977	34.087
c_2	35.988	35.021	32.956	33.638

Table.D.1. The lateral coordinates of the points to measure the track gauge.

Another important geometric parameter associated with a rail is the position of the point by means of which the track gauge is defined; this point is 14mm lower than the top plane of the rails (see Fig.D1). As indicated in Table.D1, its lateral coordinate (denoted by c_j) varies with the profile function and the rail inclination.

Original Data of CTO-Measured-Profiles

Rails				Wheel for both sides					
right		left							
θ_1	ρ_1	θ_2	ρ_2	η_{0j}^*	ζ_{0j}^*				
0	33.02	0	33.08	-70.0	10.105	-20.0	1.953	30.0	-0.249
3	33.07	3	33.04	-69.0	18.008	-19.0	1.803	31.0	-0.253
6	33.19	6	33.24	-68.0	20.519	-18.0	1.646	32.0	-0.264
9	33.38	9	33.51	-67.0	22.370	-17.0	1.505	33.0	-0.281
12	33.71	12	33.88	-66.0	23.855	-16.0	1.381	34.0	-0.293
15	34.12	15	34.34	-65.0	25.091	-15.0	1.264	35.0	-0.322
18	34.77	18	34.92	-64.0	26.182	-14.0	1.144	36.0	-0.352
21	35.48	21	35.69	-63.0	27.114	-13.0	1.029	37.0	-0.398
24	36.28	24	36.42	-62.0	27.879	-12.0	0.925	38.0	-0.443
26	36.99	26	36.73	-61.0	28.475	-11.0	0.812	39.0	-0.502
28	37.56	28	37.04	-60.0	28.899	-10.0	0.692	40.0	-0.556
30	38.18	30	37.29	-59.0	29.265	-9.0	0.597	41.0	-0.614
32	38.65	32	37.51	-58.0	29.561	-8.0	0.505	42.0	-0.680
34	38.90	34	37.65	-57.0	29.740	-7.0	0.425	43.0	-0.751
36	38.97	36	37.69	-56.0	29.829	-6.0	0.351	44.0	-0.820
38	38.92	38	37.61	-55.0	29.832	-5.0	0.271	45.0	-0.892
40	38.71	40	37.43	-54.0	29.747	-4.0	0.203	46.0	-0.964
42	38.36	42	37.17	-53.0	29.537	-3.0	0.136	47.0	-1.038
44	37.91	44	36.80	-52.0	29.247	-2.0	0.083	48.0	-1.113
46	37.34	46	36.35	-51.0	28.881	-1.0	0.035	49.0	-1.191
48	36.78	48	35.89	-50.0	28.414	0.0	-0.004	50.0	-1.265
50	36.14	50	35.36	-49.0	27.795	1.0	-0.048	51.0	-1.346
52	35.55	52	34.84	-48.0	27.001	2.0	-0.092	52.0	-1.422
55	34.70	55	34.08	-47.0	25.972	3.0	-0.130	53.0	-1.500
58	33.94	58	33.40	-46.0	24.518	4.0	-0.168	54.0	-1.584
61	33.23	61	32.77	-45.0	22.388	5.0	-0.197	55.0	-1.662
64	32.59	64	32.18	-44.0	19.207	6.0	-0.221	56.0	-1.749
67	31.99	67	31.65	-43.0	15.614	7.0	-0.231	57.0	-1.833
70	31.49	70	31.21	-42.0	12.720	8.0	-0.252	58.0	-1.946
73	31.04	73	30.82	-41.0	11.032	9.0	-0.267	59.0	-2.086
76	30.68	76	30.49	-40.0	09.662	10.0	-0.288	60.0	-2.443
79	30.40	79	30.25	-39.0	08.587	11.0	-0.301	61.0	-3.276
82	30.22	82	30.08	-38.0	07.698	12.0	-0.311	62.0	-4.185
86	30.08	86	29.96	-37.0	06.971	13.0	-0.322	63.0	-5.144
90	30.09	90	29.98	-36.0	06.349	14.0	-0.328	64.0	-6.131
94	30.24	94	30.16	-35.0	05.843	15.0	-0.331	65.0	-11.844
98	30.53	98	30.46	-34.0	05.399	16.0	-0.338	66.0	-12.013
101	30.89	101	30.82	-33.0	05.020	17.0	-0.335	67.0	-12.032
104	31.29	104	31.25	-32.0	04.675	18.0	-0.336	68.0	-12.030
107	31.78	107	31.75	-31.0	04.355	19.0	-0.337		
110	32.42	110	32.41	-30.0	04.049	20.0	-0.334		
113	33.13	113	33.15	-29.0	03.765	21.0	-0.321		
116	33.95	116	33.98	-28.0	03.505	22.0	-0.305		
119	34.93	119	34.99	-27.0	03.255	23.0	-0.284		
122	36.01	122	36.09	-26.0	03.035	24.0	-0.270		
125	37.22	125	37.36	-25.0	02.836	25.0	-0.261		
128	38.52	128	38.72	-24.0	02.641	26.0	-0.256		
130	39.38	130	39.64	-23.0	02.456	27.0	-0.246		
132	40.10	132	40.32	-22.0	02.281	28.0	-0.243		
134	40.75	134	40.88	-21.0	02.116	29.0	-0.242		

ORE-Benchmark-Profiles

Rail Prof DBT1--MA, Measured 14/05/90

left		right	
-789.3340	18.7649	789.3123	18.7543
-788.8182	21.9150	788.6566	21.8217
-787.7553	24.8860	787.6150	24.7914
-785.9649	27.4267	785.7357	27.2476
-784.8382	28.5109	784.5823	28.2961
-783.5661	29.4485	783.2974	29.2064
-782.1594	30.2252	781.8837	29.9589
-780.6432	30.8411	780.3671	30.5552
-779.0603	31.3192	778.7982	31.0282
-777.4551	31.6945	777.2312	31.4276
-775.8100	31.9342	775.6705	31.7555
-774.1959	32.1187	774.0940	31.9784
-771.1006	32.3912	771.0330	32.2831
-768.1944	32.6006	768.1474	32.5124
-765.4279	32.7194	765.4015	32.6600
-762.7926	32.7835	762.7794	32.7475
-760.2745	32.8311	760.2701	32.8159
-757.8377	32.8258	757.8368	32.8217
-755.4717	32.8117	755.4720	32.8142
-753.1523	32.7766	753.1527	32.7825
-750.8603	32.7275	750.8603	32.7350
-748.5772	32.6503	748.5762	32.6644
-746.2843	32.5600	746.2819	32.5773
-743.9659	32.4354	743.9604	32.4615
-741.6065	32.2719	741.5961	32.3080
-739.1985	32.0404	739.1743	32.1069
-736.7343	31.7274	736.6892	31.8287
-734.2074	31.3196	734.1381	31.4498
-731.5990	30.8244	731.4970	30.9876
-728.9153	30.2046	728.7973	30.3671
-727.5596	29.8235	727.4251	29.9956
-726.1949	29.3950	726.0524	29.5648
-724.8662	28.8693	724.7263	29.0247
-723.5845	28.2448	723.4612	28.3725
-722.4080	27.4760	722.3037	27.5767
-721.3296	26.5895	721.2280	26.6810
-720.2932	25.6488	720.2140	25.7152
-719.4036	24.5766	719.3110	24.6490
-718.6196	23.4241	718.5340	23.4864
-717.9820	22.1766	717.8805	22.2451
-717.5214	20.8324	717.4451	20.8801
-717.1741	19.4487	717.1337	19.4720
-716.8918	18.0613	716.8940	18.0601
-716.7601	16.6317	716.7653	16.6292
-716.7356	15.1932	716.7150	15.2024
-716.7080	12.4303	716.6547	12.4497
-716.6538	9.8085	716.6202	9.8181
-716.5999	7.2822	716.5363	7.2957
-716.5707	4.8190	716.4675	4.8335
-716.5150	2.4016	716.3804	2.4110
-716.4437	-0.0001	716.3062	-0.0001
-716.4111	-2.4090	716.2266	-2.4219

Wheel Prof DBW---3B, Measured 27/06/90

left		right	
-803.7889	-2.0833	803.9563	-2.7149
-801.0829	-1.8917	801.1913	-2.4345
-797.6288	-1.6969	797.7491	-2.2075
-794.9998	-1.5261	795.0786	-2.0037
-791.6215	-1.2840	791.7179	-1.7498
-789.0507	-1.1218	789.1056	-1.5228
-785.7401	-0.9100	785.8101	-1.2304
-783.2118	-0.7723	783.2479	-1.0356
-779.9458	-0.6071	780.0051	-0.7906
-777.4416	-0.5175	777.4734	-0.6524
-774.1931	-0.4521	774.2551	-0.5388
-771.6909	-0.4119	771.7289	-0.4787
-768.4319	-0.3863	768.5049	-0.4070
-765.9152	-0.3543	765.9667	-0.3542
-762.6307	-0.3061	762.7178	-0.2918
-760.0914	-0.2398	760.1528	-0.2435
-756.7658	-0.1743	756.8620	-0.1758
-754.1887	-0.0992	754.2559	-0.1272
-750.8021	-0.0292	750.9085	-0.0375
-748.1745	0.0608	748.2607	0.0661
-744.7209	0.1833	744.8517	0.2150
-742.0471	0.3434	742.1531	0.3704
-738.5303	0.5655	738.6902	0.6348
-735.8174	0.8305	735.9460	0.8771
-732.2537	1.2072	732.4319	1.2740
-729.5156	1.6100	729.6652	1.6648
-725.9141	2.1568	726.1411	2.2826
-723.2018	2.7905	723.3693	2.8426
-719.6770	3.7051	719.8829	3.7445
-717.0673	4.6604	717.2325	4.6736
-714.0233	6.5266	714.1832	6.4575
-712.1213	8.6464	712.2198	8.5298
-710.4525	12.4757	710.4164	12.1078
-709.3994	15.5923	709.5266	15.5096
-707.9161	19.2787	708.0970	19.2138
-706.3588	21.4706	706.5378	21.4413
-703.9579	23.8004	704.2073	23.7987
-701.9276	25.3772	702.1464	25.3716
-698.8621	26.9930	699.1821	27.0381
-695.9553	27.7395	696.2961	27.8295

E. The Product $\bar{n} \cdot (\bar{s} + \bar{\omega} \times \bar{p})$

Consider a particle P moving on the surface of a body C that is fixed in an inertial frame. From Fig.E.1, we have the relation:

$$\bar{r} = \bar{s} + \bar{p}, \tag{E.1}$$

so that

$$\dot{\bar{s}} + \bar{\omega} \times \bar{p} = \dot{\bar{r}} - \dot{\bar{p}}, \tag{E.2}$$

where $\bar{\omega}$ is the angular velocity of the moving reference frame. When we denote the normal vector of C at P by $\bar{n}$, it is clear that the following relation holds:

$$\bar{n} \cdot \dot{\bar{r}} = 0. \tag{E.3}$$

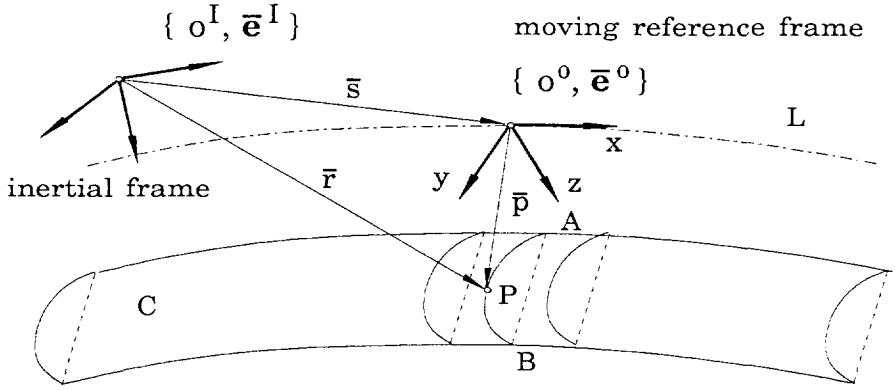

Fig.E.1. Description of the motion of the point P.

For the case that the cross-section of C is constant, we can assume that the surface C is formed by the motion of a curve AB along a trajectory L. The curve AB is always in the yz plane of the moving reference frame. Therefore, the equation of AB is only in terms of the coordinates y and z and it is independent of the inertial frame and the coordinate x:

$$f(y, z) = 0. \tag{E.4}$$

We observe the motion of P from the reference frame. First, the point P is only admitted to move along the curve AB. In this case the normal vector $\bar{n}$ is in the yz plane and

$$\bar{n} \cdot \dot{\bar{p}} = 0 , \tag{E.5}$$

so that we have from (E.2), (E.3) and (E.5)

$$\bar{n} \cdot (\dot{\bar{s}} + \bar{\omega} \times \bar{p}) = 0 . \tag{E.6}$$

When P moves on the surface nearby AB, in general, Eq.(E.5) does not hold because the equation of this surface, which is a function of the three coordinates x, y and z, depends on the position of the reference frame. Only for the special case where the body C is a toroid, in other words, when its surface equation is independent of the position of the reference frame, we may write the surface equation as

$$g(x, y, z) = 0; \tag{E.7}$$

hence the components of $\bar{n}$ are proportional to $\partial g/\partial x$, $\partial g/\partial y$, $\partial g/\partial z$, so that

$$\frac{d}{dt} g(x, y, z) = \bar{n} \cdot \dot{\bar{p}} = 0 . \tag{E.8}$$

Consequently, we obtain Eq.(E.6).

However, for the application of railway vehicle dynamics, Eq.(E.6) is always a good approximation.

F. Kinematic Analysis of an IRW System

For an IRW system, the motion of the wheels is described by

$$\dot{\bar{r}}_1 = \dot{\bar{r}} + \bar{\omega}_1 \times \bar{l}, \tag{F.1}$$

$$\dot{\bar{r}}_2 = \dot{\bar{r}} + \bar{\omega}_2 \times (-\bar{l}), \tag{F.2}$$

$$\bar{\omega}_2 = \bar{\omega}_1 + \bar{\omega}_{21}, \tag{F.3}$$

where

$$\bar{\omega}_{21} = [\, 0 , \dot{\chi}_{21} , 0 \,]\, \bar{e}^2 . \tag{F.4}$$

So the accelerations are:

$$\ddot{\bar{r}}_1 = \ddot{\bar{r}} + \dot{\bar{\omega}}_1 \times \bar{l} + \bar{\omega}_1 \times (\bar{\omega}_1 \times \bar{l}), \tag{F.5}$$

$$\ddot{\bar{r}}_2 = \ddot{\bar{r}} - \dot{\bar{\omega}}_2 \times \bar{l} - \bar{\omega}_2 \times (\bar{\omega}_2 \times \bar{l}), \tag{F.6}$$

$$\dot{\bar{\omega}}_2 = \dot{\bar{\omega}}_2 + \dot{\bar{\omega}}_{21} + \dot{\bar{h}}_{\theta 21}, \tag{F.7}$$

with

$$\bar{h}_{\theta 21} = \bar{\omega}_1 \times \bar{\omega}_{21} = \boldsymbol{h}_{\theta 21}^T \bar{e}^2 = [\, -\dot{\chi}_{21}\omega_{13},\ 0,\ \dot{\chi}_{21}\omega_{11}\,]\,\bar{e}^2. \tag{F.8}$$

Substituting (F.3) and (F.7) into Eq.(F.6) yields:

$$\ddot{\bar{r}}_2 = \ddot{\bar{r}} - \dot{\bar{\omega}}_1 \times \bar{l} - \bar{\omega}_1 \times (\bar{\omega}_1 \times \bar{l}), \tag{F.9}$$

Writing Eqs.(F.6)-(F.9) in algebraic form we can find $\boldsymbol{b}_{\mathrm{IRW}}$ in Eq.(5.16).

References

Ahmed, A.K.W., Sankar, S., Steady-State Curving Performance of Railway Freight Truck with Damper-Coupled Wheelsets, Vehicle System Dynamics, Vol.17 (1988), pp.295-315.

Bailey, J.R., Wormley, D.N., A Comparison of Analytical and Experimental Performance Data for a Two-Axle Freight Car, ASME J. of Dynamic Systems, Measurement, and Control, Vol.114(1992), pp.141-147.

Besseling, J.F., Jonker, J.B., Schwab, A., Kinematics and Dynamics of Mechanisms, Papers presented to the Symposium 'Non-linear Dynamics' dedicated to Prof. dr. ir. A.D. de Pater on the occasion of his retirement from Delft University of Technology, Delft Progress Report, Vol.10(1985), pp.160-172.

Bommel, P. Van, Applications de la theorie des vibrations non-lineaires sur le problem du mouvement de lacet d'un vehicule de chemin de fer, Ph.D. Thesis, Delft University of Technology, 1964.

Bowen, R.M., Wang, C.C., Introduction to Vectors and Tensors, Plenum Press, 1980.

Broersen, P.M.T., Evaluation of Railway Systems Dynamics by Model Adjustment, Ph.D. Thesis, Delft University of Technology, 1976.

Burton, T.D., Whitman, A.M., Nonlinear Contact Geometry Effects on Wheelset Dynamics, ASME J. of App. Mech., Vol.47(1980), pp.155-160.

Carter, F., On the Action of a Locomotive Driving, Wheel. Proc. Royal. Society. Series A, Vol.112(1926), pp.151-157.

Castelazo, I.A., Hedrick, J.K., Stability Analysis of a Nonlinear Wheelset Rolling on a Rough Track, ASME J. of Dynamic Systems, Measurement, and Control, Vol.111(1989), pp.277-285.

Cheng, B., Analytical Dynamics (in Chinese), Beijing University Press, 1987.

Chollet, H., Ayasse, J.B., Pascal, J.P., Measurement of the Transversal Creep force in a Wheel-Rail Contact Area, Proc. 11th IAVSD Symposium, R. Anderson (ed.), Kingston, Canada, 1989, pp.97-107.

Cooperrider, N.K., Hedrick, J.K., Law, E.H., and Malstrom, C.W., The Application of Quasi-linearization Techniques to the Prediction of Nonlinear Railway Vehicle Response, Vehicle System Dynamics, Vol.10(1975), pp.141-148.

Cooperrider. N.K., Law, E.H., et al., Analytical and Experimental Determination of Nonlinear Wheel/Rail Constraints, Proc. ASME Symposium on Railroad Equipment Dynamics, 1976.

Duffek, W., Kortüm, W., Wallrapp, O., A General Purpose Program for the Simulation of Vehicle-Guideway Interaction Dynamics, Proc. 5th IAVSD -2nd IUTAM Symposium, A. Slibar et al.(eds.), Vienna, 1977. pp.104-126.

Duffek, W., Contact Geometry in Wheel Rail Vehicle, Proc. Symp. Contact Mechanics and Wear of Rail/Wheel System, J. Kalousek et al.(eds.), University of Waterloo Press, 1982, pp.161-179.

Dukkipati, R.V., Narayana S.S., Osman, M.O.M., Independently Rotating Wheel Systems for Railway Vehicles - A survey of the State of the Art, The Archives of Transport, Vol.3(1991), pp.513-539.

Eickhoff, B.M., and Harvey, R.F., Theoretical and Experimental Evaluation of Independently Rotating Wheels for Railway Vehicles, Proc. 11th IAVSD Symposium, R. Anderson (ed.), Kingston, Canada, 1989, pp.190-202.

Elkins, J.A. and R.J. Gostling, A General Quasi-static Curving Theory for Railway Vehicles, Proc. 5th IAVSD - 2nd IUTAM Symposium, A. Slibar et al.(ed.), Vienna, 1977, pp.388-406.

Elkins, J.A., Wilson, N.G., Train Resistance Measurements Using a Roller Rig, Proc. 9th IAVSD-Symposium, O. Nordstrom (ed.), Linkoping, 1985, pp.86-99.

Elkins, J.A., Prediction of Wheel/Rail Interaction: the state-of-the-Art, Proc. 12th IAVSD Symposium, G. Sauvage (ed.), Lyon, 1991, pp.1-27.

Endlicher, K.-O., Lugner, P., Computer-simulation of the Dynamical Curving Behaviour of a Railway-Bogie, Vehicle Syst. Dyn. Vol.19(1990), pp.71-95.

Fisette, P., Samin, J.C., Lateral Dynamics of a Light Railway Vehicle with Independent Wheels, Proc. 12th IAVSD Symposium, G. Sauvage (ed.), Lyon, 1991, pp.157-171.

Fisette, P., Results of the Robotran Programme, Report of Universite Catholique de Louvain, 1991.

Fortin, C., Dynamic Curving Simulation of Forced-Steering Rail Vehicles, Ph.D Thesis, Queens University at Kingston, Canada, 1984.

Garg, V.K., Dukkipati, R.V., Dynamics of Railway Vehicle Systems, Academic Press, 1984.

Geuenich, W., Guenther, C. and Leo, R., Dynamics of Fiber Composite Bogies with Creep-Controlled Wheelsets, Proc. 8th IAVSD Symposium, J.K. Hedrick (ed.), Cambridge, U.S.A, 1983, pp.225-238.

Gimenez, J.G. *et al.*, IAVSD Railway Benchmark #2 - SIDIVE and VOCO Code Solutions, Proc. 12th IAVSD Symposium, G. Sauvage (ed.), Lyon, 1991, pp.172-194.

Hahn, H., and Mikulcik, E.C., Numerical Simulation and Experimental Verification of the German Roller Rig for Rail Vehicles, Vehicle System Dynamics, Vol.

15(1986), pp.303-334.

Haug, E.J., (ed.), Computer Aided Analysis and Optimization of Mechanical System Dynamics, NATO ASI Series, Vol.9(1984).

Haug, E.J., Computer Aided Kinematics and Dynamics of Mechanical Systems, Allyn and Bacon, Boston, 1989.

Hauschild, W., Design of a Limit Cycle Controller for the Nonlinear Wheel-Rail-System, Proc. 7th IAVSD Symposium, A.H. Wickens (ed.), Cambridge, UK, 1981, pp.427-440.

Hedrick, J.K., Castelazo, I.A., Statistical Linearization of the Nonlinear Rail Vehicle Wheelset, Proc. 6th IAVSD Symposium, H.P. Willumeit (ed.), Berlin, 1979, pp.164-178.

Hedrick, J.K., Generic Properties and Performance Characteristics of Passenger Rail Vehicles, First Course on Advanced Vehicle System Dynamics, ICTS-PFT Proc. Series, A.D. de Pater and H.B. Pacejka (eds.), 1982, pp.363-402.

Heliot, C., Small-scale Test Method for Railway Dynamics, Proc. 9th IAVSD Symposium, O. Nordstrom (ed.), Linkoping, 1985, pp.197-207.

Higaki, H. et al., An Active Pneumatic Tilting System for Railway Cars, Proc. 12th IAVSD Symposium, G. Sauvage (ed.), Lyon, 1991, pp.254-268.

Illingworth, R., Railway wheelset lateral excitation by track irregularities, 5th VSD - 2nd IUTAM Symposium, A. Slibar et al. (ed.), Vienna, 1977, pp.450-458.

Jaschinski, A., Duffek, W., Evaluation of Bogie Models with Respect to Dynamic Curving Performance of Rail Vehicles, Proc. 8th IAVSD Symposium, J.K. Hedrick (ed.), Cambridge, U.S.A., 1984, pp.266-279.

Jaschinski, A., On the Application of Similarity Laws to a Scaled Railway Bogie Model, Ph.D Thesis, Delft University of Technology, 1990.

Kalker, J. J., On the Rolling Contact of two Elastic Bodies in the Presence of Dry Friction, Ph.D Thesis, Delft University of Technology, 1967.

Kalker, J.J., A Fast Algorithm for the Simplified Theory of Rolling Contact, Vehicle System Dynamics Vol.11(1982), pp.1-13.

Kalker, J.J., Two Algorithms for the Contact Problem in Elastostatics, Proc. Symp. Contact Mechanics and Wear of Rail/Wheel System, J. Kalousek et al.(eds.), University of Waterloo Press, 1982b, pp.103-120.

Kalker, J.J., The Three-dimensional Elastic Bodies in Rolling Contact, Kluwer Academic Publishers, 1990.

Kalker, J.J., Wheel-Rail Rolling Contact Theory, Proc. Symp. Contact Mechanics and Wear of Rail/Wheel System III, S.L. Grassie (ed.), 1990b, pp.243-262.

Keizer, C.P., A Theory on Multi-wheelset Systems Applied to Three Wheelsets, Proc. 9th IAVSD Symp., O. Nordstrom (ed.), Linkoping, 1985, pp.233-249.

Keller, H.B., Numerical Methods in Bifurcation Problems, Springer-Verlag, 1987.

Kik, W., Comparison of the Behaviour of Different Wheelset-Track Models, Proc. 12th IAVSD Symposium, G. Sauvage (ed.), Lyon, France, 1991, pp.325-339.

Kik, W., Pascal, J.P., Railway Benchmark Model #2 - Bogie Vehicle, Nov. 1991.

Klingel, Uber den Lauf der Eisenbahnwagen auf gerader Bahn, Organ Fortschr. Eisenbahnwesens, Vol.38(1883), pp.113-123.

Knothe, K, Die geometrisch nichtlinearen Beziehungen für einen starren Radsatz, der auf einer starren Schiene querverschoben wird, TU Berlin, Inst. für Luft- und Raumfahrt Report ILR Mitt. 17, 1975.

Knothe, K., Moelle, D., Nonlinear Behaviour of Running Gear of Railway Vehicles, First Course on Advanced Vehicle System Dynamics, ICTS-PFT Proc. Series, ed. Pater, A.D. de and Pacejka, H.B., 1982, pp.405-442.

Knothe, K., Gross-Thebing, A., Derivation of Frequency Dependent Creep Coefficients Based on an Elastic Half-Space Model, Vehicle System Dynamics, Vol.15(1986), pp.133-153.

Kortüm, W., Wormley, D.N., Dynamic Interactions between Travelling Vehicles and Guideway System, Vehicle System Dynamics, Vol.10(1981), pp.285-317.

Kortüm, W., Schiehlen, W., General Purpose Vehicle System Dynamics Software Based on Multibody Formalisms, Vehicle System Dynamics., Vol.14(1985), pp.229-263

Kortüm, W., Sharp, R.S., Pater, A.D.de, Application of Multibody Computer Codes to Vehicle System Dynamics, Progress Report to the 12th IAVSD Symposium on a Workshop and Resulting Activities, 1991.

Kumar, S., Kim, J.,S., Rajkumar, B.R., A laboratory Study of the Dynamic Nature of Rail/Wheel Contact, Proc. Symp. Contact Mechanics and Wear of Rail/ Wheel System, J. Kalousek et al.(eds.), University of Waterloo Press, 1982, pp.565-583.

Lanczos, C., The Variational Principles of Mechanics, Oxford University Press, London, 1957.

Law, E.H., and Brand, R.P., Analysis of the Nonlinear Dynamics of a Railway Vehicle Wheelset, ASME J. of Dynamic Systems, Measurement, and Control, Vol.95(1973), pp.28-35.

Lohe, M.A., Huilgol, R.R., Flange Force Effects on the Motion of a Train Wheelset, Vehicle System Dynamics, Vol.11(1982) pp.283-303.

Love, A.E.H; A treatise on the Mathematical Theory of Elasticity. 4th ed. Cambridge, 1927.

Meijaard, J.P., Dynamics of Mechanical Systems, Ph.D Thesis, Delft University of Technology, 1991.

Meijers, P., Private Communications.

Mufti, I.H., Dukkipati, R.V., On the Dynamics of a Wheelset for NRC Curved Track Simulator, Proc. Symp. Contact Mechanics and Wear of Rail/Wheel System, J. Kalousek et al.(eds.), University of Waterloo Press, 1982, pp.545-564.

Nayfeh, A.H., Perturbation method, John Wiley and Sons, New York, 1976.

Nikravesh, P.E., Some Methods for Dynamic Analysis of Constrained Mechanical Systems: A Survey, Computer Aided Analysis and Optimization of Mechanical System Dynamics, Haug, E.J.,(ed.), 1984, pp.351-368.

ORE, ORE Benchmarking of Vehicle Dynamics Programs, 1991.

Papastavridis, J.G., On Jourdain's Principle, Int. J. Engng Sci. Vol.30(1992), pp.135-140.

Pascal, J.P., The Railway Dynamic Codes "VOCO", INRETS-LTN Report, 1990.

Pascal, J.P., Sauvage, G., New Method for Reducing the Multicontact Wheel/Rail Problem to One Equivalent Contact Patch, Proc. 12th IAVSD Symposium, G. Sauvage, Lyon, 1991, pp.325-339.

Pater, A.D. de, The Approximate Determination of the Hunting Movement of a Railway Vehicle by Aid of the Method of Krylov and Bogoljubov, Appl. sci. Res., Vol.10(1961), pp.205-228

Pater, A.D. de, On the Reciprocal Pressure between Two Elastic Bodies, Proc. of Sym. on Rolling Contact Phenomena, J.B. Bidwell (ed.), 1962, pp.29-75.

Pater, A.D. de, The Exact Theory of the Motion of a Single Wheelset Moving on a Purely Straight Track, Delft University of Technology, Dept. of Mech. Engg., Lab. for Engg. Mechs., Report No.648 (1979).

Pater, A.D. de, The General Theory of the Motion of a Single Wheelset Moving Through a Curve with Constant Radius and Cant, Z. angew. Math. u. Mech., Vol.61(1981), pp.277-292.

Pater, A.D. de, Railway Vehicles with Perfect Curving Behaviour Which are Asymptotically Stable at Vanishing Speed, Vehicle System Dynamics, Vol. 11 (1982), pp.121-141.

Pater, A.D. de, The Equations of Motion of a Dicone Moving on a Pair of Circular Cylinders, Int. J. Non-Linear Mechanics, Vol.20(1985), pp.439-449.

Pater, A.D. de, Optimal Design of Railway Vehicles, Ingenieur-Archiv, Vol.57 (1987), pp.25-38.

Pater, A.D. de, The Equations of Motion of a Single Wheelset Moving Along a Perfect Track, Proc. 10th IAVSD Symposium, M. Apetaur (ed.), Prague, pp.287-299.

Pater, A.D. de, The Geometrical Contact between Track and Wheelset, Vehicle System Dynamics Vol.17(1988), pp.127-140.

Pater, A.D.de, The Optimal Design of Running Gears, Vehicle System Dynamics, Vol.18(1989), pp.243-380.

Pater, A.D. de, Yang, G. The Geometric Contact between a Pair of Rollers and a Wheelset in a Railway Vehicle Roller Rig, Proc. IUTAM Sym. on Dynamical Problems of Rigid-Elastic Systems and Structures, Moscow, USSR, 1990.

Pater, A.D. de, The equations of motion of railway wheelset moving over a tangent track, LTM Report 985, Delft University of Technology, 1992.

Piotrowski, J., A Theory of Wheelset Forces for Two Point Contact Between Wheel and Rail, Vehicle System Dynamics Vol.11(1982), pp.69-87.

Rheinboldt, Numerical Analysis of Parametrized Nonlinear Equations, Wiley and Sons, 1986.

Roberson, R.E., Schwertassek, R, Dynamics of Multibody Systems, Springer Verlag, Berlin, 1988.

Rocard, Y., La Stabtilité de route des locomotives, première partie, Paris(1935).

Rosenberg, R.M., Analytical Dynamics of Discrete Systems, Plenum Press, 1977.

Samin, J.C., A Multibody Approach for Dynamic Investigation of Rolling System, Ingenieur Archiv, Vol.54(1984), pp.1-15.

Satou, E., and Miyamoto, M., Dynamics of a Bogie with Independently Rotating Wheels, Proc.12th IAVSD Sym., G. Sauvage (ed.), Lyon, 1991, pp.519-536.

Sauvage, G., Nonlinear Model for the Study of Railway Vehicle Dynamics, Proc. of IUTAM Symposium, H.B. Pacejka (ed.), Delft, 1975, pp.326-344.

Scheffel, H., The Dynamic Stability of Two Railway Wheelsets Coupled to Each Other in the Lateral Plane by Elastic and Viscous Constraints, Proc. 7th IAVSD Symposium, A.H. Wickens (ed.), Cambridge, UK, 1981, pp.385-400.

Schiehlen, W., Non-linear Phenomena in Multibody System Dynamics, Papers presented to the Symposium 'Non-linear Dynamics' dedicated to Prof. dr. ir. A.D. de Pater on the occasion of his retirement from Delft University of Technology, Delft Progress Report, Vol.10(1985), pp.105-120

Schiehlen, W., (ed.), Multibody System Handbook, Springer Verlag, 1990.

Seydel, R., From Equilibrium to Chaos, Elsevier, 1988.

Shen, Z.Y., Hedrick, J.K. and Elkins, J.A., A comparison of Alternative Creep Force Models for Rail Vehicle Dynamic Analysis, Proc. 8th IAVSD Symposium, J.K. Hedrick (ed.), Cambridge, U.S.A., 1983, p.591-605.

Shen, Z.Y., Yan, J.M., Zeng, J. and Lu, J.X., Dynamical Behaviour of A Forced Steering Three-piece Freight Car Truck, Proc. 10th IAVSD Symposium, M. Apetaur (ed.), Prague, pp.407-418.

Simeon, B., Duhrer, C., Rentrop, P., Differential-algebraic Equations in Vehicle System Dynamics, Surv. Math. Ind. Vol.I(1991), pp.1-37.

Smith, R.E., Anderson, R.J., Characteristics of Guided-Steering Railway Trucks, Vehicle System Dynamics, Vol.17, 1988, pp.1-36.

Stassen, H.G., Random lateral Motions of Railway Vehicles, Ph.D Thesis, Delft University of Technology, 1967.

True, H., Kaas-Petersen, C., A Bifurcation Analysis of Nonlinear Oscillations in Railway Vehicles, Proc. 8th IAVSD Symp. J.K. Hedrick (ed.), Cambridge, U.S.A., 1983, pp.655-665.

Ul-Haque and Law, Estimation of Creep Coefficients from Tests of the SOAC Vehicle on the Roll Dynamics Unit, Proc. Symp. Contact Mechanics and Wear of Rail/Wheel System, J. Kalousek et al.(eds.), University of Waterloo Press, 1982, pp.229-244

Vermeulen, P.J., Johnson, K.L., Contact of Nonspherical Elastic Bodies Transmitting Tangential Forces, ASME Journal of Applied Mechanics, Vol.31, (1964), pp.338-340.

Wickens, A.H., The Dynamic Stability of Railway Vehicle Wheelsets and Bogies Having Profiled Wheels, Int. J. of Solids Structures, Vol.1(1965), pp.319-341.

Wickens, A.H., Steering and Dynamic Stability of Railway Vehicles, Vehicle System Dynamics, Vol.5(1975), pp.15-46.

Wickens, A.H., Non-linear Dynamics of Railway Vehicles, Vehicle System Dynamics, Vol.15(1986), pp.289-301.

Yang, G., A Numerical Procedure for Solving the Non-linear Equations of the Geometrical Contact between Wheelset and Track, MEMT Report 7, Delft University of Technology, 1990.

Yang, G., Pater, A.D. de, The Determination of the Nonlinear Motion of a Railway Vehicle, Proc. 12th IAVSD Symposium, G. Sauvage (ed.), Lyon, pp.225-239.

Yang, G., Pater, A.D. de, Meijers, P., Theoretical and Numerical Analyses of a Railway Vehicle Negotiating a Curved Track, to be published in Proc. ITTG93 Symposium, Lille, France, 1993.

Samenvatting

Gebaseerd op methoden voor multibody-systemen is in het proefschrift een algemeen mechanisch model ontwikkeld om het dynamisch gedrag van spoorwegvoertuig-systemen te voorspellen. De interactie tussen rail en wiel zorgt niet alleen voor de geleiding en de stabiliteit van het voertuig maar veroorzaakt ook schade door hoge contactkrachten. Deze factoren moeten bij het ontwerpen van spoorwegvoertuigen in rekening gebracht worden. Speciale aandacht wordt besteed aan de geometrische, kinematische en dynamische aspecten van het spoor-wielstel systeem. In het model zijn de geometrische en fysische niet-lineariteiten ten gevolge van het contact opgenomen; niet-lineariteiten in de ondersteuningen kunnen eveneens in rekening gebracht worden. Het model is verwerkt in een computerprogramma.

Door te veronderstellen dat de twee met elkaar in contact zijnde lichamen onvervormbaar zijn, leidt het geometrisch contact tussen rail en wielstel tot een zuiver geometrisch probleem in de driedimensionale ruimte. Met de noodzakelijke en voldoende voorwaarden voor twee onvervormbare lichamen die in contact zijn, kunnen de locaties van de contactpunten op de spoorstaaf- en wieloppervlakken gevonden worden, uitgedrukt in twee onafhankelijke gegeneraliseerde coördinaten. Dit vereist de oplossing van een stelsel niet-lineaire algebraïsche vergelijkingen. Ook wordt dan het verband tussen de afhankelijke en de onafhankelijke gegeneraliseerde coördinaten verkregen. Een overeenkomstige analyse is ook uitgevoerd voor een rolproefstand.

Om de rekentijd te verminderen, wordt het stelsel niet-lineaire vergelijkingen gereduceerd tot een stelsel niet-lineaire vergelijkingen voor het twee-dimensionale contact of het wordt vereenvoudigd door middel van de zogenaamde eerste-ordetheorie. De numerieke resultaten geven aan dat de eerste-ordevergelijkingen een voldoende nauwkeurige oplossing geven voor het driedimensionale contact. De singulariteit van het stelsel niet-lineaire vergelijkingen, die verbonden is met het optreden van dubbelcontact, is analytisch en numeriek onderzocht. Het lokale effect van controleparameters wordt gebruikt om de niet-lineaire vergelijkingen op te lossen. Ook wordt een numerieke methode voor het bepalen van dubbel-contactposities gepresenteerd. Met de eerste-ordevergelijkingen is de numerieke analyse uitgevoerd voor de bekende combinatie van UIC60 - en S 1002 - profielen en ook voor twee gemeten asymmetrische profiel combinaties:"CTO-Measured-Profiles" en "ORE-Benchmark-Profiles". De invloed van de spoorbreedte en de spoorstaafhelling wordt eveneens gegeven.

In het mechanische model wordt de beweging van het voertuig beschreven door de nominale beweging, die de beweging van het referentie-coördinatensysteem van het spoor ("track reference frame") aangeeft en de relatieve beweging die de beweging van het lichaam of het aan het lichaam bevestigde coördinatensysteem ten opzichte van de nominale beweging definieert. De nominale beweging wordt beschreven als een functie van de nominale snelheid van het voertuig en de nominale geometrie van het spoor. Ten gevolge van de verbindingen die voortvloeien uit het contact tussen spoor en wielstel, heeft een conventioneel wielstel slechts vier graden van vrijheid. Door gebruik te maken van de corresponderende kinematische verbindingen, worden de algemene bewegingsvergelijkingen van het wielstel bewegend langs een willekeurig spoor afgeleid en uitgedrukt in de vier onafhankelijke gegeneraliseerde coördinaten. Twee hiervan zijn de relatieve verplaatsing in langsrichting en de rotatie van het wielstel om zijn as. Tevens worden de normale componenten van de contactkrachten tussen het spoor en het wielstel bepaald. De theorieën voor het rollend contact worden in het kort besproken en de vereenvoudigde theorie van Kalker wordt toegepast om de tangentiële componenten van de contactkrachten te berekenen. Bovendien worden de bewegingsvergelijkingen voor een wielstel met onafhankelijk roterende wielen afgeleid.

In de dynamische simulatie kunnen vier algemene vormafwijkingen in rechtspoor worden beschouwd. De afwijking van de spoorbreedte en de scheluwte ("cross-level") worden opgenomen in de bepaling van de contact posities; de afwijkingen in zijdelingse en verticale richting worden opgenomen in de beweging van het referentie-coördinatensysteem van het spoor. De bewegingsvergelijkingen voor een wielstel worden gelineariseerd om de stabiliteit van de stationaire beweging op een volkomen recht spoor te analyseren.

Zowel losse wielstellen als complete voertuigsystemen worden gesimuleerd. Eerst worden de oplossingen van enkele opgaven, opgenomen in de spoorweg-"benchmark" problemen van Pascal en Kik, gedemonstreerd. Vergelijking van het dynamisch gedrag van voertuigen met verschillende combinaties geeft aan dat een sprong van een contactpunt de beweging van het voertuig destabiliseert. Vervolgens worden voertuigen met onafhankelijk roterende wielen numeriek onderzocht. Het schijnt dat een volledige ontkoppeling van de rotaties van de beide wielen om hun gemeenschappelijke omwentelingsas destabiliserend werkt op het systeem; op dit punt is verder onderzoek noodzakelijk.